This is to certify that the

dissertation entitled

DESIGN AND DEVELOPMENT OF ADVANCED
VANED DIFFUSERS FOR CETRIFUGAL
COMPRESSORS

presented by

Naresh Kumar Amineni

has been accepted towards fulfillment
of the requirements for

___Ph.D.___ degree in __Mechanical_Engineering

_____
Major professor

Date___05 - 14 - 96___

0-12771

PLACE IN RETURN BOX to remove this checkout from your record.
TO AVOID FINES return on or before date due.

DATE DUE	DATE DUE	DATE DUE
_____	_____	_____
_____	_____	_____
_____	_____	_____
_____	_____	_____
_____	_____	_____
_____	_____	_____
_____	_____	_____

MSU Is An Affirmative Action/Equal Opportunity Institution

c:\circ\datedue.pm3-p.1

DESIGN AND DEVELOPMENT OF ADVANCED
VANED DIFFUSERS FOR CENTRIFUGAL COMPRESSORS

By

Naresh Kumar Amineni

A DISSERTATION

Submitted to
Michigan State University
in partial fulfillment of the requirements
for the degree of

DOCTOR OF PHILOSOPHY

Department of Mechanical Engineering

1996

ABSTRACT

DESIGN AND DEVELOPMENT OF ADVANCED VANED DIFFUSERS FOR CENTRIFUGAL COMPRESSORS

By

Naresh Kumar Amineni

Typically downstream of a centrifugal impeller, three types of radial diffusers are used: 1) vaneless diffuser, 2) conventional vaned diffuser and 3) low solidity vaned diffuser. Each of these diffusers has its own merits and demerits. However, recent investigations have shown that a low solidity vaned diffuser is a good compromise between the vaneless diffuser and the conventional vaned diffuser.

Some of the experimentally tested low solidity vaned diffusers were first analyzed with 3-D viscous calculations to understand the flow phenomena inside the diffuser. The effect of the geometric parameters of the low solidity vaned diffuser on the flow characteristics was also investigated by numerical experimentation. The results showed that low solidity vaned diffusers stall when the vane suction surface separation was accompanied by the end wall separation; and this qualitatively compared well with the experiments. Moreover, the design parameters: incidence angle, blade turning angle and solidity were found to have considerable bearing on the performance of the diffuser.

Based on the observations of numerical analysis, four new low solidity vaned diffusers were designed for experimental analysis. These four low solidity vaned diffusers along with a conventional vaned diffuser and two vaneless diffusers were tested downstream of the same impeller to study the pressure recovery phenomenon in each of the three types of diffusers. The low solidity vaned diffusers were divided into three sections the upstream vaneless space, the vaned region, and the downstream vaneless space. The pressure recovery in each of these corresponding sections of all diffusers was compared.

The experimental data showed that the pressure recovery in the region between the impeller exit and the vane trailing edge radius of the low solidity vaned diffuser was similar to the pressure recovery of the conventional vaned diffuser inlet to the throat section. It was found that, nearly 75% of the total pressure recovery in the low solidity vaned diffusers occurred in this region. It was also observed that the low solidity vanes functioned as deswirling vanes and did not contribute significantly to the overall pressure recovery of the low solidity vaned diffuser.

To my parents, my brother and all my teachers

ACKNOWLEDGMENTS

TABLE OF CONTENTS

LIST OF TABLES

LIST OF FIGURES

NOMENCLATURE

a	sonic velocity (m/s)
b	passage hub to shroud width (mm)
C	absolute velocity (m/s)
c	vane chord length (mm)
c_p	specific heat (J/Kg K)
Cp	pressure recovery
CVND	conventional vaned diffuser
d	diameter (mm)
I	incidence (deg)
LSVD	low solidity vaned diffuser
M	Mach number
M_t	impeller tip Mach number
P	pressure (N/m^2)
p	pitch (mm)
PS	pressure surface
$\bar{q}$	relative velocity (m/s)
r	radius
SS	suction surface
T	temperature (°C)
U	tip speed (m/s)
V_x	axial velocity (m/s)
V_r	radial velocity (m/s)
V_θ	tangential velocity (m/s)
VNL	vaneless diffuser
w	channel width (mm)
Z	vane number
z	axial coordinate

α	flow angle with respect to tangent (deg)
β	vane angle with respect to tangent (deg)
ϕ	inlet flow coefficient
γ	ratio of specific heats
η	efficiency
μ	work coefficient
π	pressure ratio
θ	blade turning angle (deg)
ρ	density (kg/m^3)
t	temperature ratio, stress tensor
σ	solidity
Ω	rotational speed (rpm)
ξ	loss coefficient
ψ	head coefficient

Subscripts

N	normalized
0	total condition
1	stage inlet
2	impeller exit
2a	impeller exit - measurement station
3	vane leading edge station based on LSVD
4	vane trailing edge station based on LSVD
5	diffuser exit
6	stage exit

1. INTRODUCTION

1.1 Demands and challenges to centrifugal compressors

In turbocompressors the required pressure rise and flow is imparted to the fluid medium by transferring kinetic energy to the process gas. The centrifugal compressor is a class of turbocompressors in which the flow enters axially and leaves the compressor radially.

Although centrifugal compressors found wide use in the early stages of gas turbine development, by the early 1950s the axial machines largely superseded them for aeronautical applications. Interest in the centrifugal compressors was renewed when they became attractive for helicopter engines. Since then, the benefits of stable performance and high single stage pressure ratio have led to several applications. The advantages of centrifugal compressors are that they are reliable, compact, and robust; have better resistance to foreign object damage; and are less affected by performance degradation due to fouling. Centrifugal compressors are found in small gas turbine engines, turbochargers, and refrigerators and are used extensively in the petrochemical and process industry.

Since the centrifugal compressor finds a wide variety of application, each application places its own demands on the design of the compressor. The gas turbine compressors are usually the most demanding from the standpoint of performance and mechanical factors. The requirements for these machines include medium to high pressure ratio, higher efficiency demands at diverse speeds, restricted overall diameters, low impeller inertia, strict life demands, and some performance trade off to match gas generator

1

(turbine) needs. However, range demands are usually not as great as for the other applications.

Turbochargers by contrast require an extremely robust design and frequently employ cast materials. They are exposed to very harsh operating environments and require moderately thick leading edges in order to resist foreign object damage and to have good first bending vibratory stress tolerance. In many cases, a very high flow coefficient or high specific speed, design is required both from the fundamental thermodynamics point of view and to keep overall size and inertia down. An exceedingly wide range is required for automotive turbocharger applications and for four-stroke diesel-engine trucks, while large locomotive engines are generally more tolerant of the operating range.

Process compressors cover an exceedingly wide range of applications and operate with very diverse gases. The molecular weight and distribution of component gases may vary significantly during the lifetime of a given compressor. It is not uncommon to find applications that require 30 or 40 percent stable operating range (design flow to surge flow) to meet the diverse changes in possible operating conditions.

The refrigeration compressors are quite similar to the process compressors except that their stage pressure ratio and flow conditions are defined by a unique thermodynamic cycle. Due to the thermodynamic properties of refrigerants, one is frequently operating quite close to the top of the vapor dome and thus design calculations with real gas properties often become mandatory. Perhaps the most distinguishing feature of the refrigeration compressor is the requirement for operation during very wide climatic conditions through summer and winter, thus requiring loads anywhere from 10 to 110 percent of the design load.

This wide range of demands on centrifugal compressors brings many design considerations that need to be accomplished. Most of the design requirements need solutions to two major problems : stress and aerodynamics. The stress problems are caused by to the material strength limitations, and the capability to accurately predict, blade and

rotor steady state and vibrational stress for complex impeller shapes and at high rotational speeds.

The aerodynamic problem is to efficiently accomplish, large air deflections and diffusion at high flow velocity, with the added difficulty of very small passage flow areas required to get good efficiency and high pressure ratio. Even though the individual components of the compressor are capable of achieving high efficiency, it is the efficiency of the whole stage that is of great importance. Thus, component matching is an essential aspect of design. It is often required to redesign one or more components of the compressor due to improper matching and sometimes the efficiency of a component is sacrificed to achieve good matching.

1.2 The importance of vaned diffusers in centrifugal compressor

A centrifugal compressor consists of three major components: the impeller, the diffuser, and the collector. The impeller is the heart of the compressor and adds energy to the fluid. The diffuser receives gas from the impeller at high velocity, and it has to practically diffuse all of the velocity head into static pressure with minimum losses. The diffused gas after leaving the diffuser is collected in a collector for further use depending on the application.

The flow discharged by the impeller is very complex and non uniform. A rotating wake system and impeller blade pitch distortions cause pulses in the flow at blade passing frequency. Furthermore, the flow varies in pressure, velocity, and angle across the width of the channel. Thus, depending on the impeller exit flow conditions and the pressure rise and flow range required, a centrifugal compressor can employ either a vaneless diffuser or a vaned diffuser.

The largest part of the velocity head entering into the radial diffuser is tangential to the impeller tip. For absolute flow angles of 15 to 20 degrees, this part is almost 80 to 85

percent. Thus, attempted diffusion of the radial component will pay little dividend, and the principle objective of the radial diffuser is to reduce the tangential velocity effectively. Due to the radial movement of the gas, the velocity will be reduced naturally by the conservation of the angular momentum without the use of diffuser vanes. However, the radial distance to achieve sufficient reduction in velocity is usually prohibitively large. Also, the sidewalls of the passage present an uninterrupted path for inward boundary layer flow caused by the radial pressure gradient. Large losses occur due to the mixing of the contrary or secondary flows. For the high speed and high pressure ratio machines, in which the required diffusion is large, a vaned system becomes essential to inhibit such loss producing cross flows.

Since in most applications high pressure rise and high efficiency are basic requirements as was mentioned previously, the vaned diffusers find extensive use in centrifugal compressors. The vaned diffusers usually constrain the operating flow range of the compressor by choking at high mass flow rates and by stalling at low mass flow rates. However, in applications where the wide operating flow range and insensitivity to operating conditions are essential, the vaneless diffusers are used.

1.3 Objective of the present work

A typical, centrifugal compressor stage can have an overall efficiency of about $85 \pm 2\%$ in the range of 2 to 6 pressure ratio. For such a compressor if operating at favorable speeds the impeller efficiency can be above 90%, which is a remarkably high value in view of the large energy added, and compares well with the best transonic and supersonic axial compressor rotors that add much lower energy per stage.

The high impeller performance has been achieved within the confines of mechanical limitations that permit very little variation in the blade or rotor design. Thus, it can be said

that any improvement in radial impeller efficiency can only be incremental, with a very significant amount of development effort.

Therefore, diffuser design and development is the area, that can provide further improvement in centrifugal compressor performance . Moreover, a diffuser is much less restricted by the mechanical limitations when compared to the impeller of a centrifugal compressor. For a compressor with an overall efficiency of 80%, even though the impeller efficiency would be about 90%, the diffusion efficiency of the diffuser ranges only between 65 to 75%. Thus, if the radial diffuser efficiency of 85 to 90% can be attained, an improvement of 4 to 5 percentage points in overall efficiency of the centrifugal compressor can be achieved.

It has been possible to obtain high diffuser efficiency (up to 85%) with the help of specifically designed vaned diffusers. But the major disadvantage of the vaned diffusers is that they limit the range of operation of the compressor. In this work the vaned diffuser design is studied in detail with a view to understand all the parameters that help in attaining high efficiency. At the same time to identify the parameters which restrict the flow range of the compressor as wide flow range is very important for most compressor applications.

The knowledge gained is used to study the Low Solidity Vaned Diffusers (LSVD). The low solidity vaned diffusers have significant advantage over both the vaneless and the conventional vaned diffusers because they are able to attain efficiency equivalent to vaned diffusers and the range equivalent to the vaneless diffusers. The low solidity vaned diffusers were analyzed theoretically using 3-D viscous code and experimentally tested to understand and study the influence of vital aerodynamic and geometric parameters on the flow phenomena.

The flow physics and the parameters controlling the flow behaviors in the low solidity vaned diffusers were initially studied using the diffusers designed and tested by Holhweg et al. (1993). These experimentally tested diffusers were modeled for analysis with 3-D viscous code (BTOB3D) of Dawes (1991). The results obtained by 3-D viscous

code analysis are compared with the experimental results. The influence of the geometric design parameters on the flow was investigated through numerical experimentation. Based on these numerical results, four new low solidity vaned diffusers were designed for experimental analysis.

The four new low solidity vaned diffusers along with one conventional vaned diffuser and two vaneless diffusers were tested downstream of the same impeller at Michigan State University's Turbomachinery Laboratory. This work contains the results of these tests. The overall steady and unsteady performance of the compressor with different diffusers is compared along with the detailed individual diffuser performance and loss analysis, which would assist in the development of a design methodology for LSVDs.

2. FLOW IN VANED DIFFUSERS

2.1 Radial Diffusers for Centrifugal Compressors

In centrifugal compressors a large amount of energy is transferred to the fluid by the impeller. Even though the centrifugal impellers are designed for very good diffusion within the blade passage, nearly 20 - 50% of the energy imparted to the fluid remains as kinetic energy at the impeller exit. Therefore, for an efficient centrifugal stage, this kinetic energy must be efficiently recovered as static pressure. Thus, a diffuser is a very important component downstream of the impeller in a centrifugal compressor.

The diffuser (in a compressor) serves to convert kinetic energy of the gas at the impeller exit into static pressure by one or both of the two principle conversion techniques:

1. by increasing the flow area, which will reduce the velocity and in turn increase the static pressure

$$\rho_1 C_{r1} A_1 = \rho_2 C_{r2} A_2 \tag{2.1}$$

2. by changing the flow path, which will bring recovery in angular velocity

$$r_1 C_{\theta 1} = r_2 C_{\theta 2} \tag{2.2}$$

The flow entering a radial diffuser has a large amount of swirl ($\alpha = \tan^{-1}(C_r/C_\theta)$); the swirl angle is typically between $10°$ - $30°$. Thus, the tangential component of momentum at low flow rates can be more than twice the radial component. The radial component of the flow diffuses due to the area increase (conservation of mass), and the tangential component diffuses as it is inversely proportional to the radius (conservation of angular momentum).

However, the radial component of the velocity has to surmount the radial pressure gradient for the tangential velocity to diffuse continuously. When reverse flow of the radial boundary layer occurs, it is not possible for the tangential component to continue diffusing, as this would imply a pressure increase in one component and not in the other. Therefore, in such cases the breakdown of flow occurs, and this breakdown can cause the diffuser to stall and produce other flow instabilities such as surge or rotating stall.

Since over the years the demands on the centrifugal compressors increased for higher pressure ratios and efficiency, different types of diffusers have been developed. These different types of diffusers can be classified as vaneless diffusers, vaned diffusers, and the low solidity vaned diffusers.

2.2 Types of Radial Diffusers

2.2.1 Vaneless Diffuser

Vaneless diffusers used in centrifugal compressors constitute a very simple geometric form for recovering the high kinetic energy leaving the impeller. These diffusers consist of two side walls between which the fluid is allowed to progress radially, converting the kinetic energy to static pressure, both by means of the deceleration of the meridional velocity due to the continuous increase in passage area and by the deceleration of the tangential velocity with the principle of conservation of angular momentum. The side walls may be parallel or converging and sometimes a part of the diffuser may even rotate with the impeller. A respectable level of static pressure recovery can be achieved with a well designed vaneless diffuser and it is inherently inexpensive. The vaneless diffuser is most frequently followed by a collector scroll that accumulates the flow and delivers.

In general, the velocity diffusion takes greater radial space than in vaned diffusers, but the vaneless diffuser has several advantages. The loss variation with the flow rate is

relatively gentle when compared to the vaned diffusers in which due to incidence and shock losses on the vanes the off design flow conditions may lead to rapid rise in losses. Also, vaneless diffusers offer no perturbances to the flow and generally produce no unfavorable pressure pulsation. Thus, centrifugal compressors for which good stable margins along with low noise is desired often have vaneless diffusers. The vaneless diffusers provide the maximum flow range for the centrifugal compressor as they do not restrict the amount of flow as in a vaned diffuser throat. The choke in a compressor with a vaneless diffuser is generally governed by the inducer choke.

There are two significant disadvantages involved with the vaneless diffuser as opposed to the advantages (wide operation range, insensitivity to changed operating conditions, simple design). The vaneless diffuser is inferior to the vaned diffuser with regards to efficiency. From the outlet velocity triangle of the impeller, it can be derived that an adequate pressure conversion can only be achieved by means of significant reduction of the tangential component of the velocity. According to the law of angular momentum for a non viscous flow, one can derive that the effectiveness of the vaneless diffuser almost exclusively depends on its diameter ratio. If good stage efficiencies are to be achieved, the radial extent of the diffuser must be large. However, an increase in the radial distance causes a longer flow path due to which the dissipation losses increase and the static pressure recovery rise is insignificant in relation to the hardware cost.

The performance of the vaneless diffuser is governed by the very complex flow field that develops in it. The velocity profile leaving the impeller is generally not uniform across the axial width. Also, the wakes generated by the impeller vanes enter the diffuser and may persist for quite some distance into the diffuser causing complicated wake mixing losses. The boundary layers that grow on the sidewalls contain momentum losses due to the wall shear stress.

2.2.2 Vaned Diffuser

At low mass flow rates the flow through a vaneless diffuser can describe an arc of approximately 360° before discharge. This long flow path results in high friction loss. The flow path length cannot be reduced easily, as a significant radius ratio is necessary to gain the required diffusion through the conservation of angular momentum. Thus, the commonly adopted approach to shorten the flow path is to insert diffuser vanes, these diffusers are called vaned diffusers.

The principle of a vaned diffuser is to provide additional reduction of the swirl over the vaneless concept by reducing the angular momentum. Typically 50% of the inlet angular momentum may be removed with vanes, which effectively halves the radial extent required for a given reduction in swirl compared to the vaneless diffusers. The additional diffusion achieved by a vaned diffuser over a vaneless diffuser can significantly reduce the losses incurred in the collection or return system which follow. The vaned diffusers are advantageous where small size is important.

In a vaned diffuser, there is a clearance between the impeller and vane leading edges. This space constitutes a vaneless diffuser and its functions are (i) to reduce the circumferential pressure gradient at the impeller tip, (ii) to smooth out velocity variations between the impeller tip and vanes, and (iii) to reduce the Mach number at entry to the vanes, so as to avoid shock or overspeeding on the vane profile. The flow follows an approximate logarithmic spiral path to the vanes after which it is constrained by the diffuser channels. For rapid diffusion, the axis of the channel is straight and tangential to the spiral. The passages between the vanes are generally designed on the basis of simple channel theory. The vaneless space is followed by a semivaneless space. The semivaneless space is very critical in the vaned diffusers as it constitutes of the vane to vane throat, which controls the choke or maximum flow through the compressor. Figure 2.1 shows the geometry of a vaned diffuser.
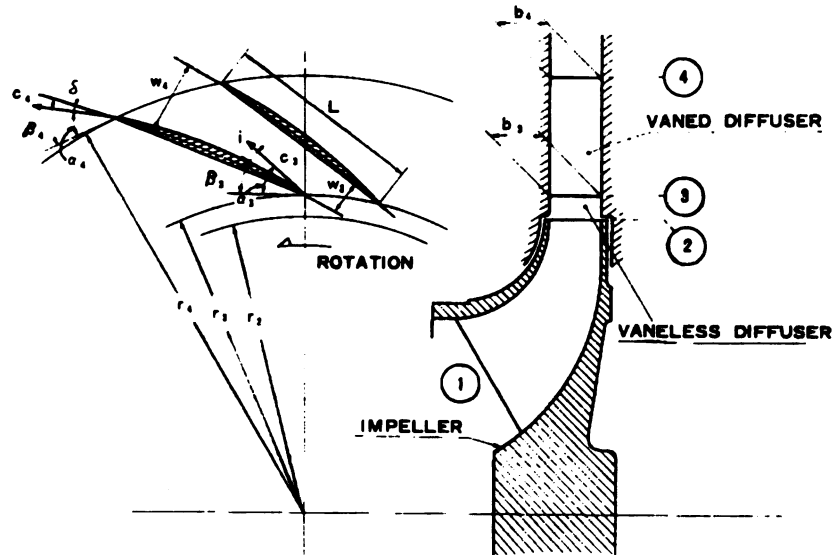
Figure 2.1. Vaned diffuser geometry

The vaned diffusers provide higher efficiency than the vaneless diffuser and at the same time have a great influence on the flow range of the compressor. The operating range of the compressor in almost all cases is reduced due to vane stall at reduced flows and throat choking at increased flows. Surge or stall is primarily due to flow separation at high positive incidence caused by low flow rates. The choke flow is controlled most often by vane to vane throat area.

The number of diffuser vanes has a direct bearing on the size and efficiency of the vaned diffuser. With large number of vanes, the angle of divergence is smaller, and the efficiency increases to the point where increased friction and blockage overcomes the advantage of more gradual diffusion. However, too many diffuser passages can have a strong adverse effect on the surge characteristics of a centrifugal compressor. With several adjacent diffuser passages sharing the gas from one impeller passage, the uneven velocity distribution from the impeller passage results in alternate diffuser passages being either starved or choked. This unstable situation leads to flow reversal in the passages and to

surge of the compressor. When the number of diffuser passages is less than the number of impeller passages, a more uniform total flow results.

Vaned diffusers can be divided into several generic classes. They are sometimes classified based on how the flow is discharged. Each channel discharges into a separate downstream element or all the channels discharge into a common scroll or collector. Most often the vaned diffusers are classified based on the type of blading. Two types of blade systems are most often found, the curved vanes and the straight channel or vane island vanes. Figure 2.2 shows some of the types of vaned diffusers.

The curved vanes are similar to the axial compressors blades. The diffusion is achieved by turning the flow radially. The curvature of the vanes is such that the divergence of the channel results in vanes with a small trailing edge thickness. This provides a smooth transition to the downstream volute or return channel. However, the flow between two successive vanes is not symmetric.

The shape of the straight channel diffusers results from the triangular vanes that are fixed between the diffuser walls and are therefore also called as vaned island diffusers. The diffusion of the flow is controlled by the divergence of the channel. A higher diffusion can be achieved in the straight channels because the flow is symmetric. However, sudden expansion losses occur at the diffuser exit due to the large trailing edge thickness.

2.2.3 Low Solidity Vaned Diffuser

In recent years the high efficiency and wide operating range requirements on the radial compressors have led to the development of low solidity vaned diffusers. Even though low solidity vaned diffusers (LSVD) were first reported in 1978, since then there has been very little information in the public domain regarding their flow characteristics and design procedures.

(a) Vane island diffuser

(b) Wedge vane diffuser

(c) Cambered vane diffuser

(d) Twisted vane diffuser

(e) Pipe diffuser

(f) Circular arc vane diffuser

Figure 2.2. Types of vaned diffusers

In a vaned diffuser, it has been established that both the minimum flow rate and the maximum flow rate are decided by the flow behavior at the throat. Thus, the presence of the throat in vaned diffusers limits the flow range and causes the associated instabilities. Hence, in LSVD the throat is eliminated by requiring the vane solidity ratio (σ = c/p) be less than 0.9.

Low solidity vaned diffusers, too, have a vaneless space between the impeller exit and the vane leading edge, similar to the vaned diffuser. The function of this vaneless space in most respects is the same in both LSVD and vaned diffusers. However, in the case of LSVD the vaned region is followed by a vaneless space, and the vaned region does not form any kind of channel as in vaned diffusers. Figure 2.3 shows the geometry of an LSVD.
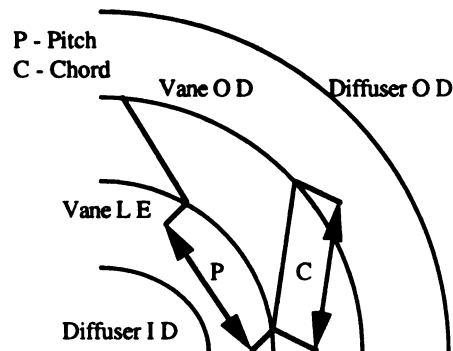
Figure 2.3. Geometry of low solidity vaned diffuser.

The LSVDs as shown in Figure 2.4 have a significant advantage over both the vaneless and the vaned diffusers. They attain higher efficiency than the vaneless diffuser with an operating range almost equal to the vaneless diffuser. Thus, with the LSVDs it is possible to enjoy the benefits of both vaned and vaneless diffusers. However, there is very little information available regarding the parameters controlling the performance of an

LSVD and the behavior of an LSVD under different diffuser inlet flow conditions. Section 2.6 reviews the little available literature in public domain.
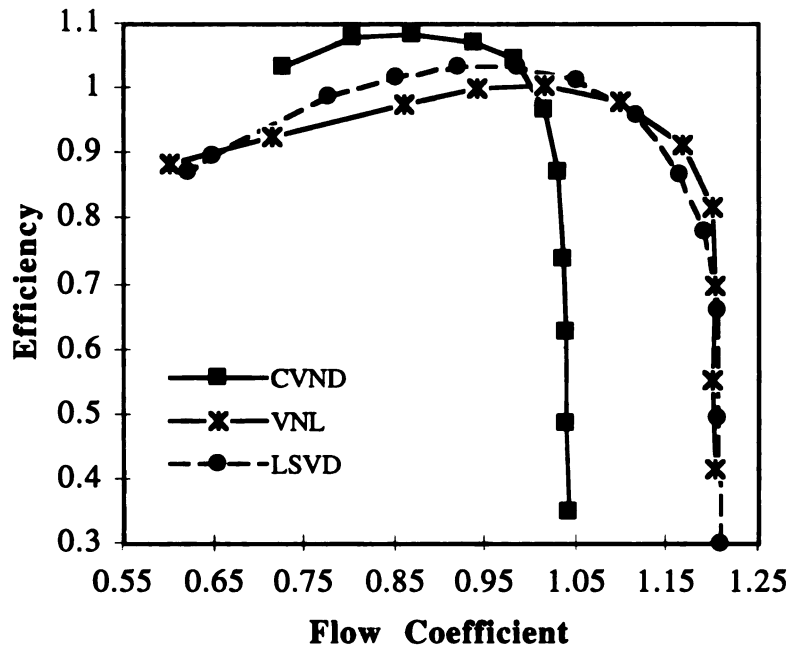
Figure 2.4. Diffuser performance characteristics

2.3 Discharge Flow of Centrifugal Impeller

The overall efficiency of a centrifugal compressor is equally dependent on the good design of both the impeller and the diffuser. In the case of the impeller, the inlet flow is usually uniform, but the diffuser has to accept the outlet flow from the impeller. The flow discharged from the impeller is most often highly non uniform with significant three-dimensional velocity components. The diffuser has to remove these nonuniformities in velocity and flow direction in order to efficiently recover the static pressure.

The flow at the centrifugal impeller exit invariably exhibits jet and wake flow pattern. These jet and wake flow patterns are generated by Coriolis, curvature, boundary

layer, and tip clearance effects that separate the flow into high (jet) and low (wake) velocity fluid. Many investigators have studied the jet-wake flow behavior at the impeller exit, in order to understand the various effects contributing to this kind of flow and how jet and wake mix in the vaneless space or diffuser downstream of the impeller.

Eckardt (1975), by measuring the relative velocity distribution just behind the impeller, showed a clear region near the flow channel suction side/shroud side corner with low mass flow, high turbulence and losses, and a region with high C_r component near the pressure side that had relatively stable flow and low total pressure losses (Figure 2.5).
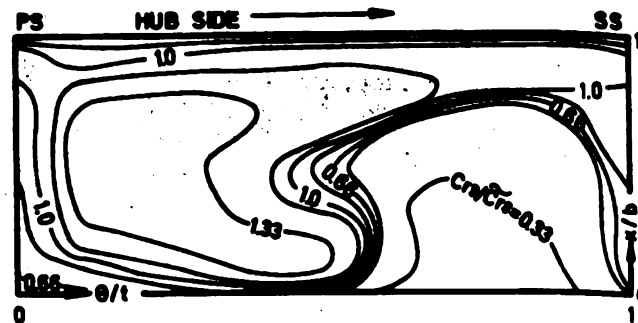
Figure 2.5. Radial velocity distribution at the exit of one blade channel (Eckardt 1975)

Thus, showing the jet-wake flow exiting the impeller. Similar measurements in the vaneless space following the impeller up to a radius ratio of $r/r_2 \approx 1.05$ showed that the jet and wake have not mixed completely, and the flow was not axisymmetric. Johnson and Moore (1980, 1982, 1983) using a ghost impeller similar to the Eckardt's impeller measured the three mutually perpendicular velocity components and rotary stagnation pressure to study the wake formation and development. They found that the wake flow was an accumulation of low rotary stagnation pressure fluid at the suction side/shroud corner of the impeller blade passage. The major flow phenomena contributing to the formation and development of the wake were:

(a) The adverse static pressure gradient between the inlet and the exit of the axial to the radial bend in the impeller near the shroud/suction side corner, which results in a substantial increase in low stagnation pressure fluid at the inlet region of the bend, and

(b) The convection of low stagnation pressure fluid by the secondary flows, which are generated in the boundary layer due to the curvature and rotation of the impeller passage.

They also showed that the mass flow rate had an influence on the location of the wake at the impeller outlet; the wake was located on the suction surface for below design flows, near the suction surface/shroud corner at design flow and on the shroud at above design flows (Figure 2.6). Since the secondary flows are a function of mass flow rate, they showed that the secondary flows in the impeller passage contribute to the formation of the wake, and that they also have strong influence on the position of the wake at the impeller exit plane.

Krain (1988), using L2F measurements, studied the flow behavior in three different types of centrifugal impellers. The impellers tested were (a) radially ending Eckardt impeller, (b) radially ending splitter blade impeller (14 + 14 blades) and (c) new backswept impeller. In his observations he noted that the new impeller had a much smoother impeller exit flow as shown in Figure 2.7. However, he concluded that secondary flows and distorted through flows found in all three impellers were caused by the swirling impeller flow inside the rotor. Moreover, he found that the vortex flow had influence on the through flow patterns , thus, it was inevitable to avoid distorted impeller discharge flow, unless the flow development is guided in such a way that the vortex flow fully disappeared at the impeller discharge. Hathaway et al. (1993) studied the flow field of the NASA low speed centrifugal compressor impeller using the laser anemometry and 3D viscous code (Dawes code). The results obtained by them were very similar to those of the Krain and others. In addition to this they also showed that 3D viscous code results were in good agreement with
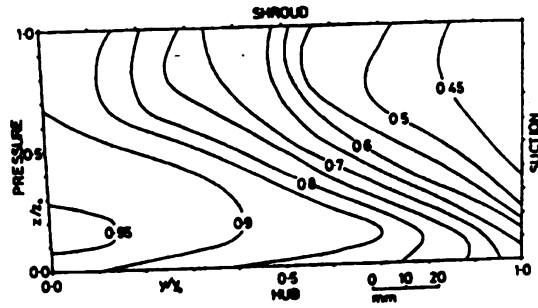
(a) 'Below Design' flow
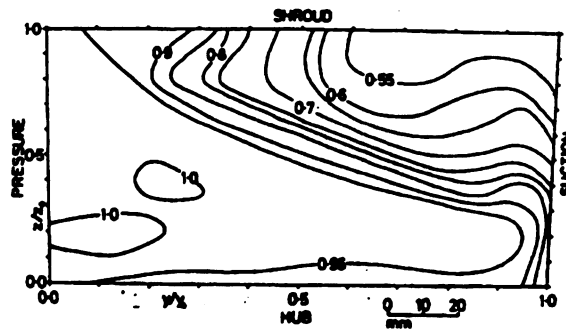
(b) 'Design' flow
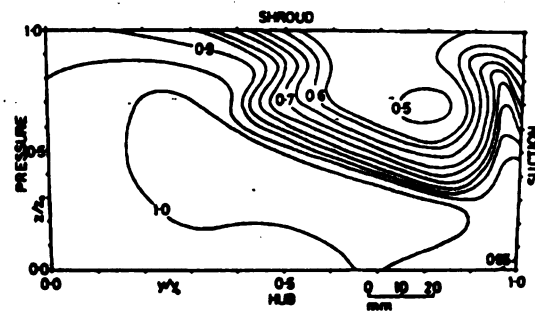
(c) 'Above Design' flow

Figure 2.6. Rotary stagnation pressure distribution at impeller exit (Johnson & Moore 1982)
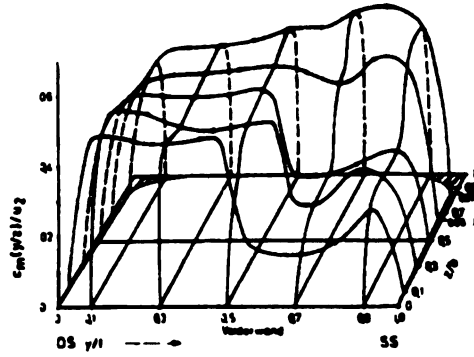
(a) Radially ending Eckardt impeller
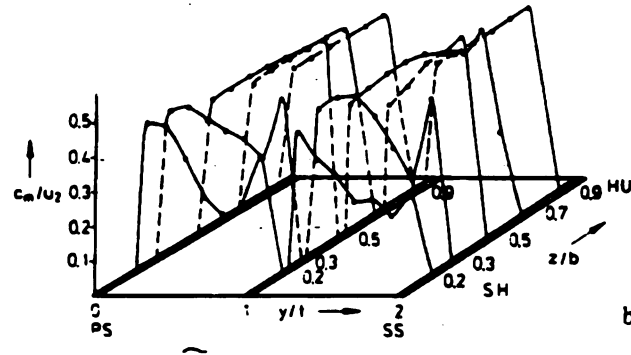
(b) Radially ending splitter-blade impeller
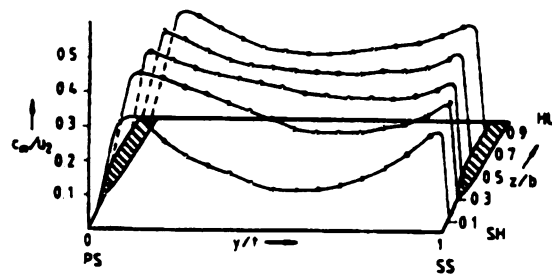
(c) new backswept impeller

Figure 2.7. Comparison of velocity profiles at the impeller discharge (Krain 1988)

the experimental results. They also compared their results with the results of the Krain's impellers and found good agreement. They found that the low momentum fluid near the blade surfaces migrates outward towards the tip of the blade. The fluid that moves up the blade pressure and suction surfaces is entrained into the tip clearance jet and the fluid is transported toward the pressure side/shroud corner of the characteristic through flow momentum wake that is found in unshrouded centrifugal impellers.

Hathaway et al. (1993) also studied the impeller wake mixing phenomenon downstream of centrifugal impeller. They measured absolute flow angles at four different locations up to an r/r_2 of 1.06 and found that the through flow momentum wake region generated as a result of tip clearance flow mixes out more slowly than does the viscous blade wake as the flow moves through the vaneless diffuser. This was concluded from the pitchwise absolute flow angle distribution study at 50% span and 90% span as shown in Figure 2.8. Thus, the flow field in the vaneless space near the shroud surface is composed of low momentum regions: one from the viscous blade wake and one from the through flow momentum wake.

Inoue and Cumpsty (1984) in their work show that the angular velocity profile did not vary as significantly as the radial velocity across the span (Figure 2.9) with radius. They also found that the circumferential distortions of the radial velocity in vaneless diffuser did not disappear even at $r / r_2 \approx 1.3$. However, the distortion patterns of tangential velocity decreased rapidly with radius, which can be attributed to the energy transfer between jet and wake regions. Mounts and Brasz (1992) with their 3D viscous calculations show that the initial dynamic variations in velocity and flow angle disappear quickly with diffuser radius ratio. However, the dynamic fluctuations in the static pressure originating from the impeller blade loading did not reduce appreciably with radius. Moreover, the steady state distortions in the hub to shroud plane, with higher through flow velocities at the hub than at the shroud persisted over a large area of the diffuser. Pinarbasi and Johnson
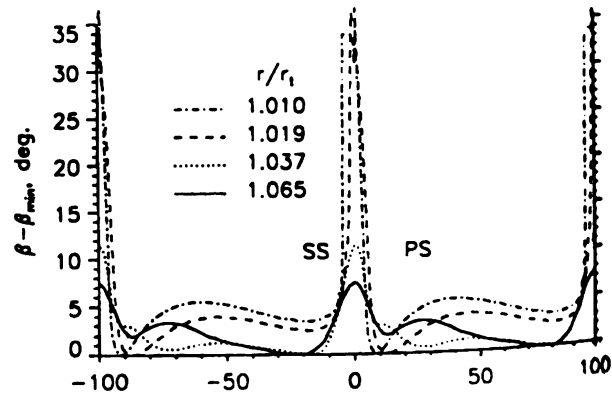
(a) At 50% span
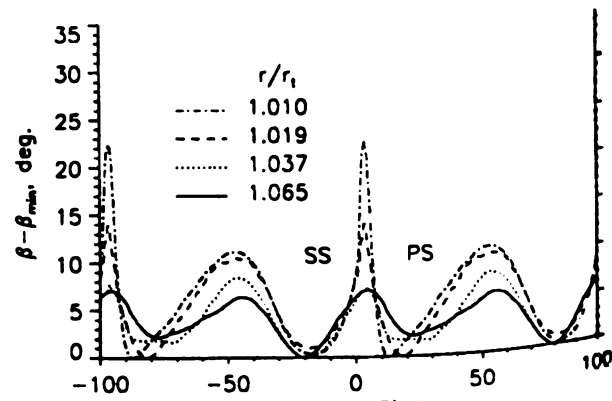
(b) At 90% span

Figure 2.8. Pitchwise distribution of absolute flow angle difference at impeller exit (Hathaway et al. 1993)
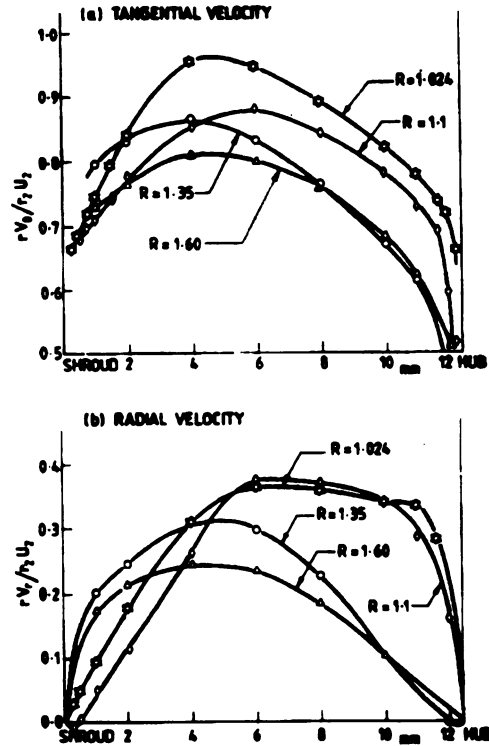
Figure 2.9. Velocity variation in axial direction in vaneless diffuser (Inoue & Cumpsty 1984)

(1994) also showed very similar results through hot wire anemometer measurements at numerous radius locations in the vaneless diffuser downstream of a backswept impeller.

Thus, the flow received by any diffuser downstream of a centrifugal compressor is very non uniform and contains jet and wake flow patterns caused by the secondary flows inside the impeller blade passage. In the vaneless space downstream of the impeller, the dynamic variations and the flow distortions in the circumferential direction tend to mix out in short radial distance. However, the passage wakes and the flow variations in the axial direction across the span tend to persist throughout the vaneless diffuser.

2.4 Rotor and Diffuser Vane Interaction

Centrifugal compressor stage optimization requires a proper impeller/diffuser matching, as this has considerable influence on the efficiency and surge limit of the stage. For a good stage performance, the efficiency of the impeller and the diffuser are of equal importance. However, the efficiencies of both these components are interdependent due to the impeller/diffuser interaction. The diffuser pressure recovery is largely affected by the highly distorted, unsteady impeller discharge flow. On the other hand, the diffuser vanes are believed to act on the internal three-dimensional impeller flows. The non uniform flow from the impeller is sensed as an unsteady flow by the vaned diffuser vanes, while the presence of diffuser vanes is seen as an unsteady disturbance by the impeller. Moreover, this interaction between the impeller and diffuser vanes is a strong source of noise and vibrational excitation. Many investigations have been made on the interaction of the impeller and the diffuser vanes on the impeller discharge flow.

Baghdadi (1977) studied the effect of impeller blade wakes on the performance of the vaned diffuser by using a vortex rig. The vortex rig could produce only the axial distortions in the flow at the diffuser inlet. Thus, he compared the results of vortex rig with the results of an actual compressor to examine the effect of impeller blade wakes. He found close agreement in the performance of the vaned diffusers used with the vortex rig and the actual compressor. Therefore, he concluded that the rotor blade wakes do not affect diffuser performance. The reason for this could be that the blade wakes mix very rapidly by energy transfer or due to the lack of response of the diffuser vanes to the high frequency flow variations imposed by the rotating wakes.

Krain (1981) performed L2F measurements both inside the impeller (near the exit) and in the diffuser with a vaneless and a vaned diffuser downstream of the impeller. The velocity patterns found inside the impeller with vaneless and vaned diffuser are shown in Figure 2.10. It can be seen that the diffuser blades have a slight effect on the velocity

profiles at the shroud, whereas the velocity patterns at the hub region were similar with both diffusers. The small effect of the diffuser vanes on the impeller flow was presumed to be due to high vane leading edge to impeller exit radius ratio of 1.1. However, the measurements in the vaneless space of the vaned diffuser showed unsteady flow angle variations of up to 17°, and up to 13° in the diffuser throat region. Thus, there does not exist any station ahead of the diffuser throat where flow is fully mixed out.
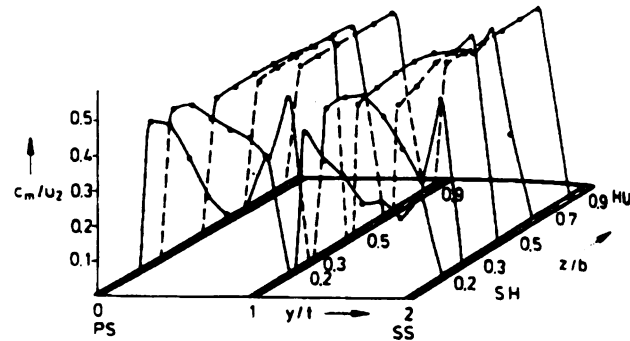
(a) Vaneless diffuser
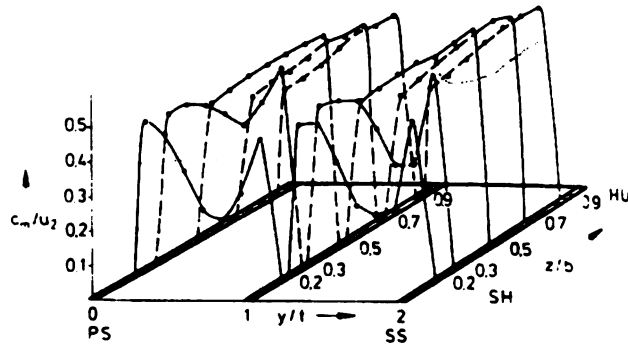
(b) Vaned diffuser

Figure 2.10. Meridional velocity distribution at diffuser inlet (Krain 1981)

Fisher and Inoue (1981) found that the vaned diffuser played a major role in establishing the circumferential variations in mean flow conditions at the diffuser inlet. They observed that by increasing the blade angle, the circumferential variations increased.

However, an increase in the number of diffuser vanes decreased the variation of the flow conditions in the circumferential direction. They also found that the vane setting radius had a major effect on the flow conditions. Figure 2.11 shows the velocity variation in circumferential direction for two different radial clearances between impeller tip and diffuser vanes (4% and 10% of r_2).

(a) $r_3/r_2 = 1.04$

(b) $r_3/r_2 = 1.10$
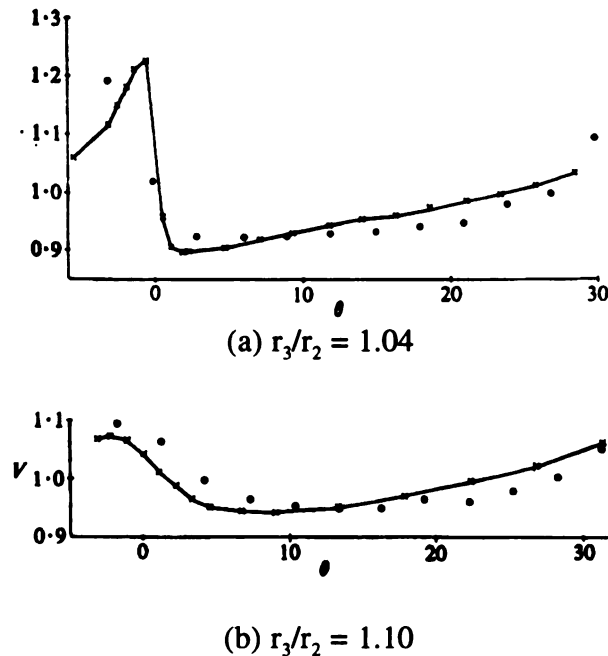
Figure 2.11. Velocity distribution at diffuser inlet (Fisher & Inoue 1981)

Inoue and Cumpsty (1984) carried out hot-wire measurements in the vaneless space between the impeller and vaned diffuser at a range of flow coefficients for three different diffusers with 10, 20, and 30 vanes set at each of three different radius ratios, 1.04, 1.1, and 1.2. It was found that the circumferential distortion of flow from the impeller was very rapidly attenuated in the entrance region of the diffuser vanes and had only minor effects on the flow inside the vaned diffuser passages. The effect of the diffuser vanes on the flow discharge from the impeller was evident and reversal of the flow back into the impeller was detected when the diffuser vanes were close to the impeller and flow rate was low. The

time mean total and static pressure at impeller outlet were found to vary over the pitch of a diffuser vane, and a variation in the strength of impeller wake was also observed. Figure 2.12 and Figure 2.13 show the variation of the reverse flow strength as a function of mass flow rate and vane number.

2.5 Design Parameters of Vaned Diffuser

The performance of the vaned diffuser is dependent on various geometric and flow parameters: the aspect ratio, the area ratio, the length to width ratio, the inlet to exit diffuser radius ratio, the impeller exit to vane leading edge radius ratio, the divergence angle of the channel, the shape of the vanes or the camberline path, and the leading and trailing edge geometry. All these parameters are related to each other in the case of a vaned diffuser, and any variation in one of them can lead to a change in other too. The various flow parameters on which the performance of the vaned diffuser can be dependent are the leading edge incidence angle, throat blockage, diffuser throat Mach number, and the Reynolds number.

2.5.1 Divergence Angle

Extensive analysis of two dimensional straight channel diffusers has been done by Kline et al. (1959,1978), Carlson et al. (1967), Reneau et al. (1967) and Runstadler et al. (1969, 1973). It was found that at a small divergence angle ($2\theta < 8°$), the flow deceleration is controlled by the geometric area ratio minus the boundary layer blockage. Decreasing the divergence angle results in longer diffusers for constant area ratio. This may result in thicker boundary layers; thus, separation may eventually occur after a large deceleration has taken place in a long diffuser but still result in high pressure recovery. However, with a
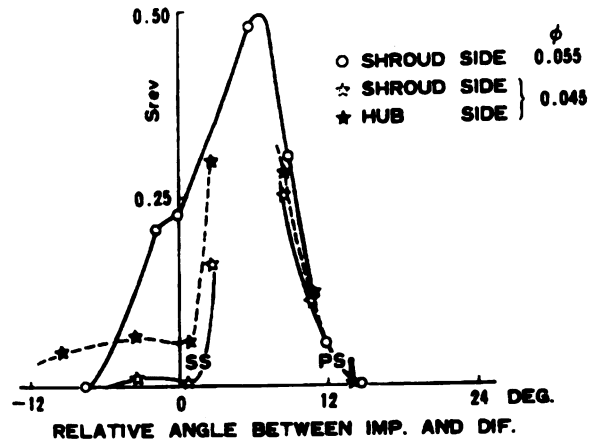
Figure 2.12. The variation in reversed flow strength as function of mass flow rate (Inoue & Cumpsty 1984)
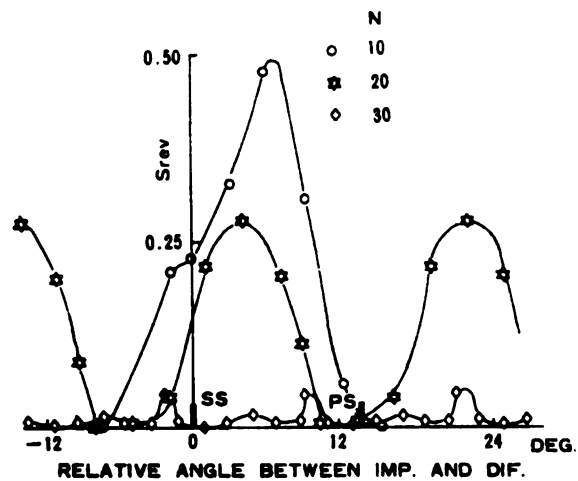
Figure 2.13. The variation of reversed flow strength as function of diffuser vane number (Inoue & Cumpsty 1984)

large divergence angle ($8° < 2\theta < 20°$) separation occurs near the diffuser channel inlet at a small area ratio resulting in much lower pressure recovery, as no diffusion takes place downstream of the separation point.

Reneau et al. (1967) showed that for a diffuser with a length to width ratio (LWR) of approximately 4, maximum pressure recovery was attained with a divergence angle of 12°. Similar results were presented by Clements and Artt (1987) for channel vaned diffusers. They found that a stage with a 12° divergence angle diffuser produced 4% higher peak efficiency than one with 4° divergence angle. It was also found that the pressure recovery increased with an increasing channel divergence angle up to 12°, and any further increase in the divergence angle did not have any significant effect on the pressure recovery (Figure 2.14).
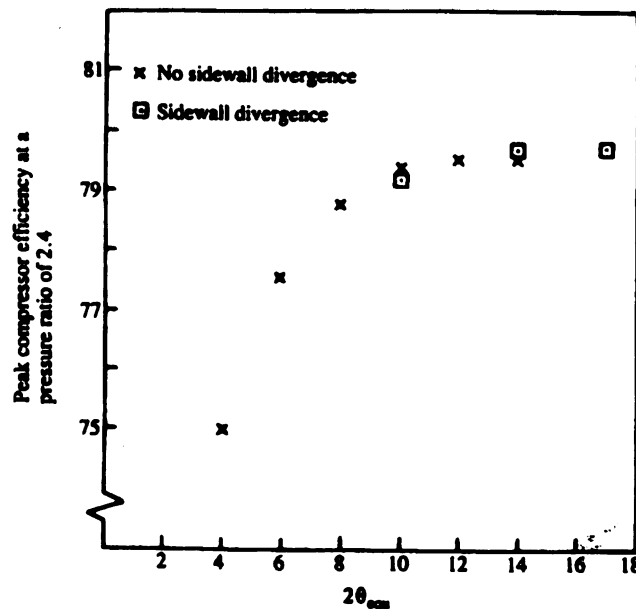
Figure 2.14. Compressor efficiency variation with divergence angle (Clements & Artt 1987)

From Figure 2.15 it is evident that an increase in the divergence angle causes the flow range to decrease. The flow range decreases due to surge at higher mass flow rates. It was also seen that with an increase in the divergence angle, the throat blockage at surge decreased. Thus, the loss of flow range with divergence angle increase can be attributed to the separation of thick boundary layers caused by large adverse pressure gradient.
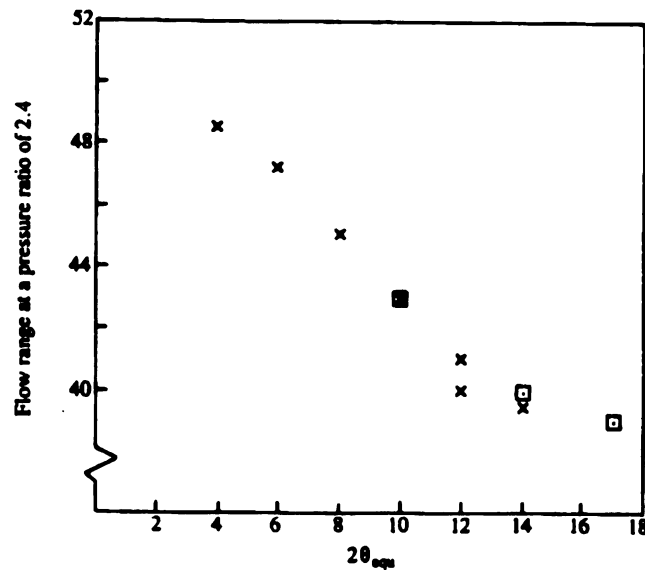
Figure 2.15. Compressor flow range as a function of divergence angle (Clements & Artt 1987)

2.5.2 Length to Width Ratio

Usually maximum diffusion in a straight channel diffuser occurs in long diffusers (LWR = 15) with small opening angle ($2\theta = 8°$) and in short diffusers (LWR = 4) with large opening angle ($2\theta = 20°$). Moreover, the static pressure rise increases with the diffuser length until the friction losses become more important and boundary layer growth prevents any further deceleration of the flow.

Clements and Artt (1988) showed that most of the channel pressure rise occurs in the first half of the channel, while the latter half of the channel contributes only a small portion of the pressure recovery (Figure 2.16). They also showed that similar pressure
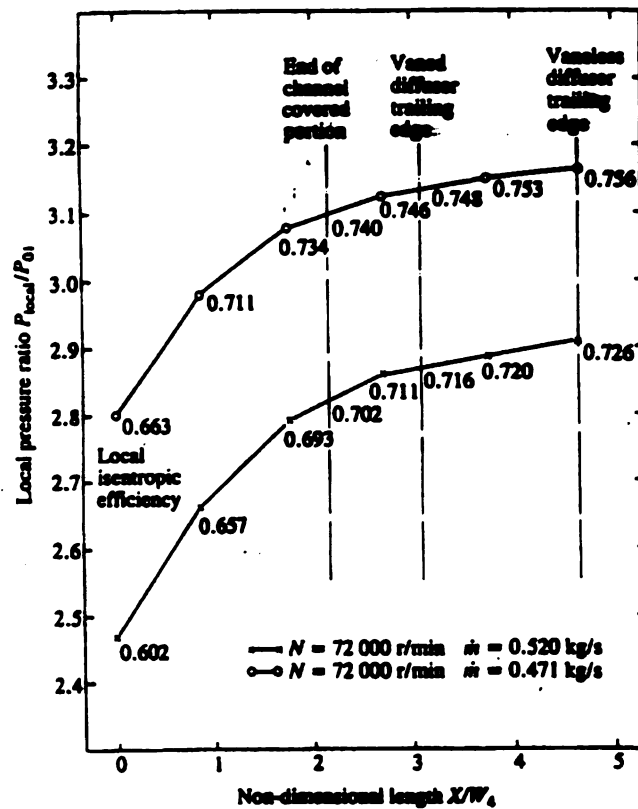
Figure 2.16. Pressure rise through the vaned diffuser (Clements & Artt 1988)

recovery could be attained by reducing the channel length and replacing it with a downstream vaneless space. Thus indicating clearly that there is optimum value of length to width ratio beyond which performance improvements are small. The low pressure recovery in the latter part of the channel is caused by unstable boundary layers whose resultant blockage prevents any further effective area increase. A factor that could contribute to channel boundary layers becoming unstable is the relatively high levels of throat blockage, since it is known that a thick boundary layer will separate much earlier than a thin boundary layer. Therefore, as the channel throat blockage increases, the point of separation will move towards the diffuser throat; and, thus, the optimum length to width ratio will decrease.

2.5.3 Area Ratio

Yoshinaga et. al. (1980), by testing 16 different vaned diffuser configurations, showed that as the area ratio of the vaned diffuser became greater than 2.0, the effectiveness and the pressure recovery of the vaned diffuser decreased (Figure 2.17). It can also be seen from Figure 2.17 that the area ratios of vaned diffusers were larger than that of the vaneless diffuser, and the pressure recoveries of the vaned diffusers were higher than those of the vaneless diffuser. Thus, it can be said that for given inlet conditions of the flow there is an optimum area ratio beyond which the diffuser effectiveness does not show any improvement. This can be explained, as the area ratio of the diffuser increases either the divergence angle or the length to width ratio increases. It is known that as the divergence angle increases, the vanes become highly loaded and the flow separates, which causes deterioration of the pressure recovery. On the other hand when the length to width ratio is increased, the boundary layers become thick and effectively reduce the area ratio, causing no significant gain in the pressure recovery.
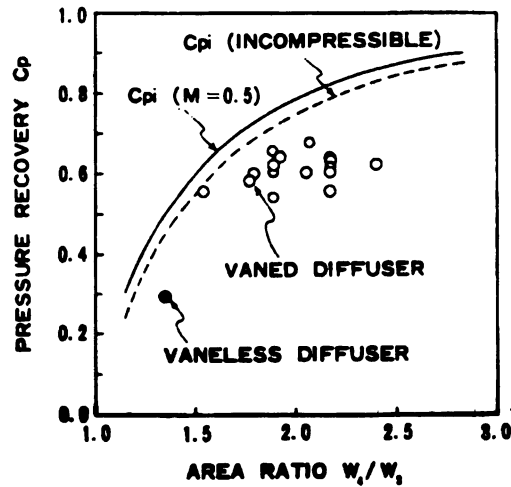
Figure 2.17. Pressure recovery of vaneless and vaned diffusers versus area ratio (Yoshinaga et al. 1980)

2.5.4 Passage Height/Width

The efficiency of the stage can be improved by reducing the passage height of the vaned diffuser, as shown by Stein and Rautenberg (1985). Figure 2.18 shows that with a narrower (b_3/d_3 = 0.0469) vaned diffuser, the efficiency increase is almost 4% more than the wider (b_3/d_3 = 0.0521) vaned diffuser. At the same time, reducing the passage height/width causes the shift in choke flow to lower mass flow rate. Also, the overall flow range of the compressor is decreased. The increase in efficiency and the decrease in flow range are more pronounced at higher shaft speeds than at lower speeds with narrow passage. There is a considerable variation in flow angle over the passage height/width (hub to shroud) at the impeller outlet, reduction of the passage height at high speeds has an equalization effect on the flow angle, which leads to improved flow conditions at the entrance to the vaned diffuser. Reducing the passage height/width seems to be favorable for good matching between the compressor components. Also by reducing the passage

height/width, one can push the surge point of a compressor with a vaned diffuser to be same as that with a vaneless diffuser.

- - - - - wide diffuser
————— narrow diffuser
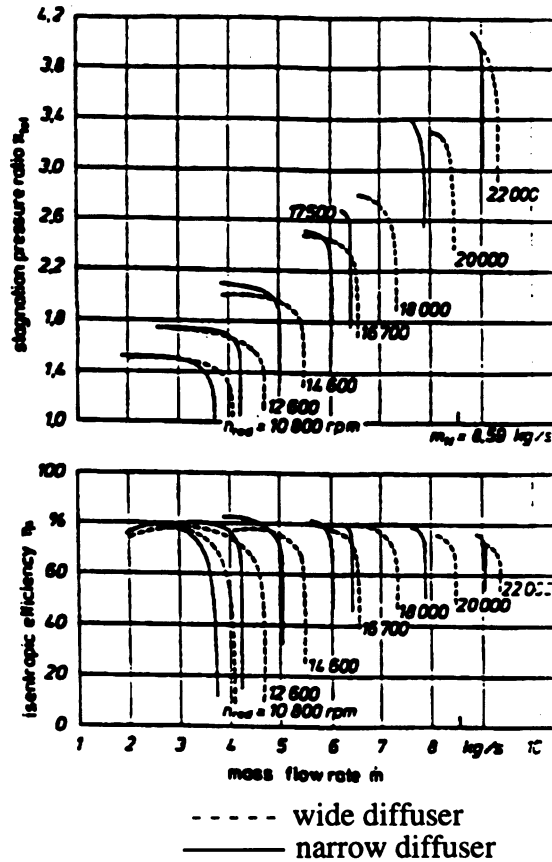
Figure 2.18. Effect of diffuser passage height (Stein & Rautenberg 1985)

2.5.5 Radius Ratio (R_i)

It has been shown by many investigators that the flow coming out of the impeller is highly distorted and has a jet-wake characteristic. It is understood that as the flow moves out into the vaneless space. The jet-wake flow mixes out with the increase in radius and provides a substantial uniform flow to enter the vaned diffuser. At the same time if the radius ratio is big, it will cause boundary layer growth which can possibly reduce the

pressure recovery. Jiang and Yang (1982) showed the effect of radial distance between the impeller exit and vaned leading edge on the blower stage efficiency. A 4% increase in efficiency was achieved by relocating the leading edge of the vanes from a radius ratio of 1.1 to a value of 1.2 (Figure 2.19). It was also seen that better mixing of circumferential distortions was achieved as the radius ratio increased from 1.05 to 1.2. These results are in agreement with those observed by Eckardt (1978). Figure 2.20 shows the relation of the total pressure loss coefficient versus the blade angle with the radius ratio as a parameter. This curve shows that the vane leading edge should be located at a radius ratio of 1.15 to 1.2 for optimum pressure recovery.
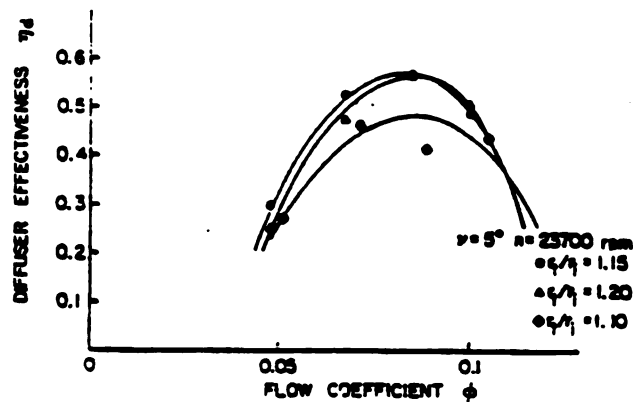
Figure 2.19. Diffuser effectiveness vs. flow coefficient as function of radius ratio (Jiang & Yang 1982)

2.5.6 Vane Profile

Bammert et. al. (1983) studied the effect of the diffuser vane shape or profile on the performance of the compressor stage. They tested three different vane shapes: cambered vanes, straight channel vanes and twisted vanes. It was seen that the performance maps of the stage equipped with a twisted diffuser were shifted towards higher mass flow rates as
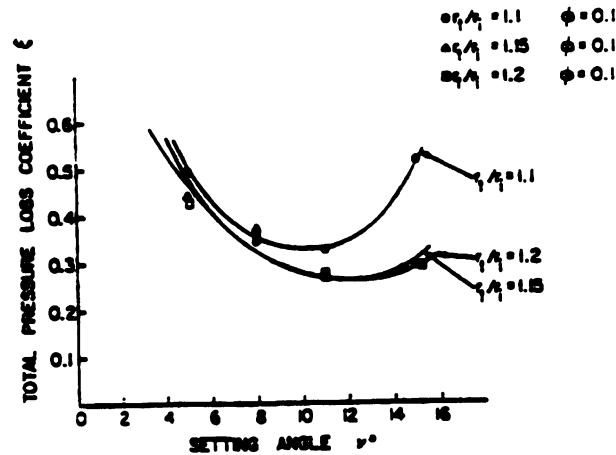
Figure 2.20. Total pressure loss coefficient vs. vane setting angle with radius ratio as parameter (Jiang & Yang 1982)

compared to the cambered vane and the straight channel diffuser, in particular at the low speed range. It was also found that the stage with twisted diffuser generally reached better efficiencies. The improvement in efficiency at low speed range was about 4% higher than the cambered vane diffuser and 3% higher than the straight channel diffuser. At higher speeds the stage with twisted vanes diffuser had wider operating range than the other two.

Figure 2.21 shows the pressure recovery of the three types of vaned diffusers. It can be seen clearly that the twisted diffuser and the straight channel diffuser achieve better pressure recovery than the cambered vane diffuser.

2.5.7 Vane Leading edge Shape

An investigation of the effect of the leading edge shapes of the vanes on the diffuser performance was performed by Yoshinaga et. al. (1980). Two different vane shapes were tried in order to match the vane inlet angle with the flow angle across the vane height. It was seen that in one case the stage efficiency decreased, and in the other case the stage efficiency increased by more than 0.5% compared to its original stage at the design point.
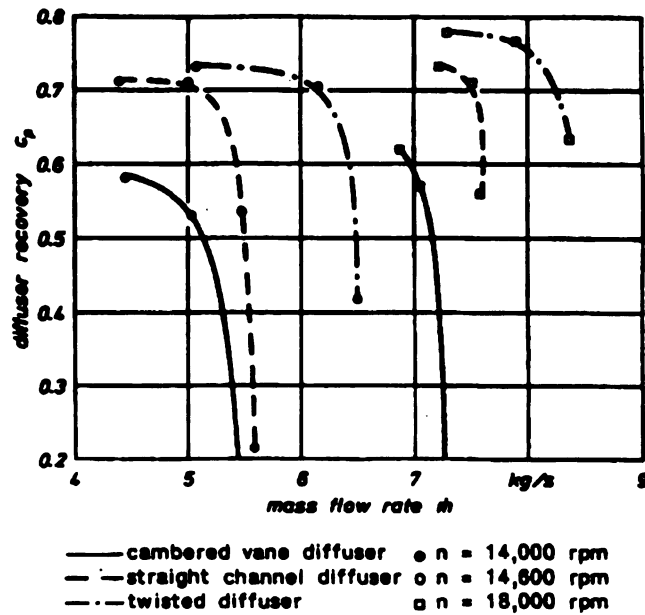
Figure 2.21. Diffuser pressure recovery for different vane profiles (Bammert et al. 1983)

The shape of the leading edge is given in Figure 2.22 and the performance comparison of the original stage and the new stages with modified vane shape is given in Figure 2.23. it is very evident that the leading edge shape of the vane have considerable influence on the performance of the diffusers.

2.5.8 Vane Number

Dean (1974) indicates that the number of vanes employed in a vane island diffuser can vary between 8 and 60. Rodgers (1982) performed tests with varying vane numbers with constant throat area, and he found that the changes in flow range (choke to surge) were minor and that the overall pressure recovery depended on the covered passage performance. Figure 2.24 shows the stage performance comparison of a high efficiency, low pressure ratio stage with 13 and 21 vane channel diffusers with the same throat area,
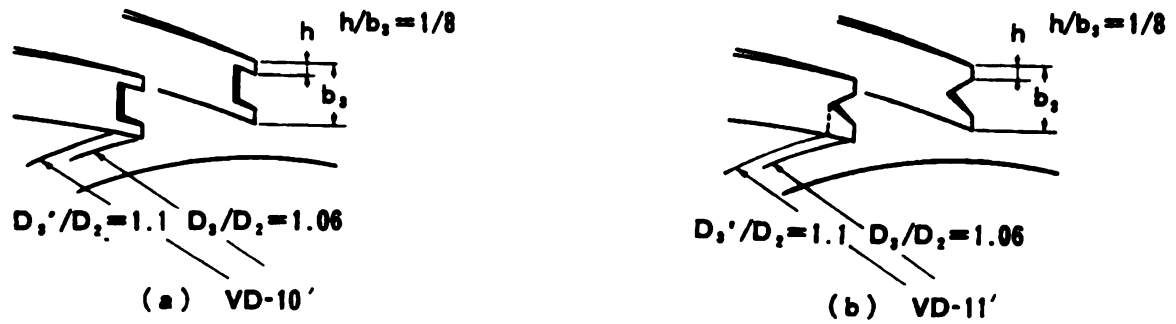
Figure 2.22. Modified vane leading edge shapes (Yoshinaga et al. 1980)
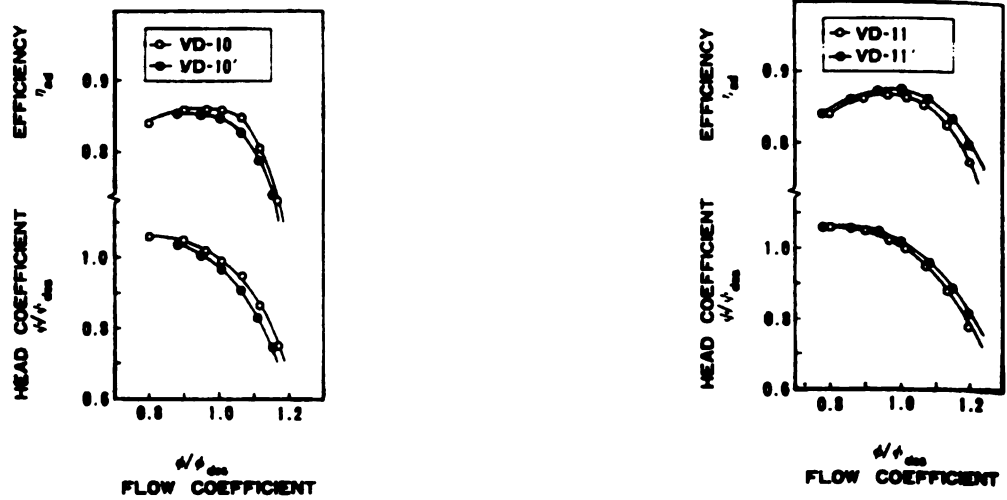
Figure 2.23. Effect of leading edge shapes of vanes on the stage efficiency (Yoshinaga et al. 1980)

O 13 VANES
● 21 VANES
THROAT AREA 22.8 SQ IN.
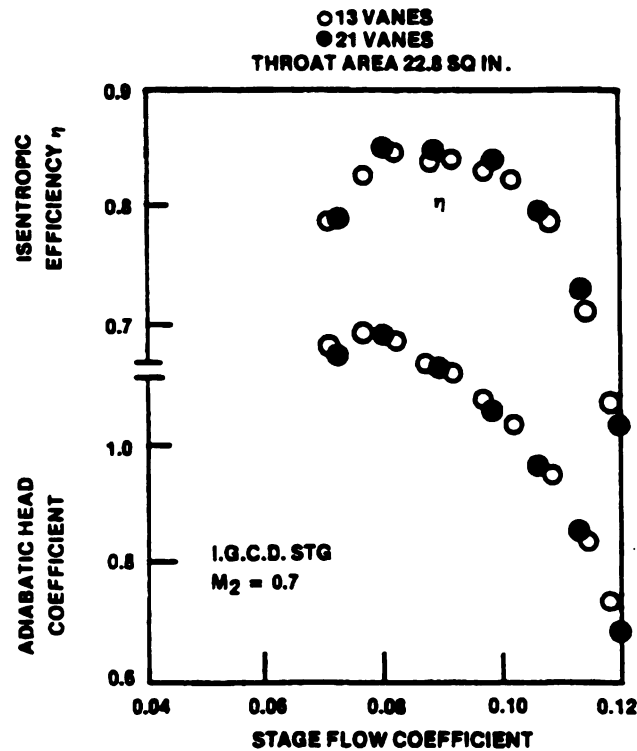
Figure 2.24. Effect of diffuser vane number (Rodgers 1982)

and it can be seen that stage performance is virtually unchanged. Thus, vane number does not seem to have a great effect on the performance of the vaned diffuser as long as the throat area is maintained constant.

Yoshinaga et al. (1980) performed an experimental analysis of the cord/pitch ratio of the vaned diffusers by varying the number of vanes up to a maximum of 27 and the inlet to exit radius ratio in the range of 1.5 to 3.3. They observed that the critical diffusion ratio for the 17 diffusers tested was 0.5 and peak pressure recovery of the vaned diffuser was attained when the length to width ratio was around 5.5 and the area ratio was around 2. These are smaller values than the two-dimensional diffusers, however the optimum divergence angle was 10° which agrees well with the two-dimensional diffusers.

Thus, the selection of the vane number should be based on the effects of the incidence needed for maximum flow range and the possible vibrational problems that could be encountered due to the impeller and diffuser vane interaction. Moreover, the vane number selected should provide optimum values for the other principal dimensions such as the LWR, area ratio and divergence angle.

2.5.9 Diffuser Arrangement

Pampreen (1972) performed tests on conventional vaned diffusers and tandem cascade vaned diffusers. He observed that the diffuser exit Mach number with the tandem arrangement was lower than the conventional diffuser. Also, the stall free range of the tandem diffuser was much larger than that of the conventional diffuser. Moreover, the minimum loss of the cascade diffuser was about 10% less than that of the conventional diffuser. In a tandem diffuser the first row, with low camber vane section, acts to reduce the Mach number and provides a wide range of stall free operation. The flow angle at the exit of the first row changes very little; thus, the vane angle of the second vane row can be set for minimum loss since there is no demand upon its stall margin. The slit between the two rows of vanes helps in moving the low momentum flow from the suction surface of the vanes of first row into the main flow by the high momentum flow of pressure surface. Therefore, cascade diffusers give a smaller overall size than the conventional diffusers for given inlet and exit conditions of the diffuser.

2.5.10 Throat Blockage

The flow range of the centrifugal compressor is known to be limited by stall and choke of the vaned diffuser. The choke flow rate not only depends on the throat area but also on the blockage factor at the throat. Kenny (1979) correlated the blockage at the throat

to the pressure rise from the leading edge to the throat of the vaned diffusers as shown in Figure 2.25 and showed that the blockage could be predicted by the boundary layer analysis. He showed that the level of blockage is also a function of the diffuser blade angle and/or the number of vanes. Conrad et al. (1980) also showed that larger vane setting angles resulted in larger throat blockage, which may be due to the longer flow path. Kenny (1972) showed that the limiting static pressure rise coefficient in vaned diffusers was about 0.4 for subsonic flows and higher for supersonic flows because of the additional pressure rise over the shock. In addition to this he also found that the static pressure rise of the diffuser was influenced by the incidence and the shape of the vane suction surface.
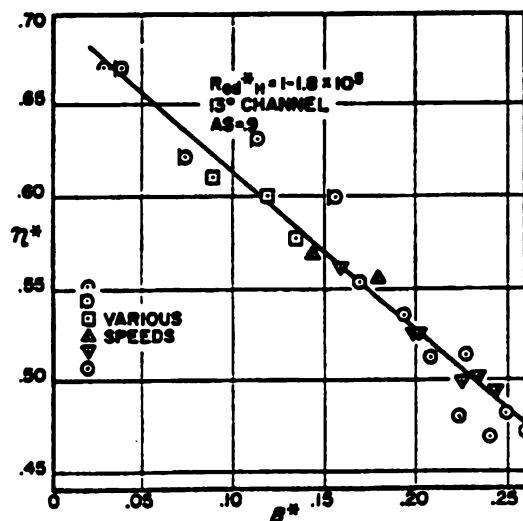
Figure 2.25. Cambered vane diffuser throat blockage as a function of static pressure rise leading edge to throat (Kenny 1979)

2.5.11 Incidence Angle (i)

The incidence relative to the vane suction surface is a significant parameter for determining the flow range of a centrifugal compressor with vaned diffuser. For wedge

type of vanes, if the divergence angle of the channel is kept constant and the number of vanes is reduced; the wedge or vane angle increases for a given blade or stagger angle, which causes the direction of the suction surface of the vane to become closer to the tangential direction. Thus, since the incidence angle is one of the main parameters for stall, the flow range of vaned diffuser is increased as the number of vanes are reduced.

Reeves (1977) correlated the flow range of pipe diffusers of compressors to the diffuser leading edge Mach number and the incidence angle. Figure 2.26 shows the effect of diffuser leading edge incidence and diffuser inlet Mach number. It is clear that the flow
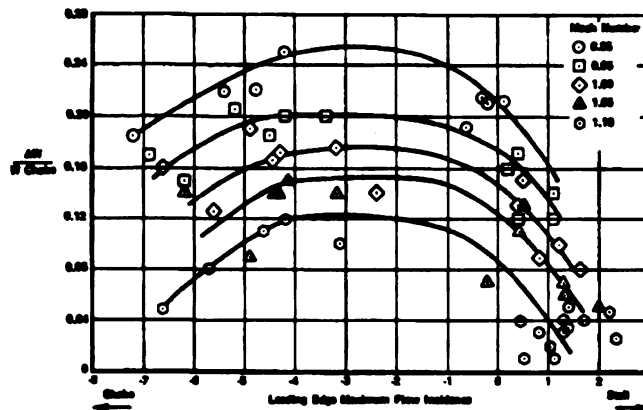
Figure 2.26. Effect of diffuser leading edge Mach number and incidence angle on range (Reeves 1977)

range varies considerably depending on the leading edge incidence angle at the choke flow. Kenny (1979) showed that minimum throat blockage occurs at - 4° negative incidence at the vane suction side leading edge and increases with increasing incidence (Figure 2.27).
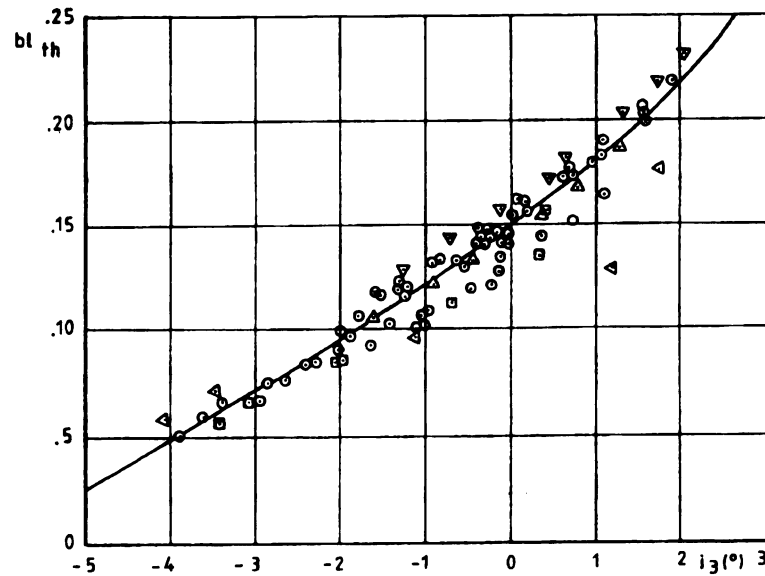
Figure 2.27. Diffuser throat blockage vs. incidence (Kenny 1979)

2.6 Status of Low Solidity Vaned Diffuser Research

The first reference to an LSVD was in a Japanese patent by Senoo (1978). In the patent, Senoo characterizes the vanes by a solidity of less than 0.9 and introduces both single and tandem row LSVDs. It also suggests that the centrifugal stage had better performance with LSVD than with the vaneless diffuser without any loss of flow range. Since then Senoo has presented a series of papers that give the details of LSVD performance.

Senoo et al. (1983) presented and discussed the results for both single and tandem row LSVDs installed in a centrifugal blower. They used USA 35B airfoil shape for the vanes by conformally mapping into a circular cascade. The single row LSVD tested had 11 blades with 0.69 solidity. The tests with this LSVD were performed with two different stagger angles of 70° and 68°. In addition, another single row LSVD with 13 vanes and 0.82 solidity was also tested. In the case of the two row tandem cascade LSVD, the first row had a solidity of 0.345 with 11 blades, and the second row had a solidity of 0.63. The

tests were performed for various combinations of vane setting or stagger angles and radius ratios between the two rows to arrive at the peak recovery in the diffuser.

The results of LSVD tests showed dramatic improvements in pressure recovery with respect to vaneless diffuser, specially near surge flow. Most importantly, they found almost no reduction in flow range with LSVDs. Near surge, the tandem cascade configurations offered a much smaller additional increase in Cp, but the improvement at high flows was nearly double that of the single row LSVDs. Further they observed that the variation in stagger angle and solidity had a small effect on the performance with relatively minor changes in surge location. The oil film patterns of the single row cascade showed strong secondary flows along the sidewalls indicating the vane suction surface boundary layers were sucked and moved towards the pressure surface of the adjacent vane. Thus, delaying the boundary layer separation on the suction surface. From the oil film patterns of two row tandem cascade it was found that the slit between the two rows redirected the accumulated boundary layer on the first row pressure surface in to the main flow, allowing new boundary layers to form on the rear row.

Senoo (1984) summarized the effect of solidity, vane number, and stagger angle on the performance of the LSVD and emphasized the need to positively use secondary flow to obtain enhanced diffuser performance. In addition to the data presented in his 1983 paper, new data for a 22 vane LSVD with the same solidity and stagger angle as for the 11 vane configuration as well as an 11 vane design with 0.82 solidity was included.

The peak Cp values were nearly same for 11 and 22 vane configurations, but the peak efficiency point was at about 20% to 25% higher flow for 22 vanes, and there was no noticeable change in surge line location with the vane number. However, the Cp drop from peak to surge was more rapid in case of 22 vane LSVD. With the increase in solidity, the peak Cp attained was lowered and moved to higher flow rate. Moreover the surge occurred at about 20% higher flow rate for LSVD with solidity of 0.82. Similar trends were

exhibited as the stagger angle increased. The peak Cp fell a small amount, and its location moved to about 35% higher flow rate.

Kanek and Ohashi (1982) used LSVD and attained better performance than the vaneless diffuser without any change in flow range. The efficiency increase was about 4% at design flow and 2% at surge flow. They suggested that LSVDs were more suited to low specific speed applications, as LSVDs increase the flow angle and reduce the flow path length and hence, the friction effects.

Osborne and Sorokes (1988) used single row LSVDs with single and multistage compressors having radial and mixed flow impellers, along with a wide range of specific speeds and various sizes and gases. From their tests it was concluded that LSVDs were successful with respect to efficiency and flow range even at high and medium specific speeds. They also showed that attractive performance gains resulted with simple flat plate vanes and for geometric parameters (such as vane number and vane setting radius ratios) which were beyond Senoo's study. However the solidity of 0.69 was retained for almost all configurations tested, and the stagger angles were maintained relatively high.

Hayami et al. (1990) showed, the LSVD with 0.69 solidity performed better than the vaneless diffuser of a transonic centrifugal compressor. The vanes were conformally transformed from linear cascade of double circular arc vanes. The LSVD also demonstrated good pressure recovery over a wide range of inflow angles, and the pressure recovery improved with increase in the inlet Mach number of up to 1.1. They also found that the LSVD had maximum pressure recovery at an incidence angle of -2° to -3°.

Sorokes and Welch (1991, 1992) developed a rotatable LSVD system, which was used to study the effect of stagger angle. In addition to stagger angle they also studied the effect of vane leading edge radius ratio (by placing the vanes at both 1.08 and 1.15 radius ratio) and the effect of chord length of the vanes by using small and many (S/M) and large and few (L/F) arrangements of the LSVD. All LSVD arrangements tested had 0.735 solidity.

They observed that the best efficiency point, head rise to surge, stability range, and choke margin all exhibit strong sensitivity to stagger angle. The overload capacity displayed a marked decrease as the stagger angle was increased. The factors contributing to this effects were, flow separation from the pressure surface of the vanes, and at high stagger angles the distance between two vanes at the trailing edge decreased tending to form a throat. On the other hand when the stagger angle was decreased, the LSVD vanes stalled, reducing the surge margin. It was also observed that the decrease in surge margin was significant even for small decrease in stagger angle.

In a comparative study of the vane leading edge radius ratio and the S/M and L/F arrangements, they found that the 1.08 L/F build had the highest pressure recovery. While the 1.15 L/F build exhibited advantage over the 1.08 L/F build in terms of surge margin, both the 1.08 and 1.15 S/M arrangements had better stall margin than their respective L/F counterparts. Thus, the 1.08 L/F build had greater sensitivity to off design incidence, even though its pressure recovery was better than the other builds. They also observed that the length and/or exit angle of the LSVD vanes had influence on the downstream components. Camatti et al. (1995) also showed similar effects of vane number and vane leading edge radius ratio.

Hohlweg et al. (1993) performed experiments on a process compressor and an air compressor with LSVDs. The LSVD used with the process compressor had 10 vanes with 0.7 solidity, while three LSVDs were tested with an air compressor, all having 16 vanes and 0.7 solidity but different design incidence of -4.1°, -1.9° and +0.3°.

In their results they found that the LSVD with highest negative incidence provided maximum flow range, while the LSVD with +0.3° incidence had small flow range and the stage efficiency was less than the other two LSVDs. However, the LSVD with -1.9° incidence had better stage peak efficiency than the one with -4.1°. Thus, they concluded that negative design incidence in general was good for LSVD performance and there should

be an optimum negative incidence based on the impeller tip Mach number that would provide both good flow range and efficiency.

From the results of low Mach number process compressor testing, they observed that the LSVD had almost the same peak efficiency as the conventional vaned diffuser, but the flow range of LSVD was considerably lower than the conventional vaned diffuser. They speculated from this observation that the low vane number might have allowed large stall cells to develop due to low flow angles at the vane leading edge, even though the design incidence of the LSVD was -3.1°.

Thus, from the review of these reports it can be said that there is no clear understanding of the effect of the vane number and solidity of the LSVD, which seem to be two major parameters in the LSVD design. However, there seems to be general agreement that LSVD, like conventional vaned diffusers, performs better with negative design incidence. Moreover, the effect of vane number and vane leading edge radius ratio on the impeller discharge flow is not clearly understood in the case of the LSVD, as some of the reports indicate that the LSVDs with small vane leading edge radius ratios performed better, which is not the case in conventional vaned diffusers.

3. NUMERICAL PREDICTION OF FLOW IN LOW SOLIDITY VANED DIFFUSERS

In order to develop a successful design procedure and performance prediction method for low solidity vaned diffusers (LSVD), it is very important to have detailed knowledge of the flow behavior in the diffuser. Thus, the flow field in a LSVD is numerically studied to define the design parameters affecting the performance, using a 3-D viscous code.

The diffusers used by Hohlweg et al. (1993) were modeled for numerical analysis of the flow field at various operating flow points. The design parameters such as incidence, blade turning angle and solidity, affecting the performance of the LSVD were varied and their effect on the flow behavior in the diffuser was studied in an attempt to understand the flow physics in LSVD near surge flows.

This chapter briefly explains the 3-D viscous code used for numerical analysis along with the results. The experimental results of the LSVDs used by Hohlweg et al. (1993) are reviewed and qualitatively compared with the numerical analysis results. The effects of some of the design parameters on the flow phenomena in LSVD are discussed; they are based on the numerical experimentation done on the corresponding parameters. Finally, the details of the new LSVD designs for experimental analysis are presented.

3.1 Experimental Results and Flow Points for Numerical Analysis

The experiments were carried out on two separate compressor test arrangements. One of the test stands was a process compressor with radial inlet and return channel

47

discharge, working on N_2 in a permanent closed loop. The other test stand was a standard production type air compressor with axial inlet and volute discharge. Details of the test stand, the measurements made, and the design parameters used for the vaned diffuser and LSVD are presented by Hohlweg et. al. (1993) along with the performance curves.

The process compressor was tested at two different speeds of $M_t = 0.53$ and $M_t = 0.70$ with one LSVD. The LSVD had $Z = 10$, $\sigma = 0.7$ and $i_d = -3.1^\circ$ (LSD10) at $M_t = 0.7$, the performance maps are shown in Figure 3.1. It can be seen from the performance curves that the efficiency of the LSVD is quite good compared to the conventional vaned diffuser and the vaneless diffuser from maximum flow to design flow; then it drops from design to the surge flow. It can be seen from the head curves that at $M_t = 0.70$ the head drops sharply for LSVD after the design flow indicating a definite diffuser stall, whereas in case of $M_t = 0.53$ the head curve tends to flatten out after the design flow. The performance curves also

(a) $M_t = 0.53$ (b) $M_t = 0.7$
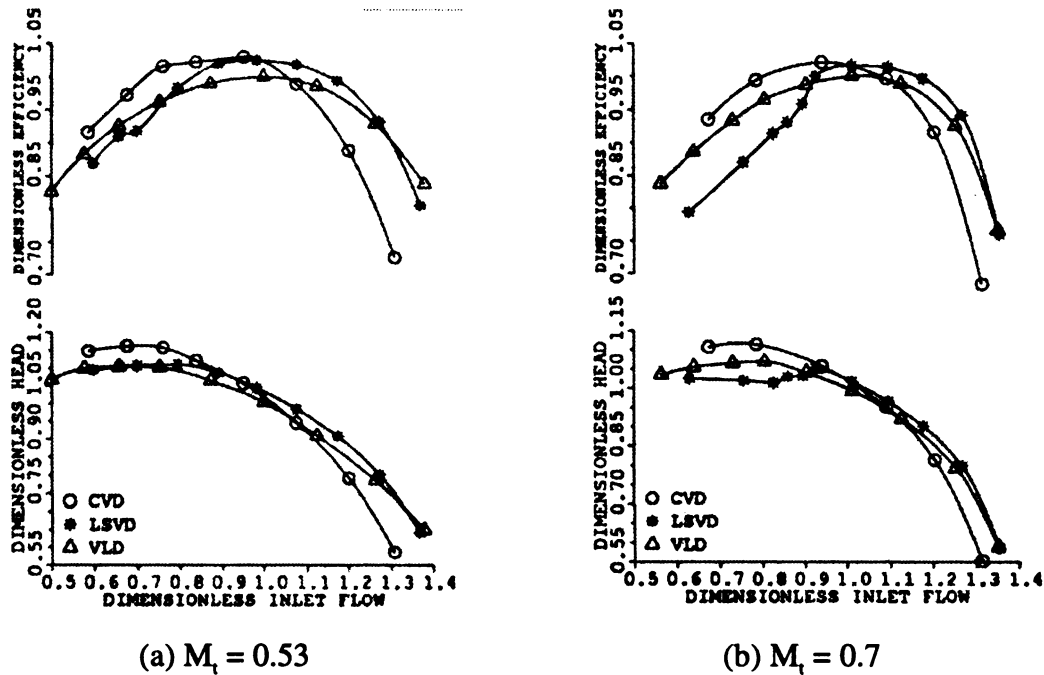
CVD - Conventional Vaned Diffuser, LSVD - Low Solidity Vaned Diffuser,
VLD - Vaneless Diffuser

Figure 3.1. Performance maps of process compressor with LSD10

(Hohlweg et al. 1993)
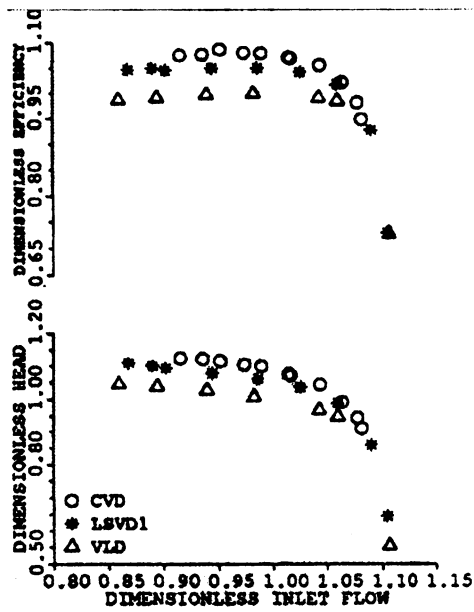
(a) LSD1
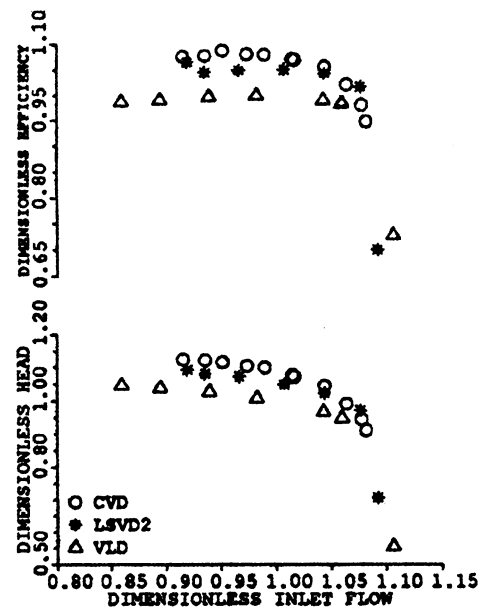
(b) LSD2
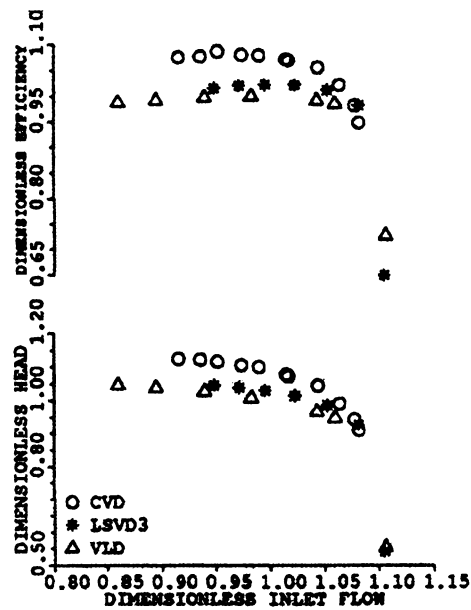
(c) LSD3

Figure 3.2. Performance maps of the air compressor at $M_t = 1.38$ (Hohlweg et al. 1993)

Table 3-1. Design Parameters of Analyzed LSVDs

Parameters	Process Compressor		Air Compressor				
	LSD10	LSD13	LSD1	LSD2	LSD3	LSD4	LSD5
σ	0.7	0.7	0.7	0.7	0.7	0.7	0.6
i_d	-3.1	-3.1	-4.3	-1.9	+0.3	+0.3	-4.3
θ	19.8	15.8	13	12.8	12.6	7.2	17.1
Z	10	13	16	16	16	20	10
b_3/b_2	1.0	1.0	1.0	1.0	1.0	1.0	1.0
r_3/r_2	1.11	1.11	1.10	1.10	1.10	1.10	1.10
r_4/r_3	1.19	1.13	1.11	1.12	1.13	1.06	1.17
Experimental	Yes	No	Yes	Yes	Yes	No	No
Numerical	Yes	Yes	Yes	Yes	Yes	Yes	Yes

show that the useful operating range of the LSD10 was very small at $M_t = 0.70$; where as at $M_t = 0.53$, the surge flow was no better than the conventional vaned diffuser.

The air compressor was tested at a constant speed of $M_t = 1.38$, with three different LSVDs. All three LSVDs had Z = 16 and $\sigma = 0.7$ but different design incidence angles: LSD1 had $i_d = -4.1°$, LSD2 had $i_d = -1.9°$ and LSD3 had $i_d = +0.3°$. The performance maps of all three LSVDs are shown in Figure 3.2. From the performance maps it is clear that LSD3 did not perform well both in terms of efficiency and flow range. On the other hand LSD1 had a flow range almost equal to the vaneless diffuser while LSD2 had better performance at the cost of flow range. Thus indicating that design incidence has a great influence on the performance of the LSVD.

In an attempt to understand these behaviors, the BTOB3D code was used to predict the flow field inside the LSVDs. In the case of LSD10, five tested flow points ranging

from 105% to 80% of design flow rate were analyzed by BTOB3D at both tested speeds of $M_t = 0.7$ and $M_t = 0.53$. An LSVD with 13 vanes (LSD13) was designed keeping the flow parameters exactly same as the LSD10. It was analyzed for the same flows as observed by LSD10 in order to study the effect of the number of blades, blade loading, and turning angle. Similarly, all three LSVDs tested with air compressors were analyzed for flow ranging from design point to the surge flow. Two LSVDs, one based on the design parameters of LSD3 designated as LSD4 and the other on LSD1 (LSD5), were designed to study the effect of blade number or blade loading and the solidity on the flow behavior in the LSVD. Table 3-1. shows the critical design parameters of all LSVDs, that were analyzed with BTOB3D code.

3.2 3D Viscous Code

The 3D viscous code used for flow field analysis was a commercially available BTOB3D program written by Dr. William Dawes (1988, 1991). The BTOB3D code solves the 3D Reynolds averaged Navier-Stokes equations in finite volume form cast in the blade relative frame using cylindrical co-ordinates (r, θ, x)

$$\frac{\partial}{\partial t} \oint_V \overline{U} dV = \oint \overline{H}.dA + \rho \overline{S} \qquad (3.1)$$

where

$$\overline{U} = \begin{bmatrix} \rho \\ \rho V_x \\ r\rho V_\theta \\ \rho V_r \\ \rho E \end{bmatrix} \qquad \overline{H} = \begin{bmatrix} \rho\overline{q} \\ \rho V_x\overline{q} + \tau \hat{i}_x \\ r\rho V_\theta\overline{q} + \tau \hat{i}_\theta \\ \rho V_r\overline{q} + \tau \hat{i}_r \\ \rho I\overline{q} \end{bmatrix} \qquad \overline{S} = \begin{bmatrix} 0 \\ 0 \\ -2\Omega r V_r \\ \dfrac{V_\theta}{r} + r\Omega^2 - 2\Omega V_\theta \\ 0 \end{bmatrix}$$

with

$\overline{q} = V_x \hat{i}_x + V_r \hat{i}_r + V_\theta \hat{i}_\theta$, the relative velocity

Ω = rotational speed

τ = the stress tensor containing both the static pressure and the viscous stresses.

and $\quad I = C_p T_{0rel} - \frac{1}{2}(\Omega r)^2$, the rothalpy.

The system is closed by an equation of state

$$P = \rho(\gamma - 1)\left[E - \frac{1}{2}(\bar{q} \cdot \bar{q} - (\Omega r)^2)\right] \quad (3.2)$$

The effects of the turbulence are modeled with a simple mixing length model. The choice of mixing length turbulence model was based on the computational cost. Since the flows typical of turbomachinery are governed largely by the effects of blockage and any turbulence model which produces enough blockage in the correct parts of the flow passage could be successful, the Baldwin - Lomax (1978) mixing length model was used.

The code automatically applies appropriate boundary conditions at the solid walls and the periodicity conditions upstream and downstream of the blade row. Thus, the boundary conditions needed to calculate the diffuser flow are the inlet and exit static pressure, inlet total pressure and total temperature profile, inlet tangential velocity and meridional velocity profile, and inlet absolute flow angle profile along the span.

The BTOB3D code was used by Dalbert et al (1993) to check the ability of the code to calculate the performance of vane diffusers and to investigate possibilities of representing the results for a better understanding of flow phenomenon. They concluded that the computed pressure distributions showed a good qualitative agreement to the measured results. They also showed that the flow visualization using the code results compared well with the experimental flow visualization, thus showing the ability of BTOB3D code to qualitatively analyze the flow behavior inside the vaned diffusers.

There have been many other reports like Sorokes (1993), Casey et al. (1992), and Drtina et al. (1993) where BTOB3D code was used for optimizing the designs of the impellers and diffusers. These reports have clearly shown that the code is capable of

predicting the flow inside the turbomachinery components. Based on these encouraging reports, BTOB3D was chosen for analyzing the flow physics in LSVD.

3.3 Computational Grid and Boundary Conditions

In order to validate the ability of the BTOB3D code, the geometry of the experimentally tested LSVDs used with the process and air compressors of Hohlweg et al. (1993) were initially modeled for analysis with the BTOB3D code. In the second stage of the present study, several new configurations of LSVD were modeled by varying the design parameters considered to be affecting the flow in LSVD. The 10 vane LSVD (LSD10) used with the process compressor and a new LSVD configuration with 13 vanes (LSD13) were modeled for BTOB3D analysis with the same upstream vaneless passage length in order to specify the process compressor flow conditions. Similarly, all three LSVDs tested with the air compressor and the new configurations designed for BTOB3D analysis had the same upstream vaneless passage lengths. Thus, the vane leading edge radius was not considered as a variable for the new designs.

In all the models used for analysis by the BTOB3D code, the computational mesh consisted of 25 gridlines in the pitchwise(K) direction, 25 gridlines in the spanwise(J) direction, and between 90 to 103 gridlines in the streamwise(I) direction (Figure 3.3). The streamwise direction gridlines varied because the length of the blade varied as the solidity and number of blades in the diffuser were changed. The number of streamwise gridlines in the upstream and downstream passages of the diffuser were held constant for all models. Since the results obtained were grid independent, no further refinement of the grid was required.

The inlet boundary conditions could be obtained from three sources: 1) from the test traverse data available at the impeller exit, 2) from the output of the BTOB3D code analysis
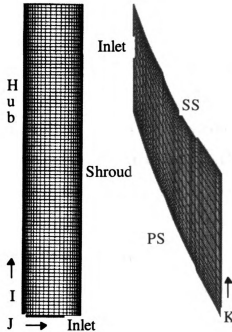
Figure 3.3. Computational Grid

of the process compressor and air compressor impellers or 3) from the output of a quasi one-dimensional stage analysis program. Since the objective of the present study is to understand and analyze the flow fields inside a LSVD, the inlet conditions to the diffusers were specified from the output of the quasi one-dimensional program; such that the inlet velocities, flow angle, and total pressure and total temperature were kept uniform across the span. The reason for this approach was to eliminate any inlet distortion or flow anomaly effects on the BTOB3D code analysis. Since the primary interest was in a qualitative rather than quantitative analysis, a uniform inlet profile provided the simplest possible flow case with which to study the flow behavior within an LSVD. The comparison of the results obtained from the code with the experimental results is justified since the performance predictions obtained from the quasi one-dimensional program of the vaneless and vaned diffuser stages were in good agreement with the corresponding experimental performance

maps. No details of the inlet boundary layer or inlet turbulence levels were specified as input.

BTOB3D code could only perform an analysis of individual components; therefore, one cannot obtain the performance map of the whole stage. This was the reason for not using the results of the BTOB3D analysis of the impeller as inlet boundary conditions for the analysis of the LSVDs, because one cannot compare the results obtained by BTOB3D with the experimental data. Moreover, the BTOB3D impeller tip flow prediction does not include the effect of the diffuser on the impeller exit flow conditions, which would be ultimately needed for accurate input flow conditions.

It would be ideal to use the test traverse data available at the impeller exit as the inlet boundary conditions, but it is known that the traverse data obtained near the surge and stall flows are not very reliable. The traverse probes are simple 2D, 3 hole probes that would not achieve a high level of accuracy near stall and surge. Also, to obtain the boundary conditions at the first streamwise gridline, one has to extrapolate the test data from the probe location radius to the first streamwise gridline radius by using some assumptions based on either the flow angles or the conservation of angular momentum. The preliminary analysis done by code showed similar flow fields in the LSVD at the design flow with both test traverse data as inlet boundary conditions and the uniform boundary conditions obtained by quasi one-dimensional performance prediction program. Although, the flow in the upstream vaneless space showed the effects of jet and wake coming out of the impeller blade channel when test traverse data was used as inlet boundary conditions. Thus, using uniform inlet conditions seemed appropriate for the present study, which is a more qualitative analysis than a quantitative prediction method.

The diffuser exit static pressure was varied until the mass flow coming out of the modeled diffuser matched with the mass flow obtained during the experimental testing. This was the criterion used for establishing a valid BTOB3D prediction to compare with corresponding test data. This, by necessity, is an iterative procedure since BTOB3D does

not permit mass flow as an input parameter to the analysis. The convergence conditions imposed on the BTOB3D code were RMS mass error of less than 0.5×10^{-3} and the percentage mass error of less than 5%. Considerably good convergence was attained in 3500 to 4500 time steps for all cases.

3.4 Flow Analysis and Comparisons

3.4.1 Process Compressor LSVD

From the performance curves (Figure 3.1)of the process compressor it can be seen that the efficiency and head follow the expected trend, relative to typical vane diffuser performance

(a)Pressure Surface   (b)Suction Surface   (c)Mid Span
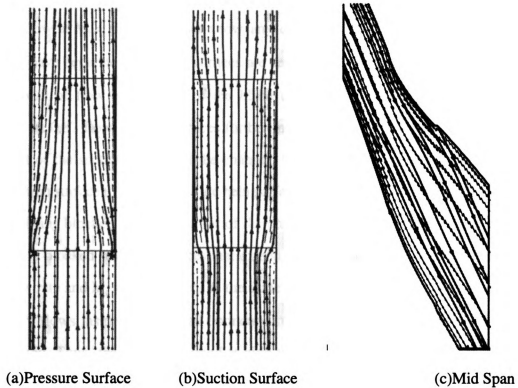
Figure 3.4. Flow patterns at $\phi_0 = 1.05$ of process compressor LSD10

versus vaneless diffuser, at the flow rate of 1.05 which is a flow point between choke flow and design flow. Therefore, one would expect the flow in the blade channel of the LSVD to be without any disturbances. The flow patterns obtained from the code support this, as shown in Figure 3.4. In Figure 3.4 the velocity vectors and the particle traces are shown at the pressure, suction surfaces and at mid span. A small amount of secondary flow seen in the hub to shroud view (Figure 3.4(a) & (b))at the leading edge of the vane indicates that the incidence is not properly matched. Because of low solidity, the vane length in LSVD is small and the vanes are very highly loaded. From this one would expect the flow to separate on the suction surface of the blade channel.

Figure 3.5 shows the flow on the suction surface of the blade at both tested speeds for the flow points of 0.95, 0.9, 0.87 and 0.8. It can be seen that as the flow rate decreases, the flow on the suction surface in general gets worse. At a 0.95 flow rate the secondary flow in the hub and shroud surface boundary layers is observed for $M_t = 0.7$, and the flow at $M_t = 0.53$ does not show any disturbances. The flow on the end walls seems to have separated, and two vortices are seen at 0.90 flow rate in case of $M_t = 0.7$. The amount of flow coming out of the blade channel at the suction surface has been reduced. At 0.87 flow rate the vortices further intensify; and very little flow is allowed to come out of the suction surface of the channel, thus indicating that more and more zones from suction surface to mid channel are being affected by the vortices and flow from these zones is being blocked from getting out of the channel. The flow on the suction surface is completely blocked with the vortices that extend from hub and shroud to the mid span at 0.80 flow rate and $M_t = 0.7$; whereas at the same flow rate and $M_t = 0.5$, we observe some secondary flows inside the end wall boundary layers but only a few xones near the walls are blocked. Thus, the vortices formed at high tip speed may be the cause for the LSVD vanes to stall, which is observed in the experimental results.

Figure 3.6 shows the blade-to-blade view of the flow inside the LSVD blade channel at mid span for different flow rates. It can be noticed that the flow on the suction

(a) $\phi_0 = 0.95$

(b) $\phi_0 = 0.90$

(c) $\phi_0 = 0.87$

(d) $\phi_0 = 0.80$
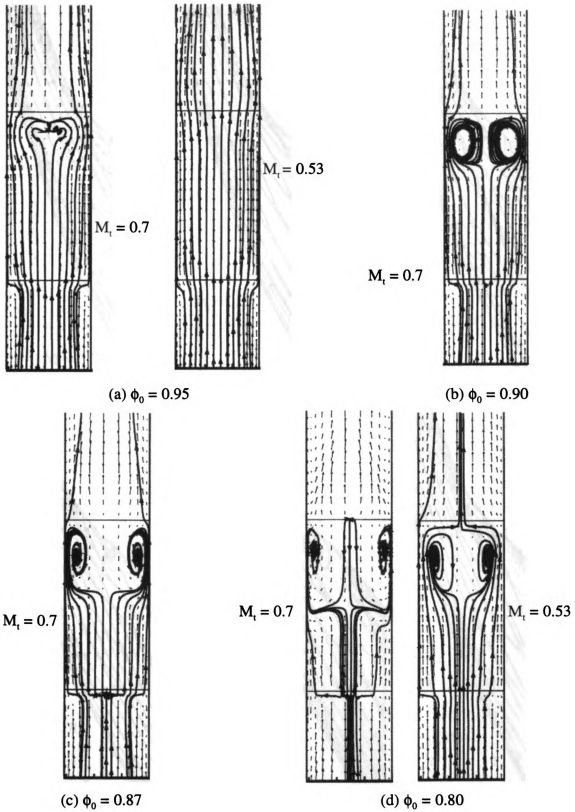
Figure 3.5. Flow on suction surface of LSD10

$M_t = 0.70$

$M_t = 0.53$

(a) $\phi_0 = 0.95$

$M_t = 0.70$

(b) $\phi_0 = 0.90$

$M_t = 0.70$

(c) $\phi_0 = 0.87$

$M_t = 0.70$

$M_t = 0.53$

(d) $\phi_0 = 0.80$
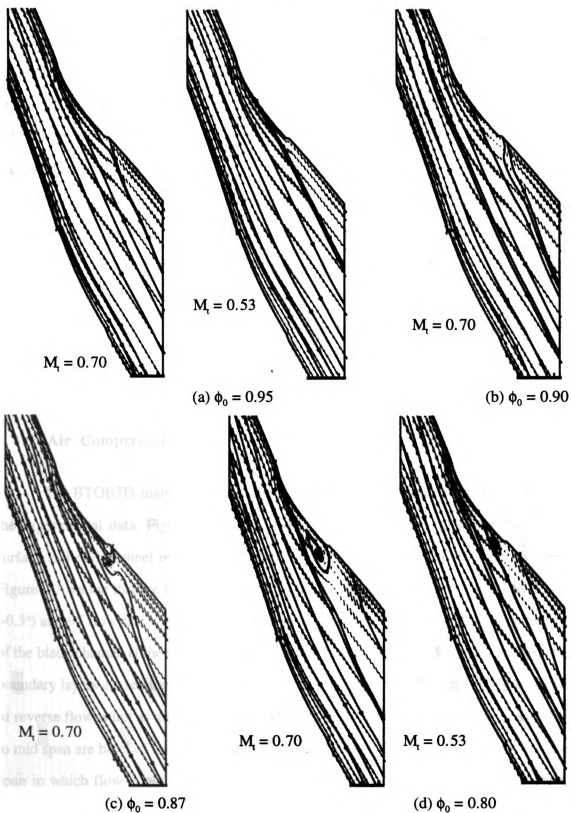
Figure 3.6. Flow at mid span of LSD10

surface is held from separating by the high velocity flow coming from the pressure side of the adjacent blade channel. One can notice a small amount of secondary flow inside the suction surface boundary layer at a 0.90 flow rate. At a 0.80 flow rate, the flow on the suction surface seem to be separated, which further supports the stall of the vanes, it also indicates that the separation on the end walls accompanied by the suction surface separation causes the loss of stability in the LSVD.

The recirculation, which is so evident near the leading edge in the hub to shroud views, does not show up in the blade-to-blade view. The reason for this is that the flow near the leading edge is being disturbed only in the end wall boundary layers. One can also notice symmetry in the flow at all cases, because of the uniform flow distributions used as inlet boundary conditions, such that flow patterns seen on the hub are the same as on the shroud.

3.4.2 Air Compressor LSVDs

The BTOB3D analysis results of the three LSVDs are compared with each other and the experimental data. Figure 3.7 & 3.8 show the velocity vector plots on the suction surface and mid channel respectively of the three LSVDs at different flow points. From Figure 3.7 we see that the flow in the end wall boundary layers is separated in LSD3 (i = +0.3°) at 0.95 flow rate which is the surge flow point (Figure 3.2). No flow is getting out of the blade channel at the suction surface indicating surge. At a 0.95 flow rate the end wall boundary layers are separated and the vortices are developed in LSD2 too, but the amount of reverse flow is not as much as seen in LSD3. Almost all the zones from suction surface to mid span are blocked in LSD3, whereas in case of LSD2 there are some zones near mid span in which flow is not blocked at 0.95 flow rate. At a 0.925 flow rate LSD2 shows flow patterns similar to LSD3 at 0.95 flow rate. 0.925 flow rate was found experimentally
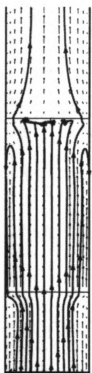
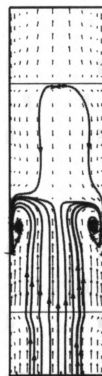LSD1 LSD2 LSD3

(a) $\phi_0 = 1.00$

LSD1 LSD2 LSD3

(b) $\phi_0 = 0.95$ **Contd**.

LSD1   (c) $\phi_0 = 0.925$ LSD2

LSD1   (d) $\phi_0 = 0.80$

Figure 3.7. Flow on suction surface of air compressor LSVDs

LSD1   (c) $\phi_0 = 0.925$ LSD2

LSD1   (d) $\phi_0 = 0.80$
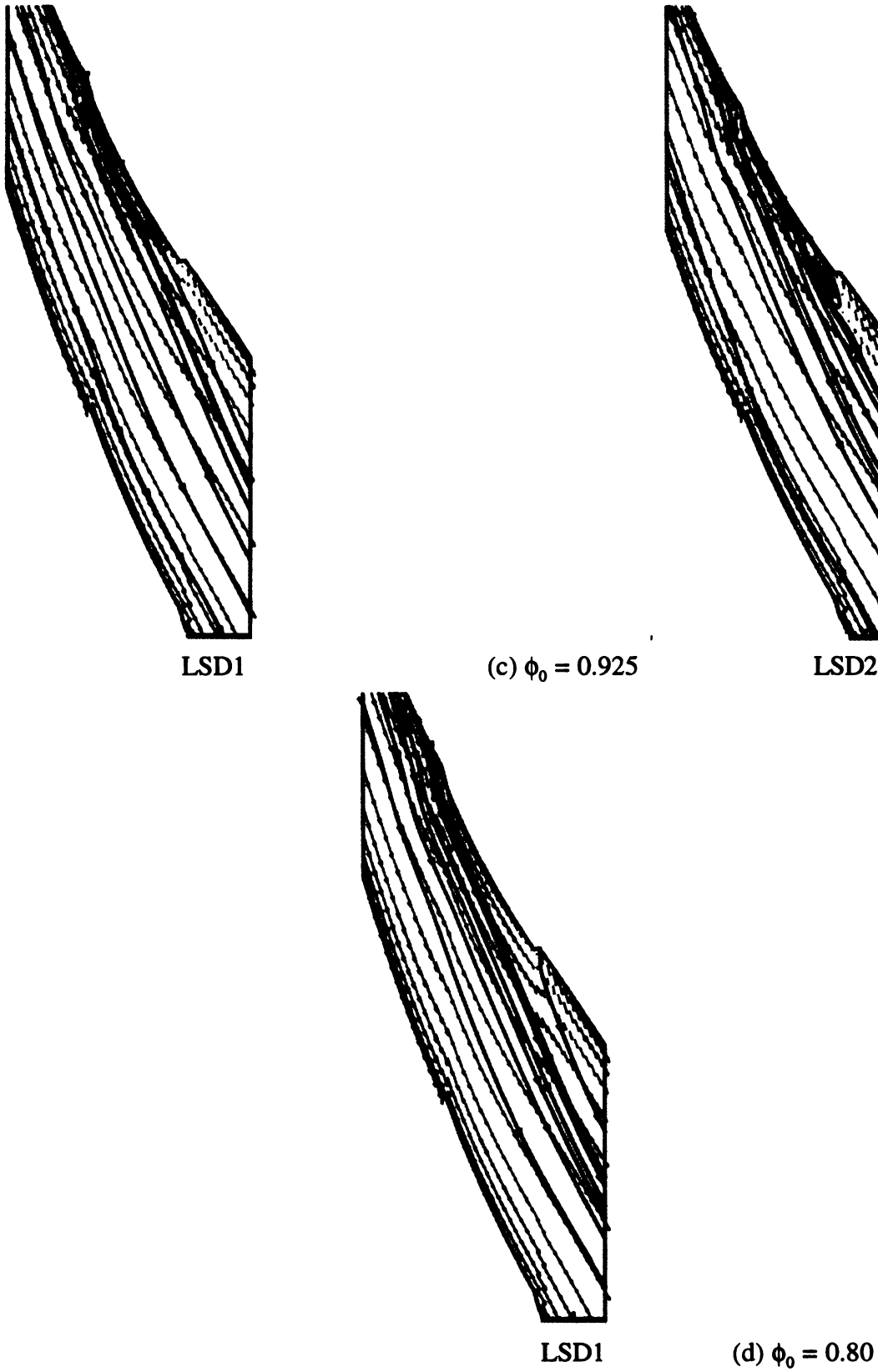
Figure 3.8. Flow at mid span of air compressor LSVDs

to be the surge flow point of the compressor with LSD2. The end wall boundary layers are separated in LSD1 at a 0.86 flow rate, but the separation is not as severe as in LSD3 at a 0.95 flow rate or LSD2 at 0.925 flow rate. This explains why the LSD1 had a larger flow range than LSD2 and LSD3, and almost equal to the vaneless diffuser (Figure 3.2). Therefore, it is possible that even though the flow in LSD1 at 0.86 flow rate is not as highly separated as in LSD3 and LSD2 at their corresponding surge flow points, the surge could have occurred due to some other unsteady phenomenon in the system, such as the inducer stall. Thus, the BTOB3D analysis observations support the experimental results by indicating that the surge at the 0.95 flow rate for LSD3 and at a 0.925 flow rate for LSD2 was caused by the flow separation in the LSVD. The numerical analysis also indicates that incidence angle has a major role in defining the stability and the flow range of the compressor when the LSVD is used downstream of the impeller, supporting the observations made by the experimental tests.

From the velocity vector plots in Figure 3.8 it is observed that the boundary layer on the suction surface of the diffuser vane separates at the experimentally found surge flow points (Figure 3.2). This point is supported by the fact that the end wall boundary layers (Figure 3.7) are separated in LSD2 at 0.95 flow point, but the suction surface boundary layer is not separated because of which the surge occurred at 0.925 flow rate. Similarly in LSD1 at a 0.86 flow rate, the end wall boundary layers are separated; but the suction surface boundary layer is not separated, which further supports the argument that the surge was caused by the unsteady phenomenon in other component(s) of the compressor and not by vane stall in LSD1. Thus, it seems that the LSVD vanes stall when the end wall boundary layers and the suction surface boundary layer are separated at a flow point. A similar conclusion was drawn from the BTOB3D analysis of the process compressor LSVD.

3.5 Parameters Affecting the Flow

3.5.1 Incidence Angle [i = β - α]

Incidence angle has a major role in the performance of the LSVD. Almost all the tests have shown that negative incidence at design, provided better performance with respect to pressure recovery and flow range. It seems that negative incidence is able to keep the flow attached to the suction surface for a longer distance. This is understandable as the flow is directed more towards the suction surface than with positive incidence. At the same time, there is a limit on the amount of negative incidence, as it can force choke to occur at lower mass flow rates. Therefore, while designing LSVDs one should aim for the vaneless diffuser choke flow and thus, investigate for a negative incidence that would retain this choke limit. Maximum negative incidence attainable with the desired choke based on efficiency considerations being fixed by the impeller is what one should target while designing LSVD. More details of incidence selection are presented in section 3.6.

3.5.2 Blade turning angle [θ = β₄ - β₃]

The blade turning angle is representative of the amount of the flow that is turned by the vanes in the LSVD; thus, the higher the blade turning angle, the higher the blade loading. It is known from the conventional vaned diffuser theory that the flow separates from a highly loaded blade. But for most LSVDs reported so far, the amount of blade loading is much higher than the acceptable conventional vaned diffuser blade loading, including the LSVDs discussed in this report. The LSD3 of the air compressor was modified to have 20 vanes with a solidity of 0.7 (LSD4), and it was noticed the flow field was much clearer, as shown in Figure 3.9. Similar results were observed by increasing the number of vanes from 10 to 13 (LSD13) in the case of the process compressor LSVD (Figure 3.10). Reducing the blade loading definitely increases the stability and the flow
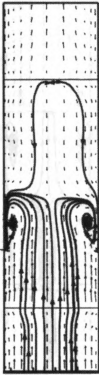
LSD3   Suction Surface   LSD4
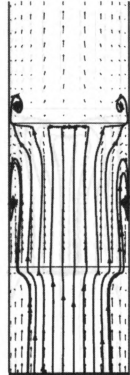
LSD3   Mid Span   LSD4

Figure 3.9. Flow in LSD3 and LSD4 at $\phi_0 = 0.95$
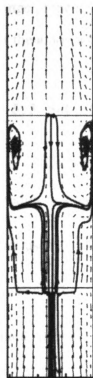
LSD10　　　　　　　Suction Surface　　　　　LSD13
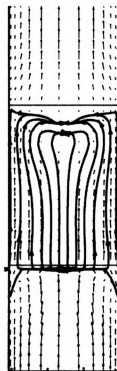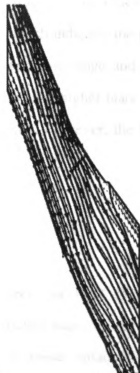
LSD10　　　　　　　　Mid Span　　　　　　LSD13

Figure 3.10. Flow in LSD10 and LSD13 at $\phi_0 = 0.80$

range of the LSVD, but it will also mean that there could be some loss in pressure recovery as the amount of flow turning is reduced.

3.5.3 Solidity [σ]

Currently, there is little or no literature available on the effects of solidity, even though this parameter seems to be a major factor. Senoo defined $\sigma < 0.9$ as low solidity and used $\sigma = 0.69$ in his works. From that point on, every reported work has used the same number. The solidity σ plays a major role in fixing the number of blades (Z) or the blade turning angle (θ) for a given inlet blade angle (β_3) in a design. Figure 3.11 shows the plots of a modified LSD1, which has 10 vanes and $\sigma = 0.6$ (LSD5). The flow in the LSVD blade channel is comparable to that of the experimentally tested LSD1 (16 vanes), but in this case the blade turning is much more than the tested LSD1; which indicates the pressure recovery should be much better for this case, while keeping the flow range and stability same as the tested LSD1. Thus, numerical experimentation shows that higher blade loading or turning is attainable without separation by reducing the solidity. However, the limits of solidity need further investigation.

3.5.4 Blade shape at the trailing edge

From the present BTOB3D code analysis we have seen that most of the flow separation is on the suction surface of the blade and near the trailing edge. To improve the performance and the range, one should look for solutions that would curtail this trailing edge separation. It is well known that flow on a blunt object separates at the trailing edge. The designs of the blades described in this report have very blunt trailing edges. Though
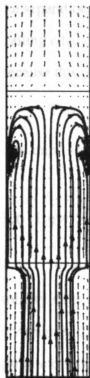
LSD1   Suction Surface   LSD5
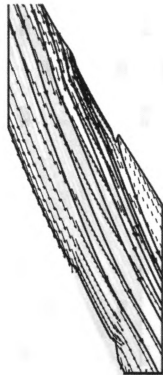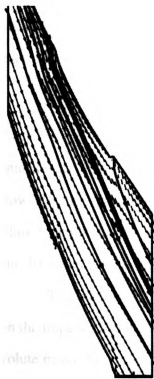

LSD1   Mid Span   LSD5
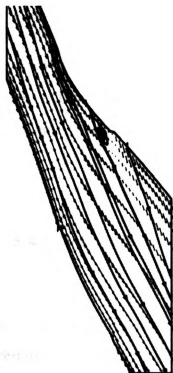
Figure 3.11. Flow in LSD1 and LSD5 at $\phi_0 = 0.80$

the separation at the trailing edge can be postponed a little by having a smooth curve at the trailing edge, its effect on the pressure recovery and the range would not be very significant because this is a very minor change in the geometry of the blade.

Thus, one will have to optimize the LSVD design based on σ, β_3, Z, and θ and then improve it further by changing the blade shape and cascade arrangement.

3.6 Low Solidity Vaned Diffuser Design For Experimental Testing

From the BTOB3D analysis it has been found that the blade turning angle and solidity have great bearing on the flow behavior and performance of the LSVD. In order to investigate the effects observed in the numerical experimentation of LSVD design parameters, four new LSVDs were designed for experimental testing.

All four LSVDs were designed with simple flat plate vanes similar to the approach taken by Hohlweg et al. (1993) and Sorokes and Welch (1991 & 1992). The choice of flat plate vanes was made based on their reported success and inexpensive design and manufacturing.

For a fixed solidity, the blade turning angle (θ), which determines the amount of blade loading of the LSVD vanes, is a function of the number of vanes (Z). The numerical analysis has shown that any increase in the number of vanes manifests into a more stable flow through the diffuser due to the reduction in blade loading or blade turning angle. Thus, to study the effect of blade turning angle on the LSVD performance, LSVDs with 14 and 16 vanes were designed.

The number of vanes were, in part, restricted by the frequency considerations based on the impeller and diffuser vane interaction. Also, on the consideration of the downstream volute matching, so that the vane discharge flow angle matched well with the volute.

Initially, two LSVDs, one with 14 and the other with 16 vanes were designed for 0.7 solidity. The remaining two LSVDs were derived from these two by trimming the

trailing edges of the vanes to obtain a solidity of 0.6. The selection of 0.7 solidity was based on the abundant literature available in the public domain for comparison, while LSVDs with 0.6 solidity were tested to study the effect of solidity on the pressure recovery of the LSVD and to compare the results obtained with the numerical observations of Section 3.5.3.

Many reports that studied the impeller discharge flow have shown that the circumferential distortions of the impeller discharge flow are considerably mixed out by a radius ratio of 1.1. However, the distortions across the width of the diffuser need much longer radial distance for mixing out. Moreover, Sorokes and Welch (1992) have shown that the LSVDs with 1.08 r_3/r_2 ratio had better pressure recovery than the 1.15 vane leading edge radius ratio. Thus, the vane leading edge radius ratio (r_3/r_2) for all four LSVDs was set at 1.09.

The final geometric parameter needed to complete the LSVD design with solidity, vane number, vane leading edge radius fixed is the vane inlet angle (β_3). The vane inlet angle is determined by first calculating the flow angle at the design point and the adding the required incidence (i) to it. The design flow angle (α_2) at the impeller exit was determined through a quasi one dimensional flow calculation through the impeller.

Both from the numerical analysis and the reports of Hohlweg et al. (1993) and Sorokes and Welch (1992) it has become very clear that the design incidence angle has a major impact on the flow range and the pressure recovery of the LSVD. Figure 3.12 shows the scatter of normalized flow range ((ϕ_c - ϕ_s)/ϕ_c) with incidence angle, the data was extracted from the various published reports of LSVD performance. It can be seen that in general the flow range tends to increase as the design incidence angle becomes negative up to a certain negative incidence; thus, indicating that there is an optimum incidence angle at which highest flow range can be attained. Moreover, this optimum design incidence angle for maximum flow range depends on the specific speed or the impeller tip Mach number as
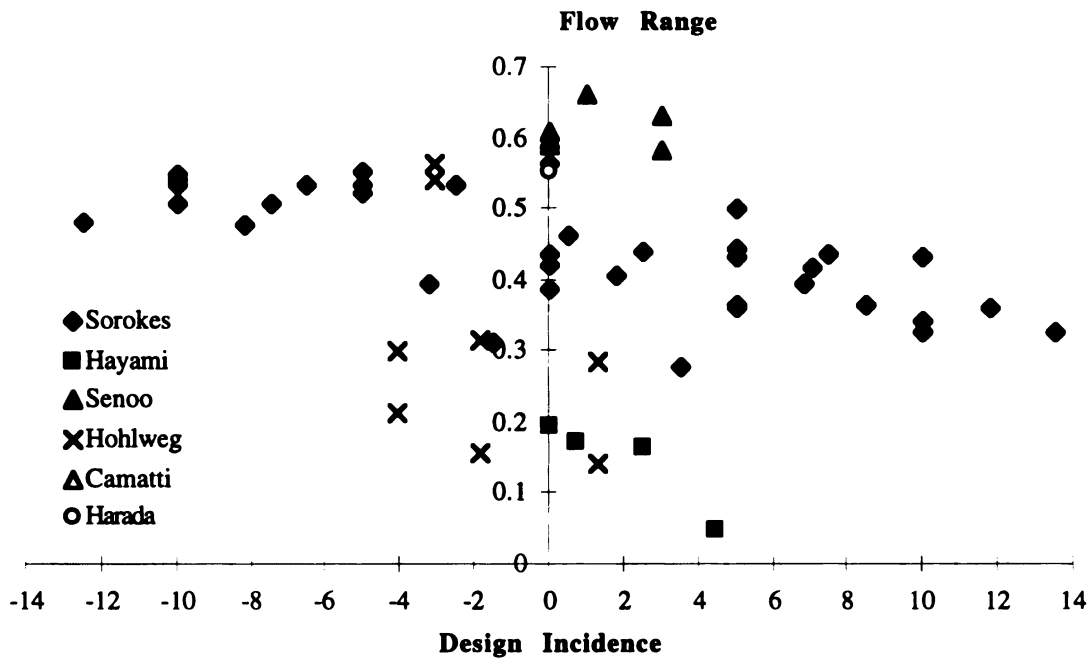
Figure 3.12. Scatter of flow range with design incidence
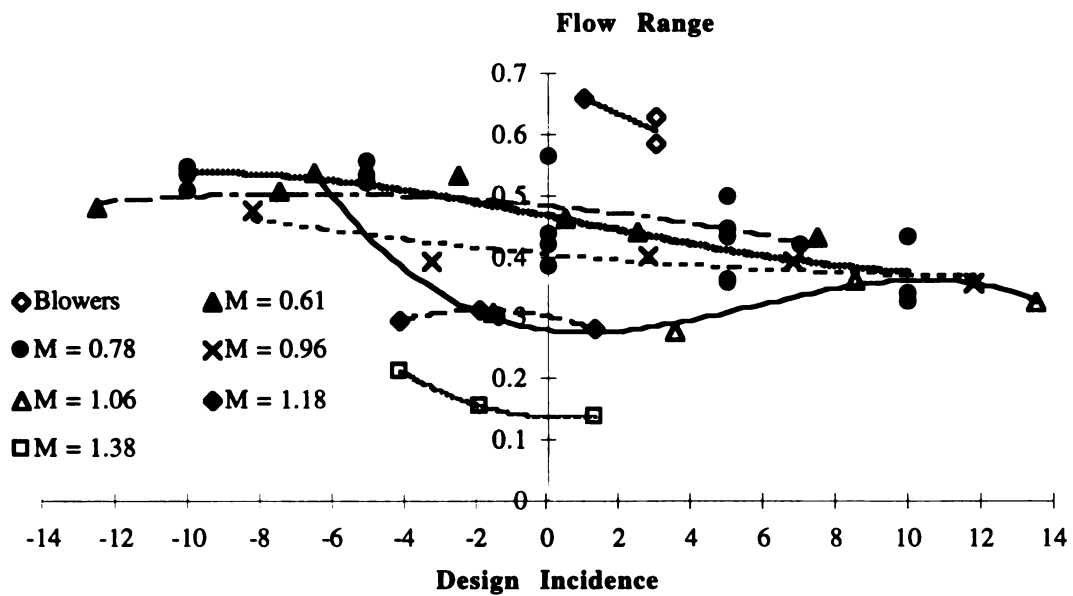
M is Impeller Tip Mach Number

Figure 3.13. Flow Range Vs design incidence as function of tip Mach number (data from Sorokes & Welch 1992)

Figure 3.14. Stage peak efficiency vs design incidence as function of tip Mach number (data from Sorokes & Welch 1992)

can be seen in Figure 3.13. It has also been observed that the incidence angle plays a key role in determining the maximum efficiency of the centrifugal stage with LSVD, as shown in Figure 3.14. Figure 3.14 contains the data from Sorokes and Welch (1992), where thenormalized peak efficiency of the stage is plotted with respect to design incidence angle as a function of impeller tip Mach number. It can be seen that the impeller tip Mach number does not seem to have any remarkable effect on the peak efficiency at design incidence of about -2° to -3°. Hohlweg et al. (1993), also obtained highest efficiency for the LSVD with -1.9° design incidence. Thus, for all four LSVDs designed for experimental testing had -2° design incidence.

Once the solidity, the diffuser inlet radius, the inlet vane angle, and the number of vanes are determined the vane exit radius and vane discharge angle can be obtained from the LSVD geometric relationship

$$[\sigma]^2 = \frac{\left(\dfrac{r_4}{r_3}\right)^2 + 1 - 2\left(\dfrac{r_4}{r_3}\right)\cos\theta}{2 - 2\cos\left(\dfrac{2\pi}{Z}\right)} \tag{3.3}$$

with $\theta = \beta_4 - \beta_3$ and for straight vanes

$$r_4 = r_3 \frac{\cos\beta_3}{\cos\beta_4} \tag{3.4}$$

4. EXPERIMENTAL SETUP

4.1 The Centrifugal Compressor Test Stand

The present investigations of performance of different diffusion systems for a centrifugal compressor were carried out on the first stage of a plant air package compressor. The schematic outline of the test rig is shown in Figure 4.1. The centrifugal compressor was driven by a variable speed motor with a maximum power input of 225 kW. The impeller and the motor were coupled through a gear box of 9.06 gear ratio. The
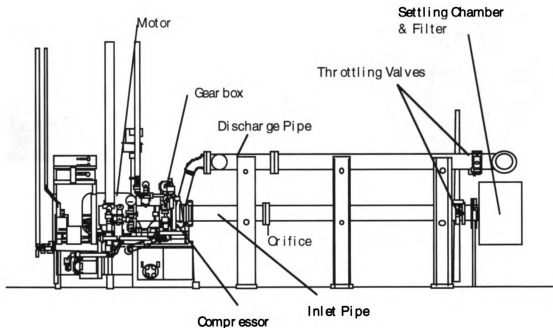
Figure 4.1. Compressor test stand

speed of the motor was accurately controlled by a frequency controller capable of adjusting the power supplied to the motor in accordance with the load on compressor.

The centrifugal impeller is shown in Figure 4.2. This unshrouded cast impeller has 19 blades with 19.3^0 backsweep. The blade camberlines have ellipsoidal shapes in cylindrical sections. The inlet hub and shroud diameters were 47.09 mm and 147.67 mm. The impeller tip diameter was 244 mm, with exit blade width of 13.33 mm.
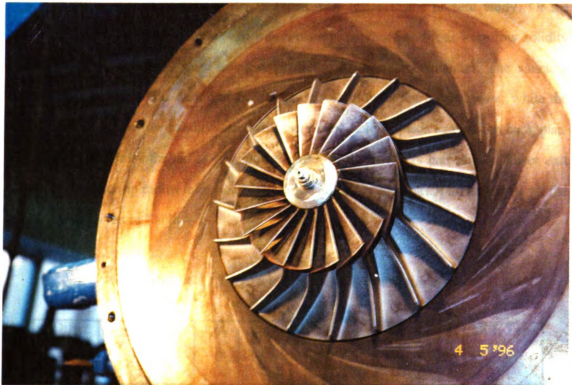
Figure 4.2. The centrifugal impeller

The compressor was tested in an open air loop. The air entered the compressor through an air filter, settling chamber, and inlet pipe. The settling chamber provided the compressor with an air supply free of the temperature stratification, thus enabling the compressor inlet temperature to be measured accurately. After being compressed in the impeller the air is discharged to the outlet pipe after passing through the diffuser and the volute of the compressor. The air in the outlet pipe is muffled before it is discharged. The

mass flow rate through the compressor could be controlled by either of the throttle valves located in the inlet or the outlet pipes. However, for the results presented here the mass flow rate was controlled by the throttle valve located in the outlet pipe.

4.2 Investigated Diffusers

Seven diffusers of three different types were tested in the present study. Of the seven diffusers two were vaneless, one was conventional vaned and four were low solidity vaned. All these diffusers were tested downstream of the same impeller. The vaneless diffusers were fixed to the casing of the compressor with three flat head screws, while the conventional and the low solidity vaned diffusers were held in place against the back plate of the compressor by the aid of two Dowel pins. All the diffusers had same diffuser exit radius to impeller tip radius ratio (r_s/r_2) of 1.53. The major geometric parameters of all the diffusers are given in Table 4-1.

Table 4-1. Diffuser Geometric Prameters.

Diff. Name	b_{2a}/b_2	r_3/r_2	r_4/r_2	r_5/r_2	Z	θ	i	σ	Diff. Type
VNL1	0.70	1.09	-	1.53	-	-	-	-	Vaneless
VNL2	0.84	1.09	-	1.53	-	-	-	-	Vaneless
CVND	1.0	1.09	-	1.53	15	-	0°	1.15	Vaned
LSVD1	1.0	1.09	1.22	1.53	14	14.6°	-2°	0.7	LSVD
LSVD2	1.0	1.09	1.19	1.53	16	12.9°	-2°	0.7	LSVD
LSVD3	1.0	1.09	1.20	1.53	14	12.6°	-2°	0.6	LSVD
LSVD4	1.0	1.09	1.18	1.53	16	11.1°	-2°	0.6	LSVD

In order to understand the effect of diffuser width on the flow angles in the diffuser and the matching of the diffuser with the upstream impeller and the downstream volute, the two vaneless diffusers had different b_{2a} / r_2 ratio. The information obtained was used for the design of the low solidity vaned diffusers. The b_{2a} / r_2 ratio for VNL1 and VNL2 were 0.077 and 0.091. Both VNL1 and VNL2 were pinched from b_2/r_2 (0.109) to b_{2a} / r_2 in a radial distance of 0.44. The conventional vaned diffuser design was based upon the design and performance analysis procedures of Aungier (1988) and Aungier (1990). The cambered vaned diffuser (Figure 4.3) had constant width along the radial direction and the channel divergence angle ($2\theta_d$) was 10.9°.
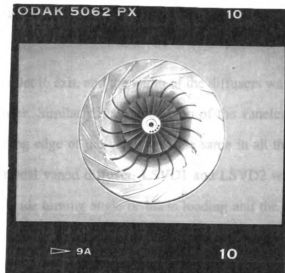
Figure 4.3. The conventional vaned diffuser

(The diffuser has wrong rotation direction relative to impeller for photographic purpose)

The vanes of all the low solidity vaned diffuser were machined on to an aluminum plate. The vanes were simple flat plates in order to reduce the manufacturing cost. Figure 4.4 shows the notation of a low solidity vaned diffuser. The low solidity vaned diffusers
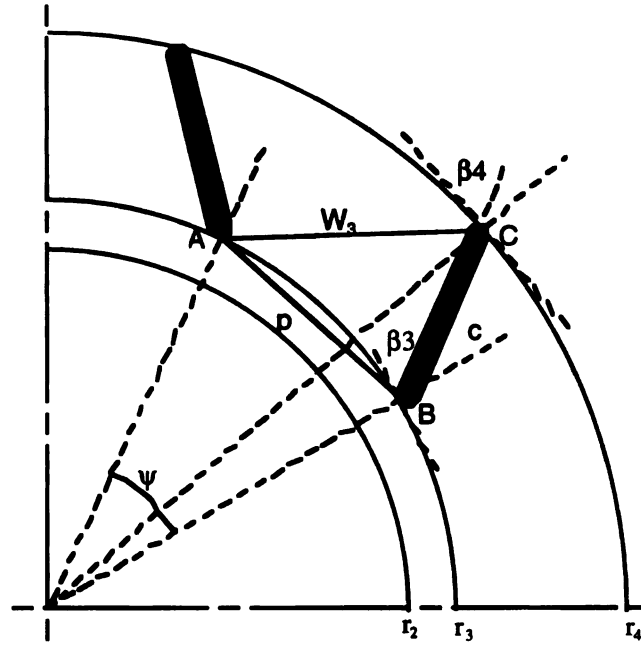
Figure 4.4. LSVD geometric notation

had constant width from inlet to exit, and the width of the diffusers was equal to that of the conventional vaned diffuser. Similarly, the radius ratio of the vaneless space between the impeller exit and the leading edge of the vanes was the same in all the low solidity vaned diffusers and the conventional vaned diffuser. LSVD1 and LSVD2 were initially designed to study the effect of the blade turning angle or blade loading and the blade number on the performance of the low solidity vaned diffuser. LSVD3 and LSVD4 were derived out of LSVD1 and LSVD2 by trimming the vane trailing edges to study the effects of solidity. Figure 4.5 shows the LSVD1 and LSVD2 diffuser plates.

4.3 Measurement Positions and Measurements

The contents of this report present both steady and unsteady results of the experiments performed with the centrifugal compressor test stand having different diffuser
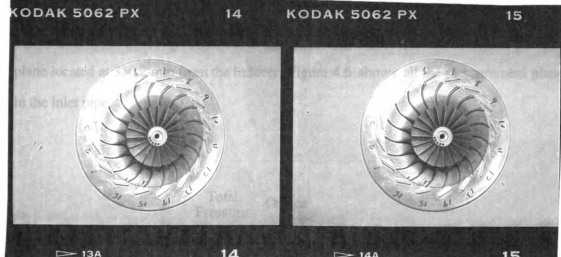
Figure 4.5. LSVD1 and LSVD2 diffusers

(The diffusers have wrong rotation direction relative to impeller for photographic purpose)

configurations described in previous sections. Several static and total temperatures along with static and total pressures and pressure fluctuations at different planes of the compressor stage were measured in order to determine the mass flow rate through the stage, overall performance, and the performance and interaction of various components of the compressor stage. This section presents the details of all the measurement locations and the measured quantities at these locations.

The mass flow rate was measured with an ASME standard orifice plate. Two total and two static temperatures were measured at different circumferential positions located opposite to each other at the same plane of the inlet pipe, upstream of the orifice. The differential pressure across the orifice plate was measured by two sets of static taps located 76.2 mm downstream and 152.4 mm upstream of the plate. The static pressure at the orifice was also measured at two locations in the same plane, 152.4 mm upstream of the plate.

The stage inlet static and total pressures were measured at two 90° apart circumferential positions each. Similarly, the inlet static and total temperatures are also measured at two different circumferential positions. The pressures are measured at a plane mid way between the orifice plate and the inducer, while the temperatures are measured at a plane located at 330.2 mm from the inducer. Figure 4.6 shows all the measurement planes in the inlet pipe.
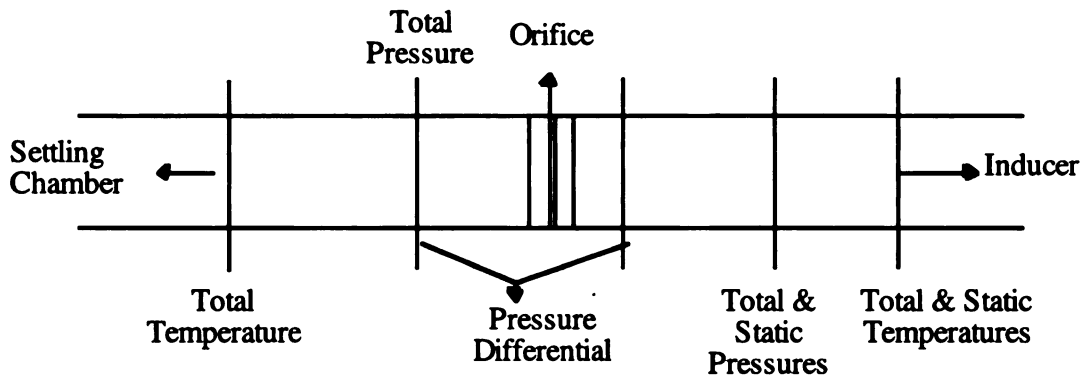
Figure 4.6. Measurement planes in inlet pipe

The inducer behavior is studied by measuring the static temperature just upstream of the inducer and the static pressures at two different axial positions in the inducer. Moreover the pressure fluctuations at the inlet of the inducer are also measured. Figure 4.7 shows the location of the different measurement probes in the compressor stage. The pressure fluctuations and the static pressure in the impeller are measured at a r_{imp}/r_2 ratio of 0.77. All measurements in the impeller are done at the same circumferential plane, and both the dynamic transducers measuring pressure fluctuations and the static pressure taps were located at an angle of 42.5° with respect to each other. All the static taps and the dynamic transducers in the inducer and the impeller were located on the casing of the compressor.
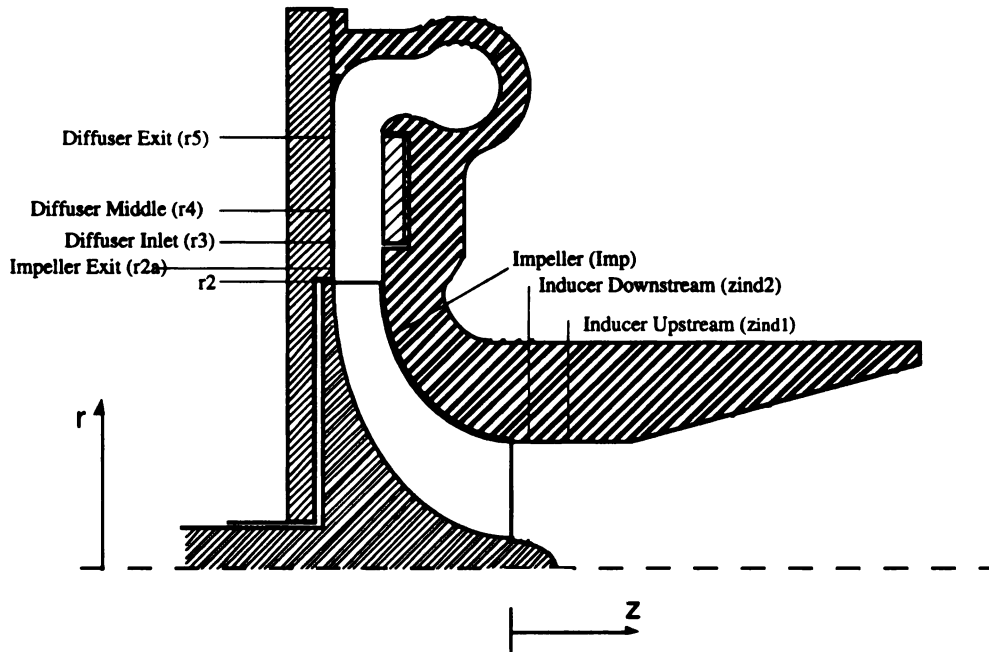
Figure 4.7. Measurement planes in the compressor stage

The pressures at the exit of the impeller and at various locations in the diffuser were measured through the taps drilled on the back plate of the compressor. All these taps were located 150° away from the volute tongue in order to minimize any flow asymmetry caused by the presence of volute. Figure 4.8 shows the location of the taps and different probes on the back plate of the compressor. In all, eight static taps were used to measure the pressure recovery from the impeller exit to the diffuser exit. A set of static taps was located at a radius ratio of (r_{2a}/r_2) 1.04 to measure the static pressure at the impeller exit. One pair was located at the leading edge radius (r_3) of all vaned diffusers, a pair was located at the trailing edge radius (r_4) of the LSVD1 and LSVD2 or the mid channel of the CVD, and the last pair was located at the diffuser exit radius (r_5). In addition to these static pressures the total pressure at the impeller exit was measured at the vane leading edge radius and the pressure fluctuations in the diffuser were measured at the LSVD1 trailing edge radius. The leading
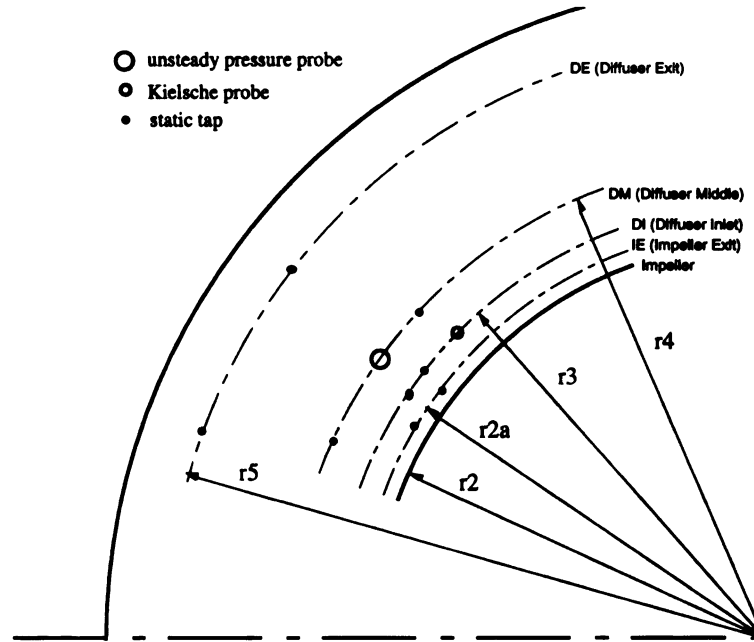
Figure 4.8. Various probe locations on the diffuser back plate

edge radius was chosen for total pressure probe location, since it is assumed that the jet and wake pattern flow coming out of the impeller is mixed out and the flow pattern becomes quasi uniform at this radius. The static taps, the total pressure probe, and the dynamic pressure transducer were placed between the two vanes of the CVD in an attempt to minimize the flow distortion effects caused by the presence of the vanes.

The stage exit pressures and temperatures are measured in the pipe connected to the volute. The exit total and static pressures are measured at four circumferential locations 90° apart in the pipe at the same plane. Similarly the exit total and static temperatures are also measured at four locations at a plane, which is 76.2 mm downstream of the plane where pressures are measured. In order to avoid the heat transfer effects on the temperature measurements the casing of the compressor was covered with insulating material. Table 4-2 summarizes all measurement locations and the quantities measured.

Table 4-2. Summary of Measurements and Measurement Locations.

Location	Position	Static pressure taps	Notation	Other probes	Unsteady pressure transducers
Orifice	as per ASME standards	2	p_{orf}		
Inlet Pipe	$\dfrac{z_1}{r_{1s}} = 5$	2	p_1	2 total pressure 2 total temperature	
Inducer Upstream	$\dfrac{z_{ind1}}{r_{1s}} = 0.74$	1	p_{ind1}		
Inducer Downstream	$\dfrac{z_{ind2}}{r_{1s}} = 0.396$	1	p_{ind2}	1 temperature	Transducer A
Impeller	$\dfrac{r_{imp}}{r_2} = 0.77$	2	p_{imp}		Transducer B & C $\Delta\phi = 42.5°$
Impeller Exit	$\dfrac{r_{2a}}{r_2} = 1.04$	2	p_2		
Diffuser Inlet	$\dfrac{r_3}{r_2} = 1.1$	2	p_3	1 Kiel probe	
Diffuser Middle	$\dfrac{r_4}{r_2} = 1.21$	2	p_4		Transducer D
Diffuser Exit	$\dfrac{r_5}{r_2} = 1.53$	2	p_5		
Discharge pipe		2	p_6	2 total pressure 2 total temperature	

4.4 Steady Performance Measurement

This section enumerates the details of the instrumentation used to obtain the steady data, along with the data reduction procedure.

4.4.1 Instrumentation

The steady static and total pressures were measured with three different types of pressure measuring devices: 1) Validyne - variable reluctance pressure transducers, 2) Omega - hand held manometers, and 3) water/mercury manometers. The water and mercury manometers had 2.54 mm resolution. One of the water manometers was used to measure the differential pressure across the orifice plate and the other measured the stage inlet static pressure, while the only mercury manometer was used to measure the stage exit static pressure. The usage of the water and mercury manometers at these locations was considered necessary to validate the proper functioning of the Validyne and Omega pressure transducers.

The static pressures were measured with 3.175 mm taps and the total pressures were measured with Kielsche type pressure probes. Flexible tubing was routed from the static pressure taps and the Kiel probes to the Validyne and Omega transducers. The Validyne transducers were connected to the Validyne digital transducer indicators with Belden type 8434 cable, while the Omega transducers had digital display integrated to the transducer. The Validyne transducers were calibrated with an Omega pressure calibrator in conjunction with the water and mercury manometers. The water and mercury manometers used during the calibration process provided an additional check. On the other hand, the Omega pressure transducers were factory calibrated, and they were checked for proper function with the water and mercury manometers before use. All pressures were read to the second decimal digit, either in mm of water or mercury.

The total temperatures were measured by, half shielded with bleed slot, total temperature probes. All temperature measurements were done by cooper-constantan (T-type) thermocouples connected to the Omega digital temperature indicators. The digital displays were calibrated by switching the display to a builtin calibration setting and applying 0.00 mV at the thermocouple input to adjust zero reading and similarly applying 39.00 mV for full scale display reading of 560.0. Once calibrated, the digital displays were capable of indicating temperatures in either °F or °C. For the present study °C display was chosen with 0.1 °C resolution.

The Validyne pressure transducers were able to measure with an accuracy of ±.0.25% of full scale, which includes the effects of linearity, hysteresis and repeatability at an operating temperature range of -17°C to 72°C. The Omega pressure transducers had an accuracy of ±2.54 mm of water. The accuracy of the Omega digital temperature indicators was ±0.5°C at 0.1° resolution setting under the operating temperatures of 5 to 45°C for T-type thermocouples.

4.4.2 Data Collection and Reduction

The compressor was tested at three different impeller tip Mach numbers ($M_t = 0.69$, 0.89, 1.02) for each diffuser configuration. At each speed the temperature and pressure measurements were collected from all probe locations for approximately 9 to 14 different mass flow rates, ranging from compressor choke to surge in order to obtain a complete speed line. As mentioned earlier, the mass flow rate through the compressor was controlled with the throttle valve located at the stage exit.

At each flow point, the data was collected when the compressor stage reached stability in terms of the temperatures. The stability criterion was the temperatures at the stage inlet and exit oscillated within ±0.1°C. The data were never collected when the temperatures monotonically increased or decreased. Thus, the stage inlet and exit

temperatures were continuously monitored and recorded every 2 minutes for 30 min, until stability was attained. Once the stage was considered stable, all the pressures and temperatures were recorded and transferred on to a PowerPC for further data reduction and processing.

The data reduction and processing were done by an EXCEL program. The program first converts the recorded pressures and temperatures into N/m^2 and $^\circ K$. At this stage the temperatures and pressures at each measurement plane are compared with each other and with downstream and upstream measurement planes. In this way any faulty or malfunctioning transducers are detected, and the data from them are eliminated before obtaining average pressures and temperatures at each measurement plane. The program uses the averaged pressures and temperatures at various planes to calculate the stage overall performance and the component performance parameters. The program is also capable of plotting these performance parameters with the mass flow rate or the impeller exit flow angles. This on-line plotting capability of the program acts as a good tool to monitor the behavior of the stage and the whole system; moreover, it also provides greater flexibility in control and operation.

The overall performance parameters calculated were the stage static and total pressure ratios, the total temperature ratio, the total-to-total isentropic efficiency of the stage, the head coefficient, the work coefficient, and the stage pressure recovery. In addition to the above mentioned overall performance parameters, individual component performance was determined by calculating the impeller pressure ratio, the impeller total-to-total efficiency, the pressure recovery of the impeller, the diffuser, and the volute.

In order to understand the pressure recovery phenomenon in all three types of diffusers, the diffusers were subdivided into three regions; and the pressure recovery in each of these regions was calculated. The subdivision was based on the low solidity vaned diffusers: 1) the vaneless space from impeller exit to the vane leading edge, 2) the vaned region, from vane leading edge to trailing edge of LSVD1, and 3) the downstream vaneless

space from vane trailing edge to the diffuser exit. The pressure recovery of each of these three regions in case of LSVD1 and the corresponding regions of all other diffusers was calculated for comparison purposes. Apart from these pressure recoveries, the isentropic pressure recovery and the loss coefficient of the region from vane leading edge to the volute exit are also calculated to understand the loss mechanisms in different kinds of diffusers.

The stage and impeller total pressure ratio compares the total pressures at the stage exit and rotor exit, with the stage inlet total pressure. As such, they are

$$\pi_{0,rotor} = \frac{P_{03}}{P_{01}} \tag{4.1}$$

and

$$\pi_{0,stage} = \frac{P_{06}}{P_{01}} \tag{4.2}$$

Similarly, the rotor and stage static pressure ratios are given as

$$\pi_{,rotor} = \frac{P_2}{P_1} \tag{4.3}$$

$$\pi_{,stage} = \frac{P_6}{P_1} \tag{4.4}$$

The isentropic efficiency can likewise be calculated for both the rotor and the stage. Efficiency is the ratio of work done in an ideal process to the actual work. For compression process between two states 1 and 2, this can be expressed as a ratio of the isentropic work (representing the ideal process) and the real work. In terms of enthalpy this becomes (Figure 4.9)

$$\eta_s = \frac{w_s}{w} = \frac{h_{02s} - h_{01}}{h_{02} - h_{01}} \tag{4.5}$$

For an ideal gas with constant C_p, the relation $dh = c_p dT$ can be used to rewrite equation (4.5) in terms of temperatures

$$\eta_s = \frac{w_s}{w} = \frac{T_{02s} - T_{01}}{T_{02} - T_{01}} \tag{4.6}$$
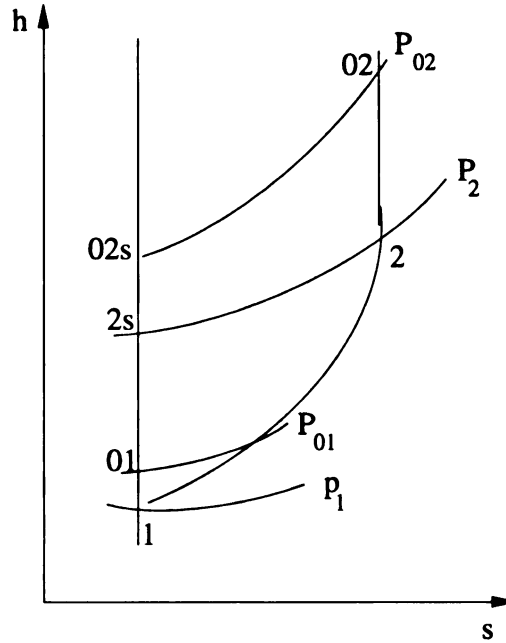
Figure 4.9. Definition of isentropic efficiency

In an isentropic process with constant properties, the pressures and temperatures are related according to

$$\frac{P_{02}}{P_{01}} = \left(\frac{T_{02s}}{T_{01}}\right)^{\left(\frac{\gamma}{\gamma-1}\right)} \tag{4.7}$$

Thus, substituting into equation (4.6), the isentropic efficiency for a compression process between state 1 and 2 can be written as

$$\eta_s = \frac{\left(\frac{P_{02}}{P_{01}}\right)^{\left(\frac{\gamma-1}{\gamma}\right)} - 1}{\frac{T_{02}}{T_{01}} - 1} \tag{4.8}$$

It is also known as total-to-total isentropic efficiency as the total conditions at the state 1 and 2 are used to for calculation.

In the present investigation equation (4.8) was used to find the isentropic total to total efficiency of the rotor and the stage. However, the heat transfer through the casing is considered to be negligible and the stage exit total temperature is used for calculating the rotor efficiency too, i.e. $T_{06} = T_{03}$. The ratio of stage exit to inlet total temperature is also given as

$$\tau_0 = \frac{T_{06}}{T_{01}} = \frac{T_{03}}{T_{01}} \tag{4.9}$$

Thus, the appropriate expressions for rotor and stage efficiency are

$$\eta_{t-t,rotor} = \frac{\left(\pi_{0,rotor}\right)^{\left(\frac{\gamma-1}{\gamma}\right)} - 1}{\tau_0 - 1} \tag{4.10}$$

and

$$\eta_{t-t,stage} = \frac{\left(\pi_{0,stage}\right)^{\left(\frac{\gamma-1}{\gamma}\right)} - 1}{\tau_0 - 1} \tag{4.11}$$

The energy transferred by the rotating blades to the gas passing through the impeller per unit mass is defined as the compressor "head". Although the compressor produces head, it cannot be measured directly. However, it can be calculated from the measured pressure ratio, inlet and exit temperatures and gas properties. Head in nondimensional form is given as

$$\psi = \frac{\Delta h_{0s}}{\frac{1}{2}U_2^2} \tag{4.12}$$

and is known as isentropic head coefficient. Using equation (4.7) the head coefficient can be written in terms of measured quantities and gas properties as

$$\psi = \frac{2C_p T_{01}\left[\left(\pi_{0,stage}\right)^{\left(\frac{\gamma-1}{\gamma}\right)} - 1\right]}{U_2^2} \tag{4.13}$$

The work coefficient relates the isentropic head coefficient and the isentropic efficiency. It is a nondimensional value of the actual head produced by the compressor and is given as

$$\mu = \frac{2C_p(T_{06} - T_{01})}{U_2^2} \tag{4.14}$$

The relation between the head coefficient, work coefficient and the efficiency is

$$\mu = \frac{\psi}{\eta} \tag{4.15}$$

The static pressure recovery between any two stations 1 and 2 was calculated as the percentage of impeller peripheral dynamic (or velocity) pressure.

$$Cp = \frac{P_2 - P_1}{\frac{1}{2}\rho_0 U_2^2} \tag{4.16}$$

Thus the pressure recovery of all the compressor components and the static pressure rise between various stations in the diffuser were calculated using equation (4.16). In addition to the static pressure recovery of the diffuser calculated as mentioned above, the static pressure rise from the vane leading edge station to the diffuser exit was also calculated as percentage of the dynamic pressure at the vane leading edge station.

$$Cp' = \frac{P_5 - P_3}{P_{03} - P_3} \tag{4.17}$$

The total pressure loss from the vane leading edge station to the volute exit was determined in terms of total pressure loss coefficient, which is expressed as

$$\xi = \frac{P_{03} - P_{06}}{\frac{1}{2}\rho_0 U_2^2} \tag{4.18}$$

The mass flow rate through the compressor was calculated from the differential pressure measured across the orifice as per the ASME standards. The equations used for the calculation are given in Miller (1992). In this report the mass flow rate is presented in nondimensional form known as flow coefficient which is given by

$$\phi = \frac{\dot{m}}{\rho_0 U_2 \frac{\pi d_2^2}{4}} \tag{4.19}$$

The flow angles at the impeller exit were calculated at the vane leading edge station as the static and total pressures at this station were measured. From the measured total and static pressures, the Mach number was determined

$$M_3 = \sqrt{\frac{2}{\gamma-1}\left[\left(\frac{P_{03}}{P_3}\right)^{\left(\frac{\gamma-1}{\gamma}\right)} - 1\right]} \tag{4.20}$$

Assuming that there was negligible heat transfer through the casing, i.e. $T_{03}=T_{06}$ and the Mach number obtained above, the static temperature at the vane leading edge station was calculated

$$T_3 = \frac{T_{06}}{1 + \frac{\gamma-1}{2}M_3^2} \tag{4.21}$$

Now the absolute flow velocity was calculated from the basic relation that relates the total and static temperature at any point

$$C_3 = \sqrt{2C_p T_{06}\left[1-\left(\frac{T_3}{T_{06}}\right)\right]} \tag{4.22}$$

On the other hand, the radial component of the velocity at vane leading edge station was calculated from the continuity

$$C_{r3} = \frac{\dot{m}}{2\pi r_3 b_3} \tag{4.23}$$

The flow angle then was obtained from equations (4.22) and (4.23)

$$\alpha_3 = \text{Sin}^{-1}\left(\frac{C_{r3}}{C_3}\right) \tag{4.24}$$

However, in this calculation of flow angle, no blockage caused by the boundary layer growth was considered. Thus, the flow angles calculated were invariably higher than the actual flow angles.

4.5 Unsteady Performance Measurement

4.5.1 Obtaining and Storing the Pressure Signal

The pressure fluctuations were measured by PCB pressure transducers. The transducers in the inducer and in the impeller were mounted on the shroud wall, where as the transducer in the diffuser was mounted on the compressor back plate. All pressure transducers were flush mounted because this eliminated any gap between the transducer diaphragm and the measurement location. Thus, no usable frequency range of the transducer was lost.

The PCB transducer uses a stack of thin piezoelectric quartz crystal wafers to convert the applied pressure on the transducer diaphragm into electric charge. The charge produced is proportional to the applied pressure. The transducer has a built in accelerometer that compensates for any acceleration and reduces distortion and resonance in high vibration environments. The transducer also has a built in temperature compensation that allows it to operate in a temperature range of $\pm 205°F$. The transducer can measure pressure fluctuations in a range of $0-6.89 \times 10^5$ N/m^2 with 13.8 N/m^2 resolution. It has a natural frequency of 250 kHz with a usable frequency of upto 80 kHz.

When a constant pressure is applied to the PCB transducers for a long time (> 100 sec), the output charge does not remain constant and decreases with time. For the transducers used for experiments described in this report the output charge would be constant for about 30-60 seconds. This makes it impossible to measure the steady absolute pressure with these transducers, and they can only measure pressure fluctuations. Thus,

the averaged static pressure was measured through the static taps and Validyne transducers at every plane where unsteady transducers were mounted.

The signal from the PCB pressure transducer was conducted to an inline amplifier through 10 feet of low-noise coaxial cable. The inline amplifier conditions the transducer output signal. This amplifier has high input impedance (10^{11} Ω) and a range capacitor in order to avoid any distortions in the signal through input capacitance shunting.

The signal was then passed on to the signal conditioner through a 50 foot low-noise coaxial cable. Even though one inline amplifier was used for each transducer, one signal conditioner was used for all four signals. The signal conditioner powered both the inline amplifier and the PCB transducer and could also amplify the signal with fixed gain of 1, 10, 100. During the system evaluation tests, it was found that the gain had no effect on the signal to noise ratio, indicating that the noise was being added to the signal before it reached the signal conditioner. Since the signal to noise ratio was unchanged with signal gain and the amplitude of the signal was small, a gain of 100 was used to obtain better resolution of the signal.

The amplified signals from the signal conditioner were transferred to a two-channel HP signal analyzer. The signals were stored and transferred to a PC for further processing and analysis through the signal analyzer and the signal processing software. The HP signal analyzer also provided the capability for on-line signal analysis through the various features available with it. It was possible to obtain the power spectrum, phase and cross-correlation between two signals for on-line monitoring of the compressor. The complete signal flow path is shown in Figure 4.10.
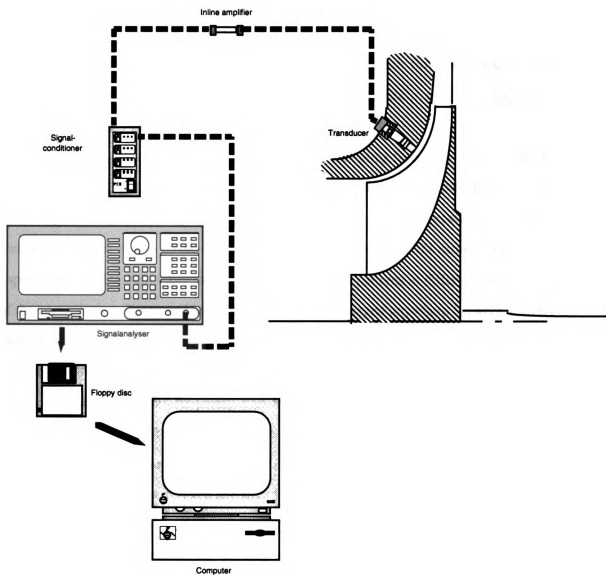
Figure 4.10. Unsteady pressure signal flow path

4.5.2 Signal Processing

Since the signal analyzer had only two channels, the signal capture through the signal analyzer was done in pairs of two transducers. Transducer B (Table 4-2) located in impeller was used as reference for all captures, i.e. signal from transducer B was captured through channel 1 and the signal from transducers A, C, and D was captured through channel 2 of the signal analyzer alternately at each flow point. Thus, at each flow point for a given capture frequency, three captures were made with BA, BC, and BD transducer combinations at the two channels of the signal analyzer.

Even though the captures could be made at any sampling frequency of up to 261.12 kHz per channel, but most captures were made at 12 kHz and 2048 Hz sampling frequency. The high frequency was used to observe the blade to blade pressure fluctuations and small captures of 5 to 10 records were taken. Each record had 1024 sample points. The captures at 2048 Hz were taken to study the unsteady flow patterns in different components of the compressors. The record lengths at this frequency ranged anywhere between 8 to 64 records. The choice of 2048 Hz was based on the available memory of the signal analyzer and the required resolution of the capture. Moreover, literature survey has shown that in most cases the rotating stall frequency was lower than the impeller rotational frequency. The maximum rotational frequency in the present experiments was 460 Hz and with 2048 Hz sampling frequency the usable frequency range was 800 Hz.

Once the capture was taken and stored on the PC, the signal data is processed using in-house signal processing software (UDACS). The software has various data preparation tools such as windowing, filtering, removal of mean, removal of linear trend etc. It also provides options to choose different kinds of filters and windowing methods. From the prepared data power spectrum, cross spectrum, amplitude spectrum, phase, and coherence are calculated. In addition to these features the software was also capable of graphical display of the raw data and the results or processed data in time or frequency domain. The

details of the software and the procedures used to accomplish the results can be found in Wilmsen (1996).

5. RESULTS AND DISCUSSION

Seven diffusers, two vaneless, one conventional vaned and four low solidity vaned diffusers were experimentally tested downstream of the same impeller. The results of this testing are presented here. All diffusers were tested at three different speeds corresponding to the impeller tip Mach number (M_t) of 0.69, 0.88 and 1.02.

The overall performance of each of these seven diffusers is compared with each other in order to enumerate the advantages and disadvantages of the three types of diffusers used in centrifugal compressor stages. In addition to this the range of operation, peak efficiency and the pressure ratio obtained by the low solidity vaned diffusers is compared with the vaneless and conventional vaned diffusers. Moreover the effect of the LSVD vane number and solidity on the overall performance of the compressor stage is also discussed.

The pressure recovery (Cp) of the LSVDs is studied by dividing the LSVD into three major regions: 1) the upstream vaneless region, 2) the vaned region and 3) the downstream vaneless region. The Cp of each of these three regions of the LSVDs is compared with the corresponding regions of the vaneless and conventional vaned diffusers in an attempt to understand the pressure recovery phenomena in LSVDs. By analyzing the pressure recovery in the four LSVDs, the effect of solidity and vane number on the LSVD performance is studied. The effect of the diffuser type on the unsteady flow patterns in the inducer, the impeller , and the diffuser of the compressor stage is also presented.

All the performance curves presented in this chapter are normalized with the design point flow and performance parameters of the VNL1 at M_t = 1.02.

99

5.1 Overall Performance Characteristics

The performance characteristics of the compressor stage with the seven diffusers and at three different M_t are given in Figure 5.1 through Figure 5.3. From the head (ψ_N) curves at all three speeds it can be seen that the VNL1 had better pressure ratio than the VNL2. However, the difference in head between VNL1 and VNL2 decreased as M_t increased and at $M_t = 1.02$ the head obtained by both was nearly same. Since, VNL1 was narrower than VNL2, the flow angles at the inlet of VNL1 were more radial, due to which the fluid had to travel shorter distance before exiting the diffuser. Thus, the frictional losses in VNL1 were lower than VNL2, providing better performance. In addition to having better head and efficiency, VNL1 also had higher flow range than the VNL2. This could again be related to the high tangential flow coming into the wider (VNL2) diffuser. At low mass flow rates the flow angle (α) is small, and if the diffuser radius ratio (r_5/r_2) is large enough, the flow tends to re-enter the compressor after describing a 360° arc, thus causing reverse flow and diffuser stall resulting in compressor surge. Therefore the better performing VNL1 is used for comparative study of LSVDs.

At $M_t = 1.02$, the characteristic curves of the VNL1, VNL2 diffusers and the LSVDs are vertical at the right end, with the mass flow rate being approximately constant for all these diffusers. On the other hand the maximum flow rate attained by the stage with CVND was about 14% less than the other diffusers. This clearly indicates that the maximum flow through the compressor was controlled by the vaned diffuser throat choke in case of the CVND and the inducer choke in case of the vaneless and LSVDs. However at lower speeds ($M_t = 0.88$ and 0.69) it can be noticed that even though the LSVDs lack a true diffuser throat, their overload capacity decreased with the speed. The loss of overload capacity by LSVDs over vaneless diffusers was about 3% at $M_t = 0.88$ and 11% at $M_t = 0.69$. This short fall in overload capacity of the LSVDs is because of the high negative
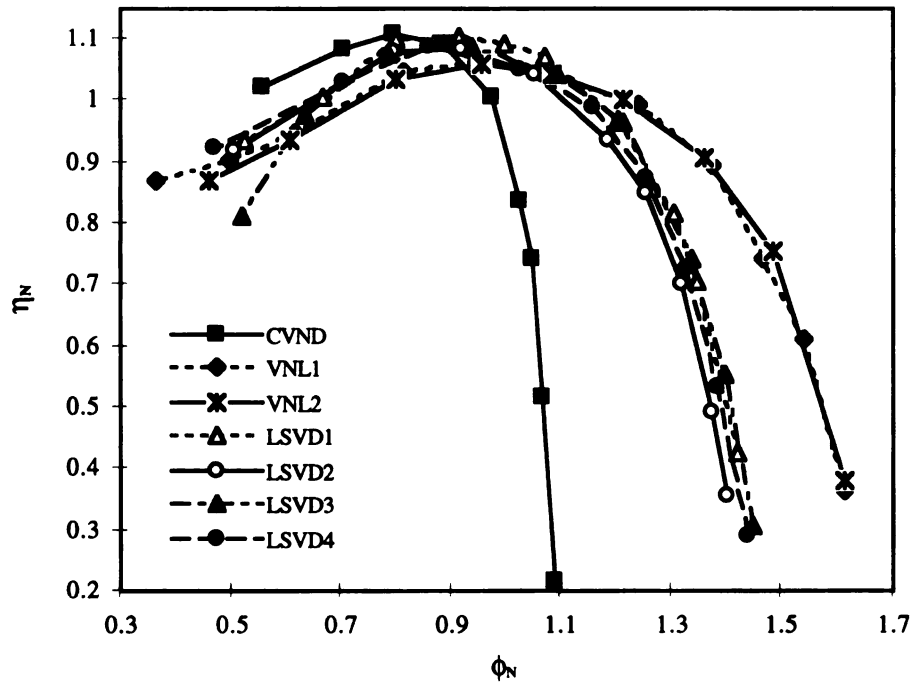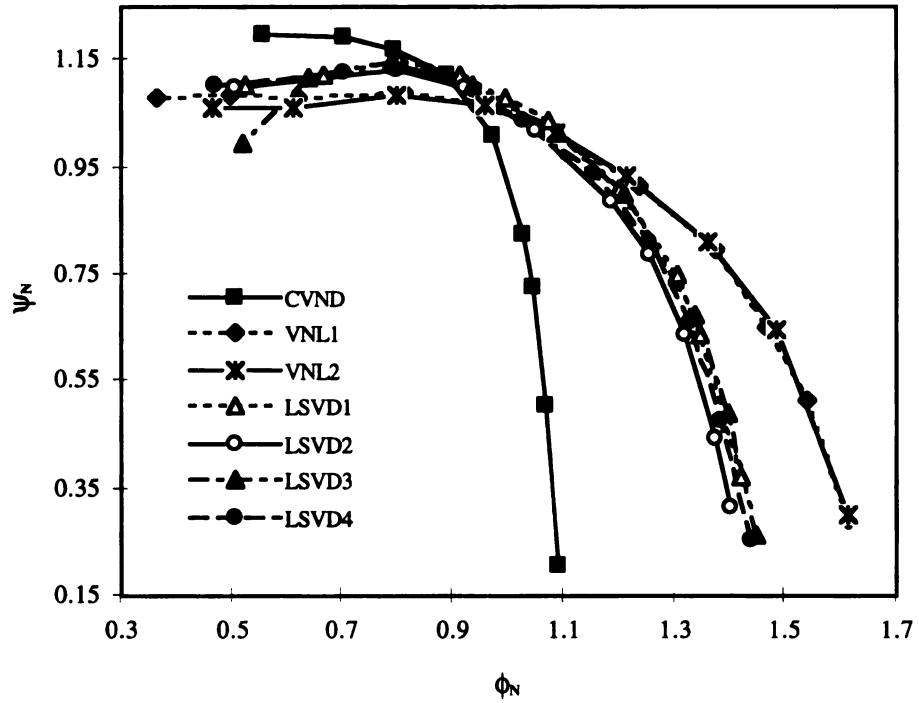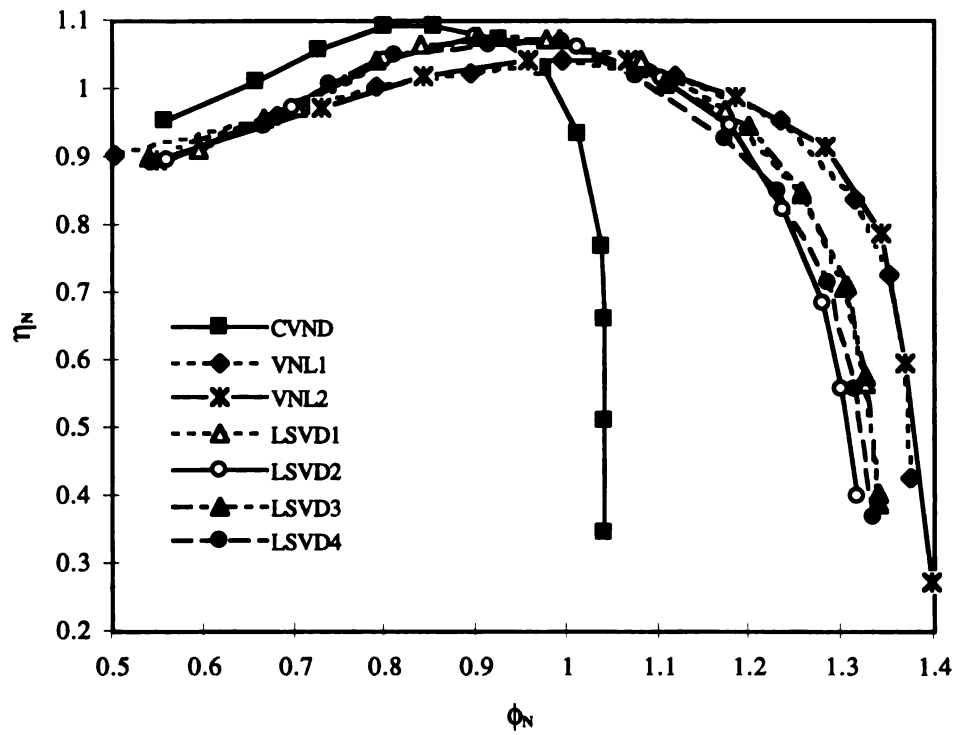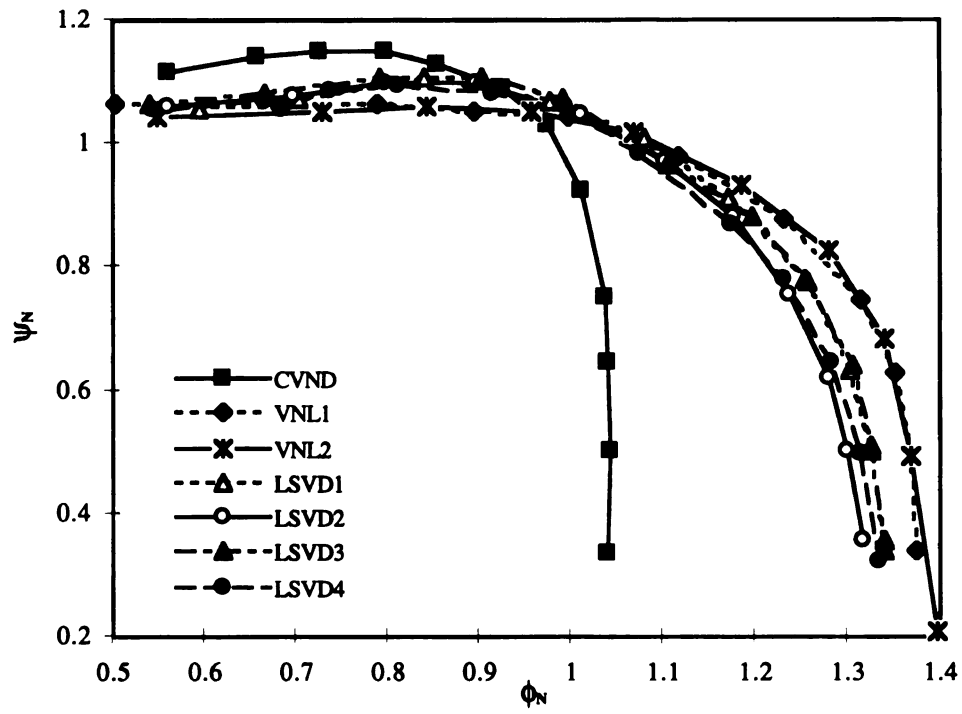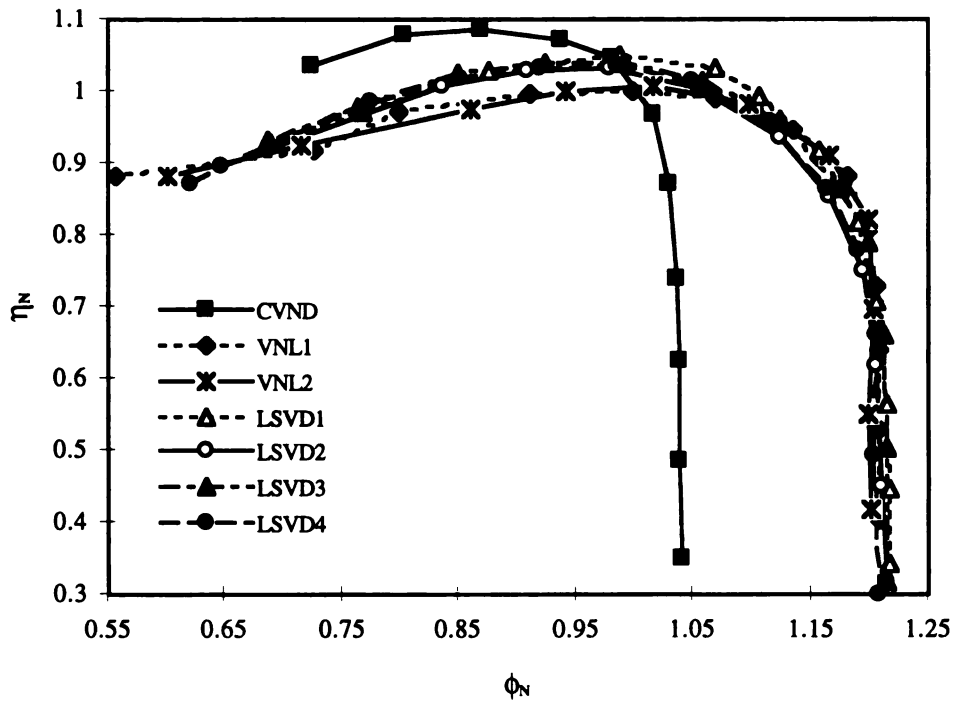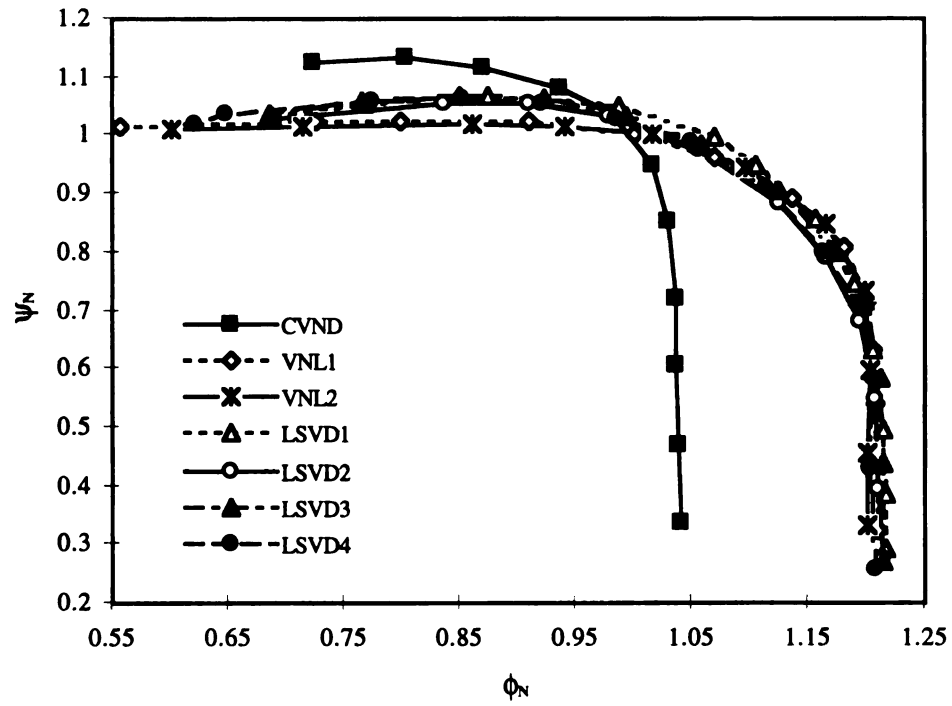
Figure 5.1. Performance Characteristics at $M_t = 0.69$

Figure 5.2. Performance characteristics at $M_t = 0.88$

Figure 5.3. Performance characteristics at $M_t = 1.02$

incidence on the vanes at lower than design speeds. The high negative incidence causes the pressure surface stall of the LSVD vanes. The vanes along with the stalled flow form a virtual throat which limits the maximum possible flow through the compressor, similar to the CVND. Thus at off design speeds the LSVDs tend to behave like the CVND in terms of overload capacity.

However, the characteristic curves show (Figure 5.1 to Figure 5.3) that the surge flow attainable by the different diffusers is different. At all three speeds the CVND in general had the highest surge mass flow rate, indicating their intolerance to the positive incidence. On the other hand the LSVDs seem to have nearly same surge flow rate at each of the three speeds. However the surge flow of the LSVDs is in general higher than that of the vaneless diffusers. Thus, with LSVDs the surge flow was lowered from the CVND but they could not provide a surge flow equivalent to the best performing vaneless diffuser (VNL1), contrary to the observations of Hayami et al. (1990) and Senoo et al. (1983) (θ = 10°). The reason for this difference could be that the LSVD vanes in the present study had higher loading or turning angle (θ) (Table 4.1) and were made of thin flat plates which are more sensitive to incidence.

The efficiency of the compressor with LSVDs was better than the vaneless diffusers for a wide range of flow at all tip speeds. But, the LSVDs fell short of the CVND efficiency at M_t = 1.02 and 0.88. However, at M_t = 0.69 the LSVD1 and LSVD3 were able to perform almost as good as the CVND over a wide flow range. Moreover, it can also be seen that the peak efficiency of the LSVDs at all speeds, was attained at higher mass flow than the CVND. Thus providing greater stable operating range between peak efficiency flow point and surge flow.

In general at all speeds the efficiency and the pressure ratio of the compressor with LSVDs were superior to the best performing vaneless diffuser over a wide flow range. The flow range obtained by the LSVDs was also comparable to the vaneless diffusers. Thus

LSVD's give greater flexibility in design as they can be adjusted to peak in performance over a wide range of impeller flow conditions.

5.1.1 Operating Range

The percentage range (choke to surge) or the total operating range of the compressor stage as function of the impeller tip Mach number is presented in

Figure 5.4. The CVND diffuser as expected has the lowest operating range at all speeds because the maximum and the minimum possible flow through the compressor is fixed by the diffuser irrespective of the speed. On the other end VNL1 has the highest operating range in which the maximum and minimum flow is fixed by the inducer. VNL2 diffuser at all speeds had approximately 4% lower range than VNL1 due to the diffuser stall at low flow rates.
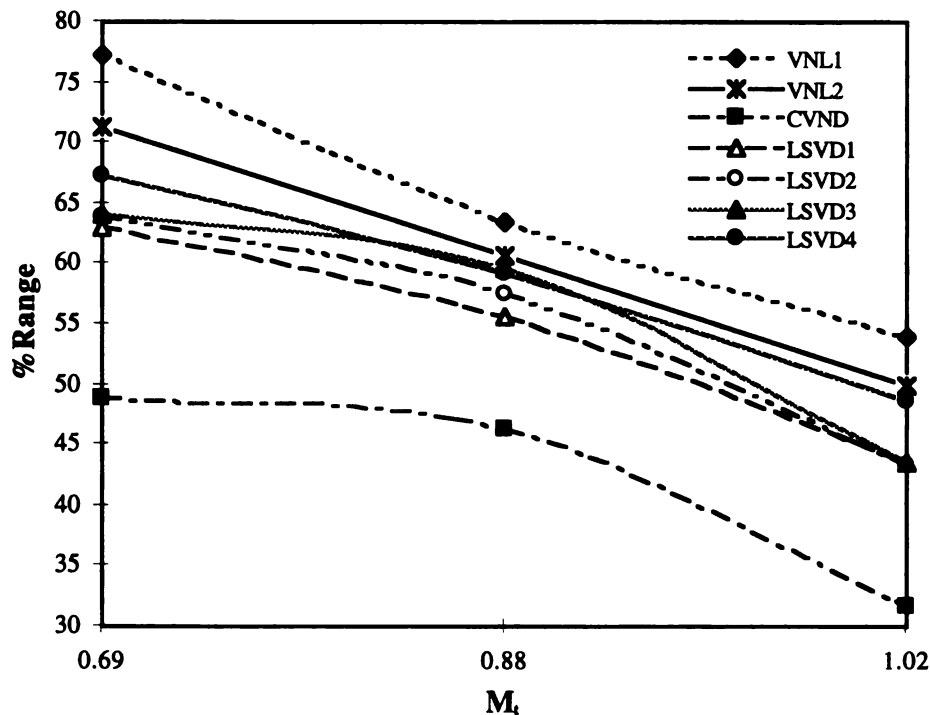

Figure 5.4. Variation of %Range with M_t

The operating range of the LSVDs seen in Figure 5.4 is in between the vaneless and the conventional vaned diffusers at all speeds. At M_t = 1.02 LSVD1, LSVD2 and LSVD3 all have same range, indicating that irrespective of the blade loading and the solidity the vanes stalled at a specific positive incidence. However, LSVD4 has 5% higher range than the others. There are two possible reasons which could have assisted LSVD4 to achieve higher flow range. First, the blade turning angle of LSVD4 is about 1.5° lower than the next higher blade turning angle LSVD (LSVD3), even though the blade turning angle does not seem to have an effect on the other three LSVDs. The lower blade turning angle means lower loading of the vanes and therefore the vanes did not stall, providing lower surge flow. Second, the solidity of LSVD4 was 0.6 and had 16 vanes due to which the cord length of the vanes was smallest of all others. It is known that the stall causing flow separation on the vanes at low flow rates occurs at the trailing edge of the suction surface. Thus, shorter vanes could provide lower surge flow.

At M_t = 0.88 and 0.69 , the LSVDs limit both the maximum and the minimum flow through the compressor. Since all four LSVDs had same design incidence of -2°, the maximum flow through the compressor was almost identical for all of them as seen in Figure 5.1 and Figure 5.2. Thus at these speeds the total operating range attained by each diffuser was dictated by their respective surge mass flow rates. It can be seen in

Figure 5.4 that the flow range decreased as the blade turning angle of the diffusers increased. However, LSVD3 at M_t = 0.69 did not have a range better than LSVD2. The reason for this is clearly seen in Figure 5.1 head curve, which indicates that some component other than diffuser stalled at this speed causing the compressor to surge at a higher mass flow rate.

An interesting observation from

Figure 5.4 is that the LSVDs (except LSVD4) and CVND have similar trend in decrease of operating range with an increase in speed. LSVD4 on the other hand behaved similar to the vaneless diffusers by showing a linear decrease in operating range as M_t

increased. Thus it could be concluded, that when the blade turning angle is below a certain optimum the LSVD tends to behave like a vaneless diffuser in terms of total operating range.

5.1.2 Peak Efficiency

Figure 5.5 shows the variation of peak efficiency of the stage with the M_t. At $M_t =$ 1.02 the LSVDs have 4 to 7% higher normalized peak efficiency than the vaneless diffusers, and this difference in peak efficiency is almost constant at all speeds. The CVND has about 3 to 5% higher normalized peak efficiency than the LSVDs at $M_t = 1.02$ and this difference in peak efficiency between the CVND and LSVDs decreases as M_t decreases. Thus LSVDs can have much promising results at lower speeds than at high speeds.
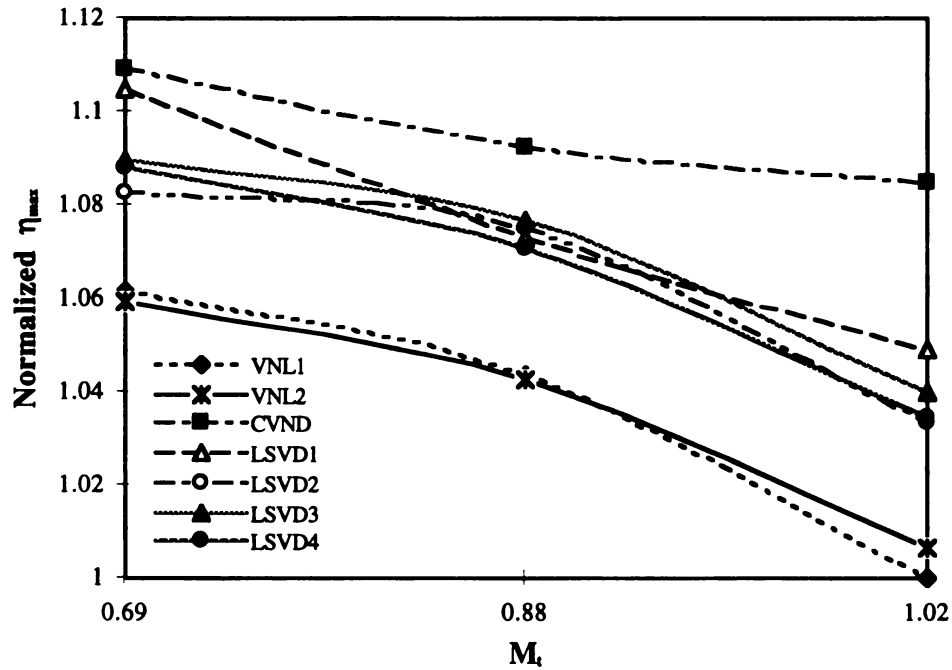

Figure 5.5. Normalized η_{peak} variation with M_t

LSVD2, LSVD3, and LSVD4 have a trend similar to the vaneless diffusers and LSVD1, with highest blade turning angle (θ = 14.6°), has a trend similar to the CVND. From this observation it can be deduced that there is an optimum blade turning angle beyond which the LSVD tend to have the peak efficiency variation with M_t similar to the conventional vaned diffusers.

At M_t = 0.88, it can be seen that LSVD2 (θ = 12.9°) and LSVD3 (θ = 12.6°) have better peak efficiency than the LSVD1 (θ = 14.6°). Therefore, it seems that at a given M_t there is an optimum blade turning angle which will provide highest peak efficiency. In the present case (M_t = 0.88) the optimum blade turning angle seems to be about 12.5°.

5.1.3 Effect of Blade Number

Figure 5.6 and Figure 5.7 show the efficiency curves of the 14 vane and 16 vane diffusers at 0.7 and 0.6 solidity respectively. For a fixed solidity and blade inlet angle, reduction in blade number causes an increase in blade turning angle or blade loading. It can be seen that at both 0.7 and 0.6 solidity the LSVD having 16 vanes had lower surge flow irrespective of the speed. Moreover the diffusers with 14 vanes were able to attain higher efficiency than the 16 vane diffusers at all speeds. It can also be noticed that the LSVDs with 14 vanes, at lower than design speeds were able to provide slightly better overload capacity than 16 vane counterparts.

When the blade turning angle and blade inlet angle are fixed, an increase in blade number causes the solidity to increase. Camati et al. (1995) have shown that with an increase in blade number, the peak efficiency increases and the flow range decreases. From Figure 5.6 and Figure 5.7 too it can be seen that the difference in peak efficiency of 14 vanes and 16 vanes LSVD is more pronounced at higher solidity. Thus the peak efficiency and the flow range are functions of the number of vanes of a LSVD.
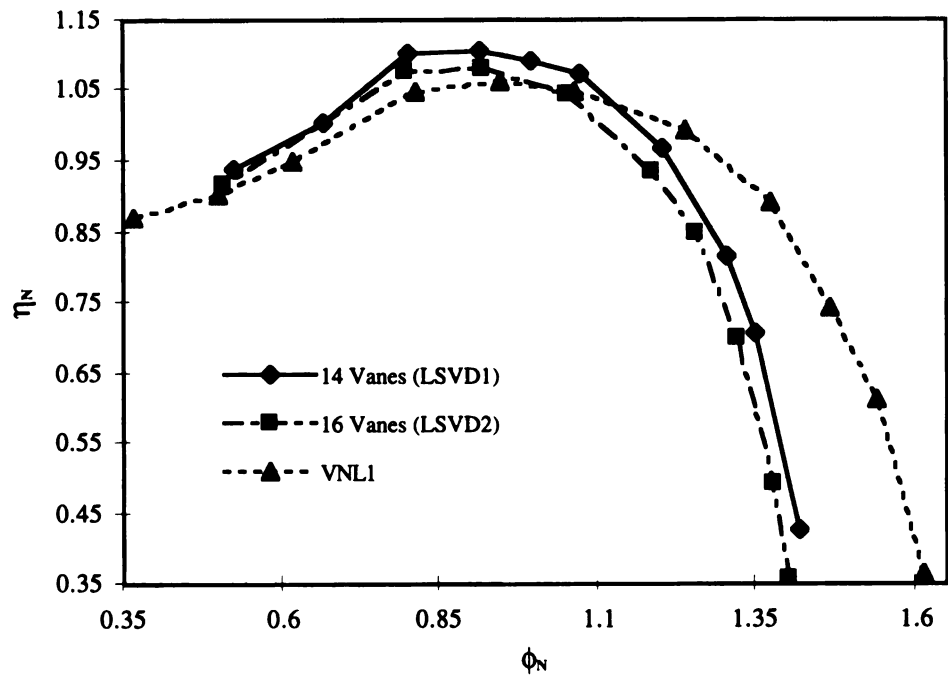
(a) $M_t = 0.69$
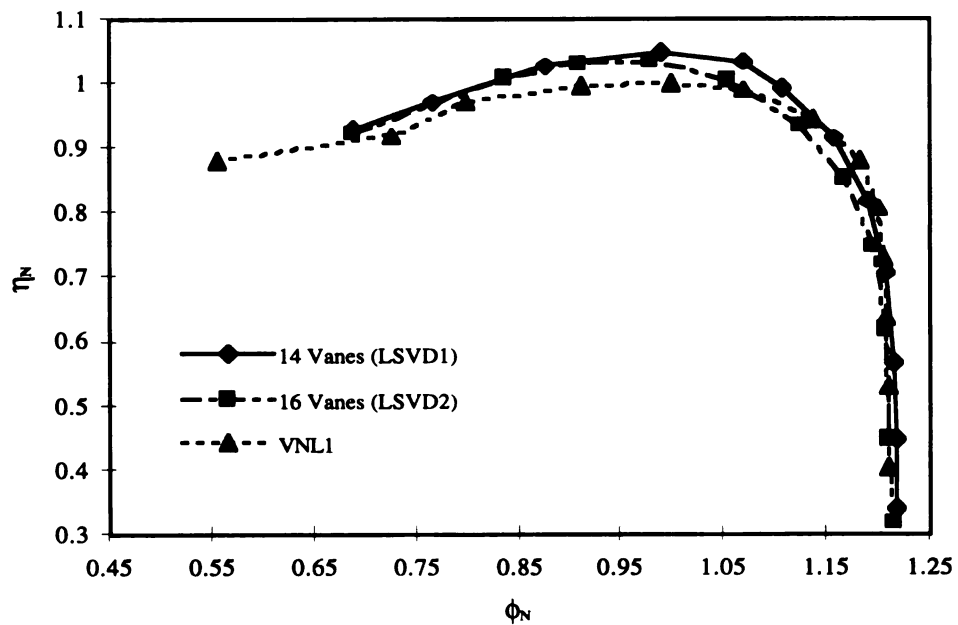
(b) $M_t = 1.02$

Figure 5.6. Effect of vane number on the performance of LSVD ($\sigma = 0.7$)
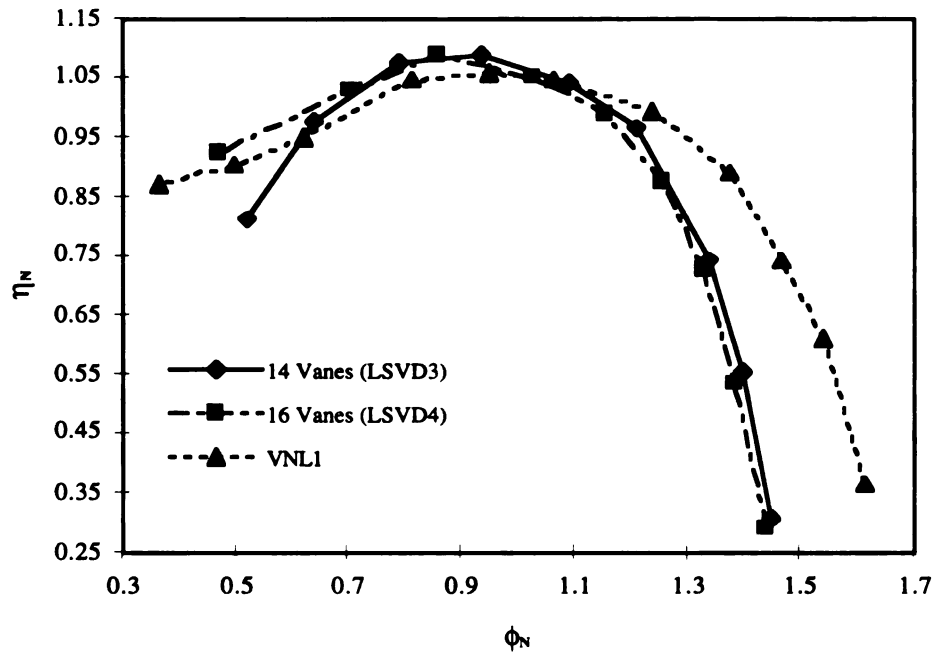
(a) $M_t = 0.69$
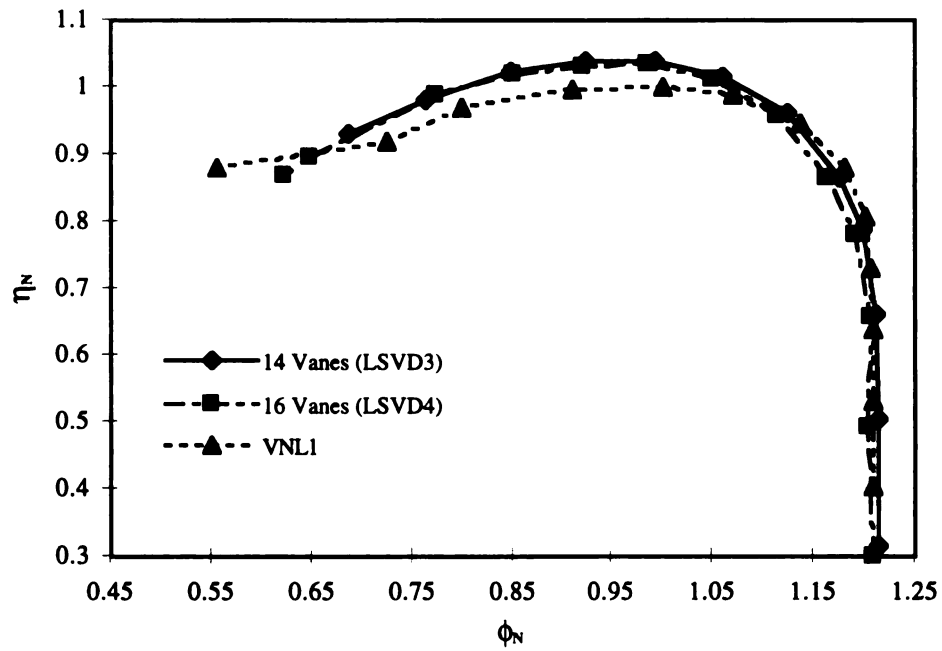
(b) $M_t = 1.02$

**Figure 5.7. Effect of vane number on the performance of LSVD ($\sigma = 0.6$)**

5.1.4 Effect of Solidity

Figure 5.8 shows the efficiency of the 0.7 and 0.6 solidity diffusers at $M_t = 1.02$. In the present study a reduction in solidity caused a reduction in blade turning angle as the vane number was kept constant. It can be seen that as the solidity decreases the flow range increases irrespective of the blade number. This can be attributed to the decrease in blade turning angle. However the peak efficiency of diffusers with 0.6 solidity did not suffer as one would have expected, due to reduction in blade turning angle. The 14 vanes and 0.6 solidity LSVD had only 1% lower peak efficiency than the 0.7 solidity and 14 vane LSVD. While 16 vanes diffusers had same peak efficiency with both 0.6 and 0.7 solidity.

These results are in agreement with the numerical experimentation results presented in Chapter 3. It was shown that the flow range can be increased by reducing the solidity of the diffuser and at the same time get an improvement in the pressure recovery of the diffuser.
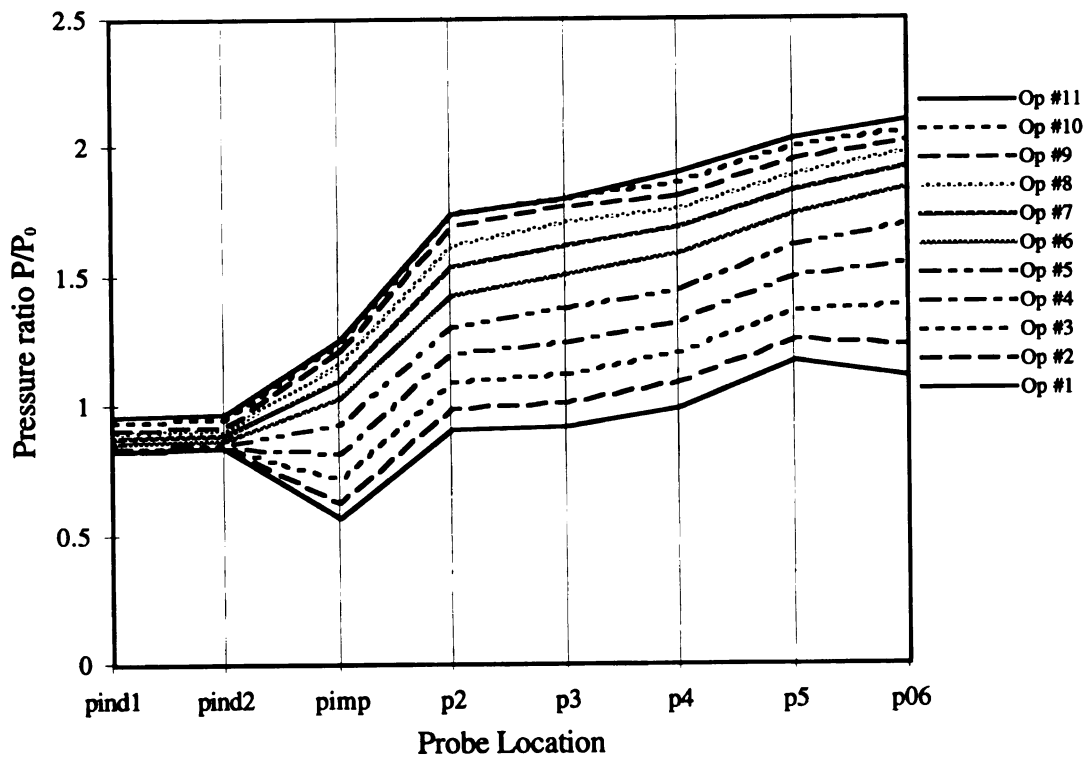
5.2 Pressure Rise in the Compressor Stage

In an attempt to understand the effect of the diffuser system on the static pressure rise in the stage, the static pressure from stage inlet to exit was measured at eight different locations. The observed differences in terms of pressure ratios among all seven diffuser configurations were similar for every tested speed. Moreover the static pressure rise characteristics of each diffuser type were also similar. Thus the data of high speed ($M_t = 1.02$) VNL2, CVND and LSVD2 are analyzed and discussed. In Figure 5.9 the ratio of the static pressure to the stage inlet total pressure is plotted, with respect to the different locations at which the pressure measurements were made for 11 different operating flow points. From the static pressure characteristics of VNL2 (Figure 5.9 (a)), the flow in the vaneless diffuser is stable. Moreover the highest pressure gain in the vaneless diffuser
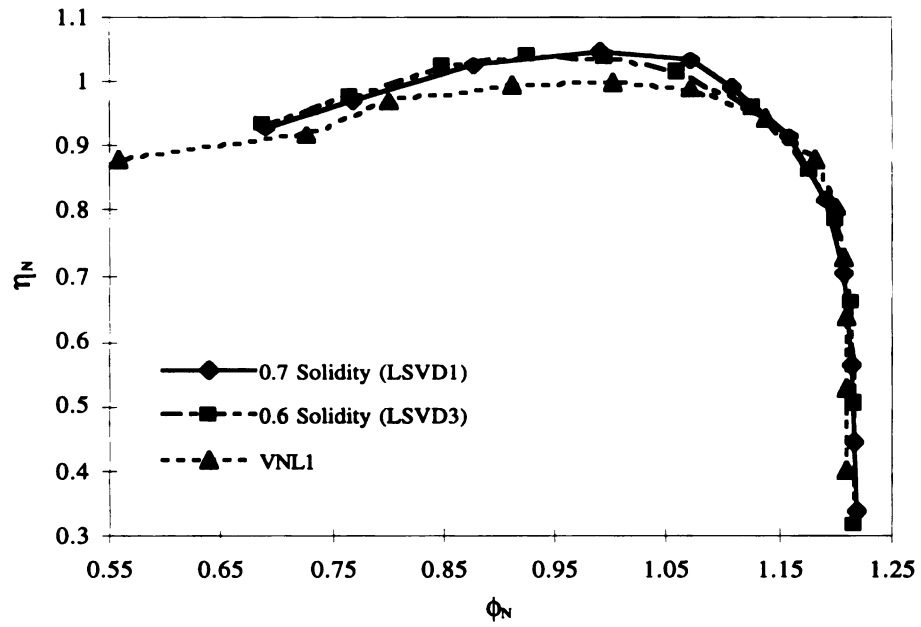
(a) Z = 14
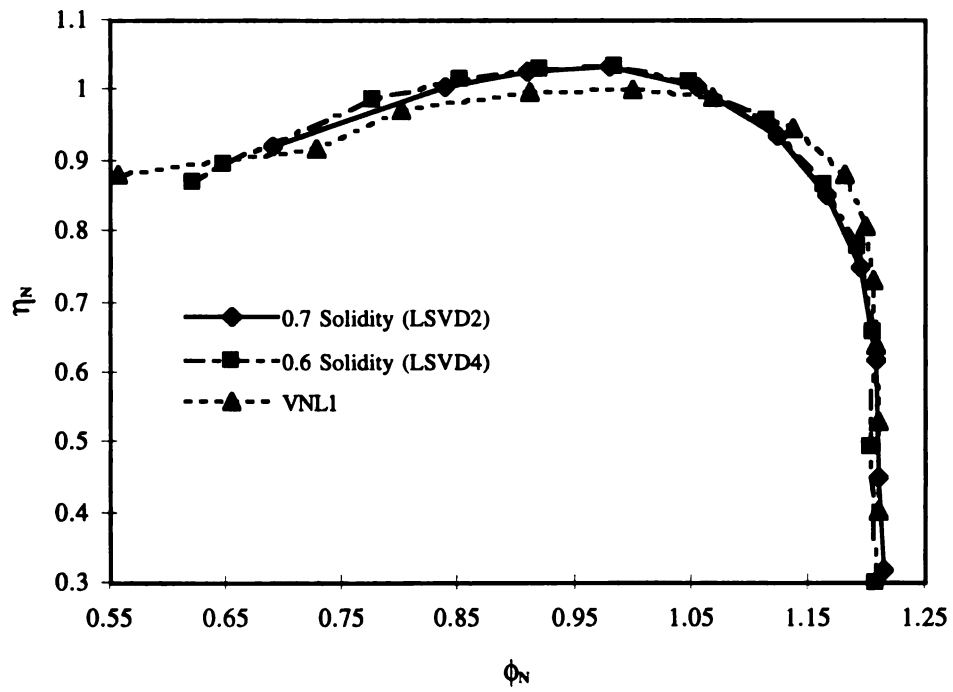
(b) Z = 16

Figure 5.8. Effect of solidity on the performance of LSVD at $M_t = 1.02$

seems to occur at high mass flow rates. This could be because at high mass flow rates the flow leaves the impeller more radially than at low mass flow rates. Since the flow angles are higher at high mass flow rates, the flow path in the diffuser is shorter leading to lower flow losses. The volute on the other hand does not contribute in any pressure rise at high mass flow rates, where as at low mass flow rates its contribution is very significant (after Op#4). As the vaneless diffuser is not the limiting component for maximum flow through the compressor, the limiting component is the inducer. This can be seen from the sudden pressure drop in the impeller at high mass flow rate (Op#1). The pressure drop is caused by the inducer choking. However, this phenomena gets alleviated as the mass flow rate is decreased through the stage.

Figure 5.9 (b) shows the static pressure rise in CVND at different mass flow rates. It can be seen that the pressures from stage inlet to the diffuser inlet are constant for the first five operating points (Op#1 to Op#5). However from diffuser inlet to stage exit the pressure rise is dependent on the mass flow rate, thus indicating that neither the inducer nor the impeller was responsible for limiting the maximum flow through the compressor. It can be seen that there is a sudden pressure drop in the diffuser at high mass flow rates. This indicates that the vaned diffuser was choked and that the pressure drop was due to the negative incidence losses. Moreover it seems that the flow upstream of the shock is not influenced by the flow conditions downstream of the shock. Therefore, the pressure up to the diffuser inlet remains constant in the first five operating points.

The pressure rise characteristics of LSVD2 (Figure 5.9 (c)) is a mixture between the characteristics of VNL1 and CVND. It can be seen that the sudden pressure drop occurs both in the impeller and in the LSVD at high mass flow rate. However the maximum flow rate attained by the stage with LSVD2 was equivalent to that of the VNL2 as seen in performance characteristics (Figure 5.3). Thus the maximum flow limiting component was the impeller even though the losses do not seem to be as high as in VNL2. On the other hand the pressure drop in the diffuser is caused by the pressure surface stall of the LSVD
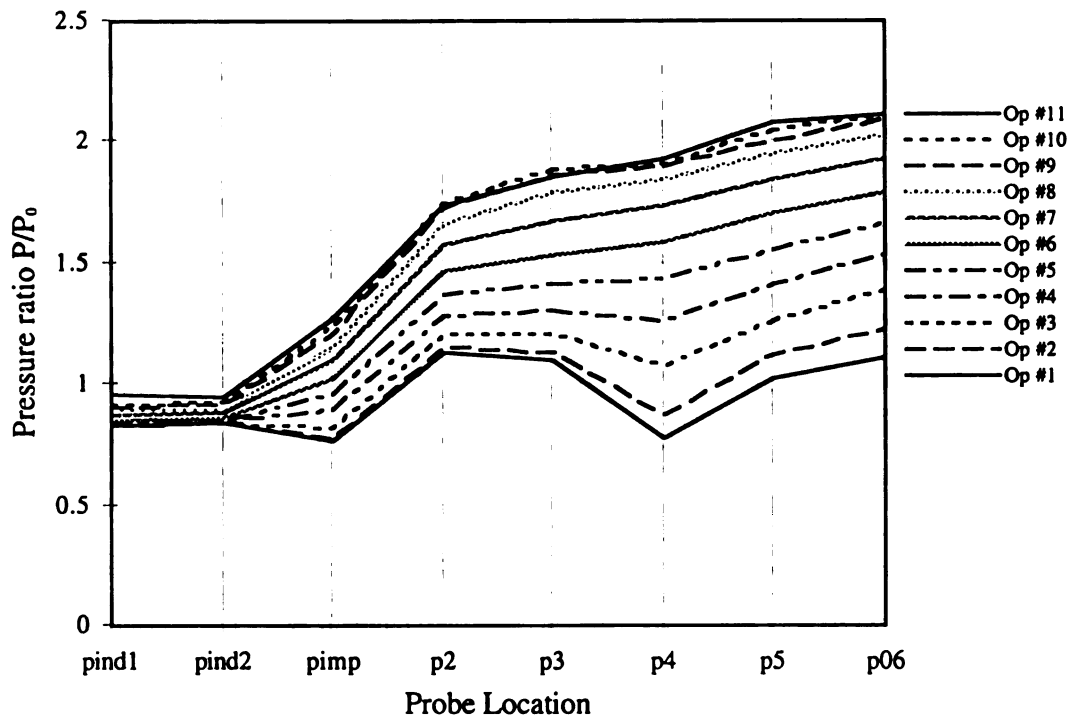
(a) Vaneless Diffuser (VNL2)
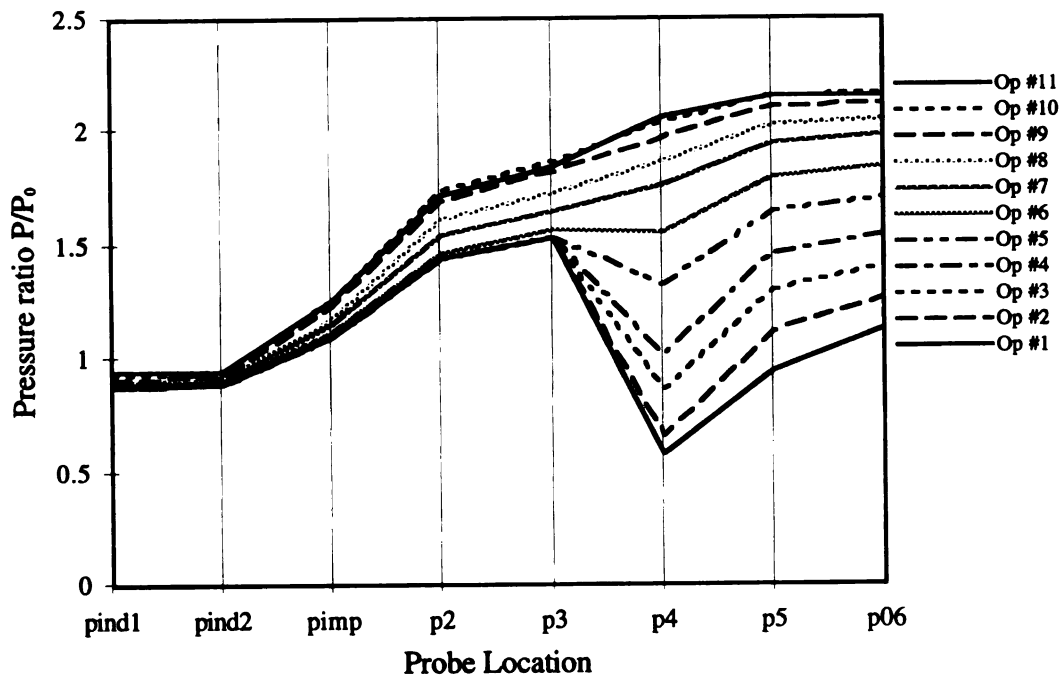
(b) Conventional Vaned Diffuser (CVND)

Contd.

(c) Low Solidity Vaned Diffuser (LSVD2)

Figure 5.9. Pressure rise in the compressor stage

vanes. At high mass flow rates the flow has very high negative incidence on the vanes due to which the flow separates on the pressure surface and forms a large stalled region. This large stalled flow, blocks a major area between two vanes forming a virtual throat and causing the flow to accelerate. These effects in the diffuser are seen only in the first three operating points and then on the pressure rise through the stage is very steady. Thus clearly showing the advantage of the LSVD in attaining smoother pressure rise over wide flow range.

5.3 Pressure Recovery of the Diffusers

Figure 5.10 through Figure 5.12 show the total pressure recovery (Cp_{2-5}) in the various diffusers at all speeds. At all speeds it can be seen that the CVND has highest peak pressure recovery and the vaneless diffusers have the lowest. The pressure recovery of the

LSVDs at all speeds is in between the vaneless diffusers and the CVND. It can also be observed that the LSVDs have a pressure recovery trend similar to the CVND, which is because of the negative incidence losses at high mass flow rates. The LSVDs with 14 vanes tend to have higher Cp_{2-5} at high mass flow rates at all speeds than the 16 vane LSVDs. This can be expected because of lower losses and blockage by the stall on the pressure surface of each vane. The same reason can also explain the slightly higher overload capacity of LSVDs with 14 vanes. On the other hand at the lower mass flow rates, specially at $M_t = 0.88$ and 0.69, the LSVDs with 0.6 solidity have better Cp_{2-5} than the LSVDs with 0.7 solidity. However at $M_t = 1.02$ this feature is not observed. The next section attempts to explain such observations by breaking the pressure recovery of the diffuser Cp_{2-5} into the pressure recovery of three different regions.

5.4 Pressure Recovery in the Diffuser Regions

5.4.1 Upstream Vaneless Space Pressure Recovery (Cp_{2-3})

The pressure recovery in the vaneless space between the impeller exit and the vane leading edge radius of the CVND and LSVDs is considerably higher than that of the corresponding region of vaneless diffusers at all speeds (Figure 5.13, Figure 5.15, and Figure 5.17). The higher Cp_{2-3} of CVND and LSVDs is due to the greater width of the diffuser and the presence of the vanes. The effect of the width can be clearly seen from the Cp_{2-3} curves of VNL1 and VNL2. The width at the impeller exit is reduced to the vaneless diffuser width in this region due to which there is a flow acceleration in addition to the diffusion by area increase. Narrower the diffuser, greater the flow acceleration and lower the area increase. The effect of the width is more remarkable as the speed increases because the absolute flow velocity coming out of the impeller increases.
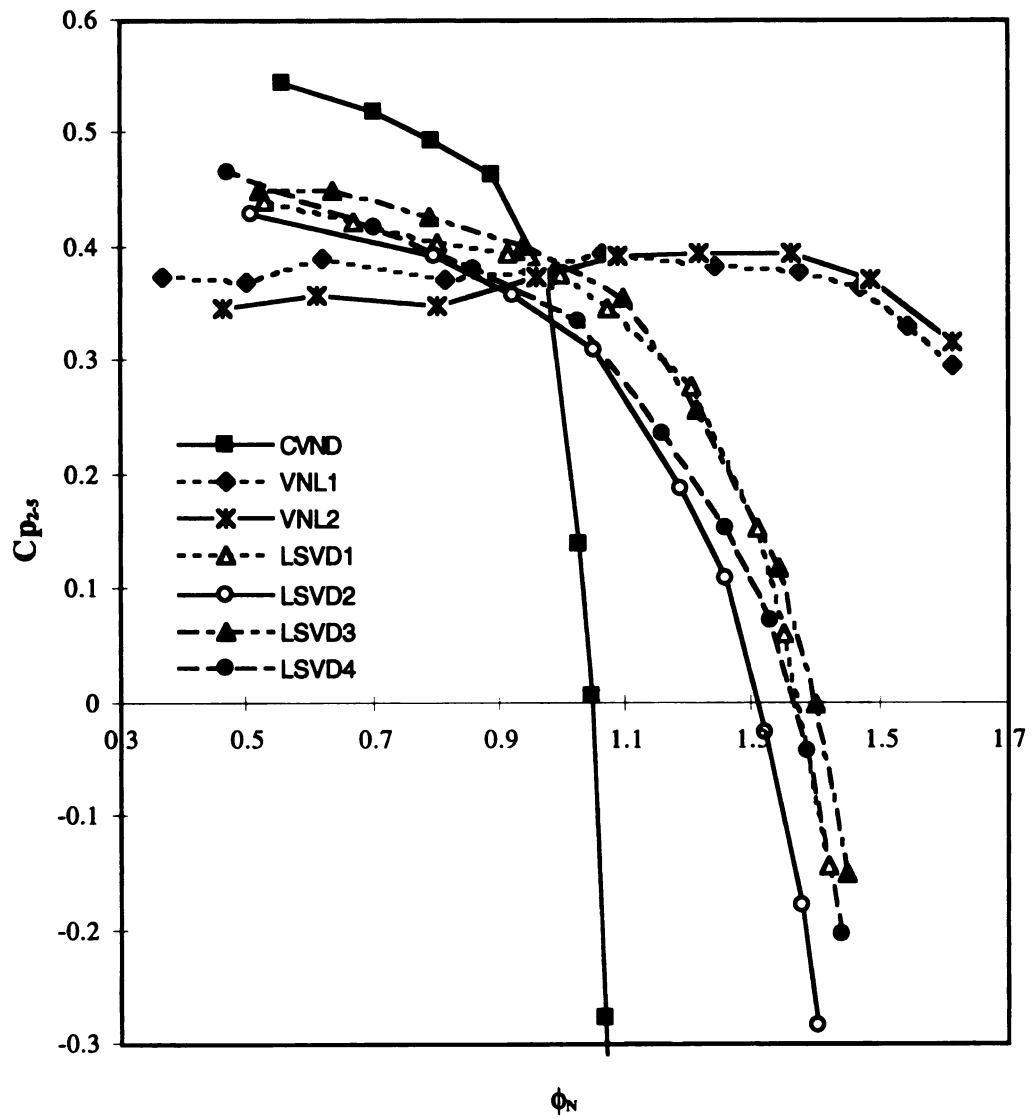
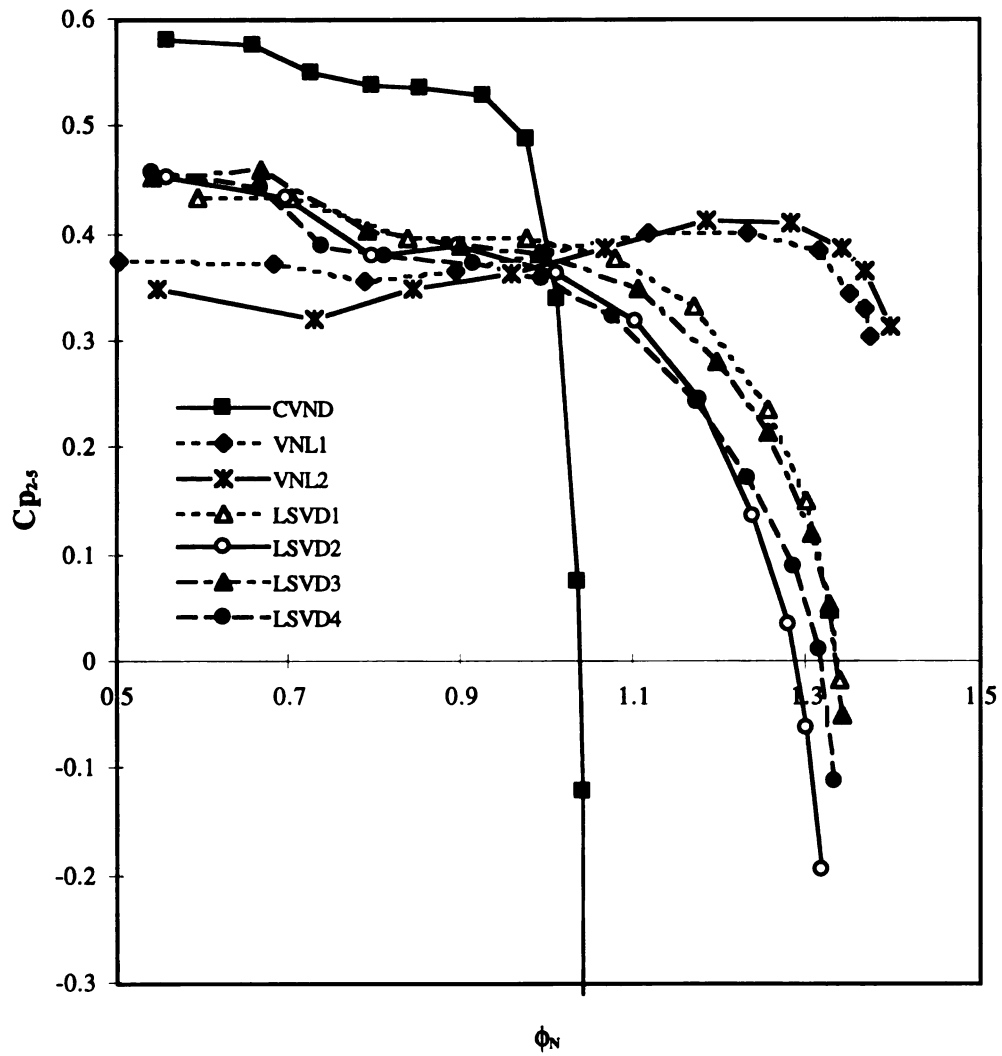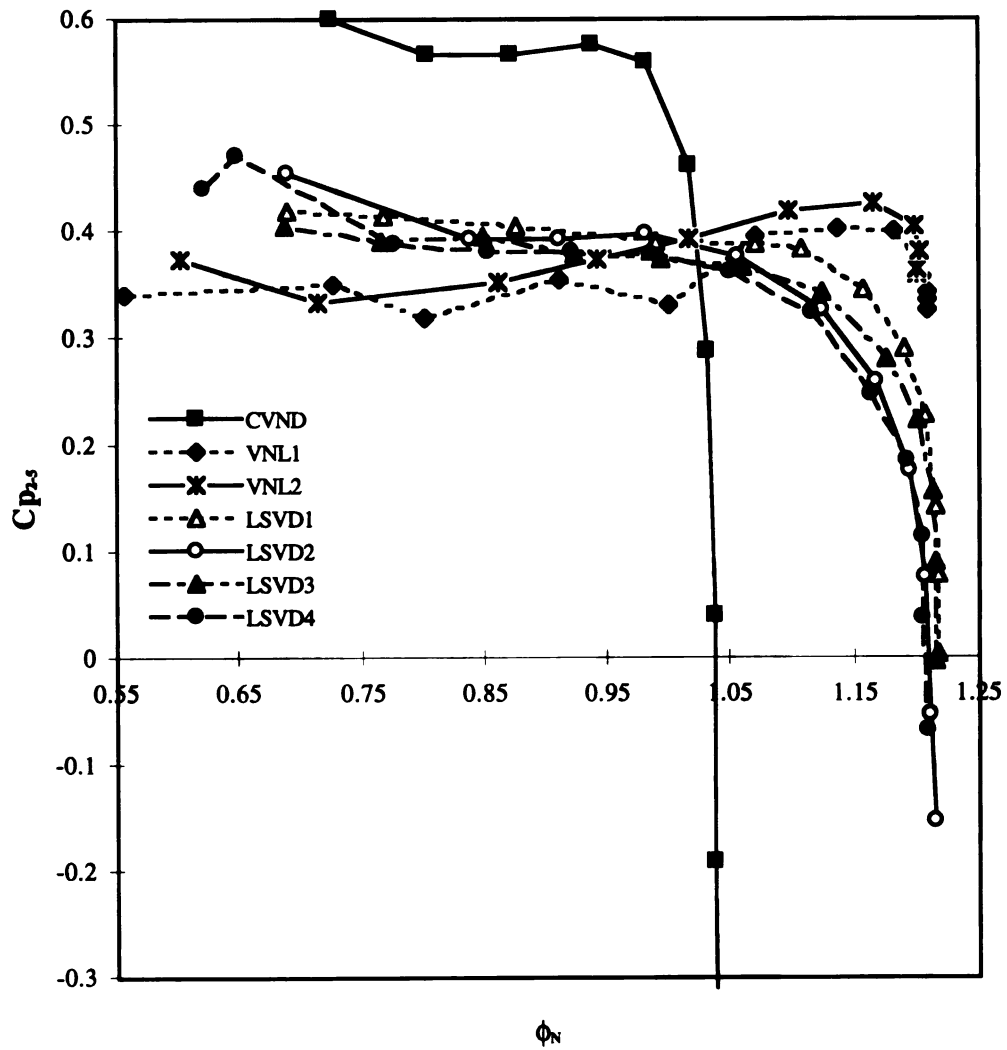**Figure 5.10. Diffuser pressure recovery at M$_t$ = 0.69**

Figure 5.11. Diffuser pressure recovery at M$_t$ = 0.88

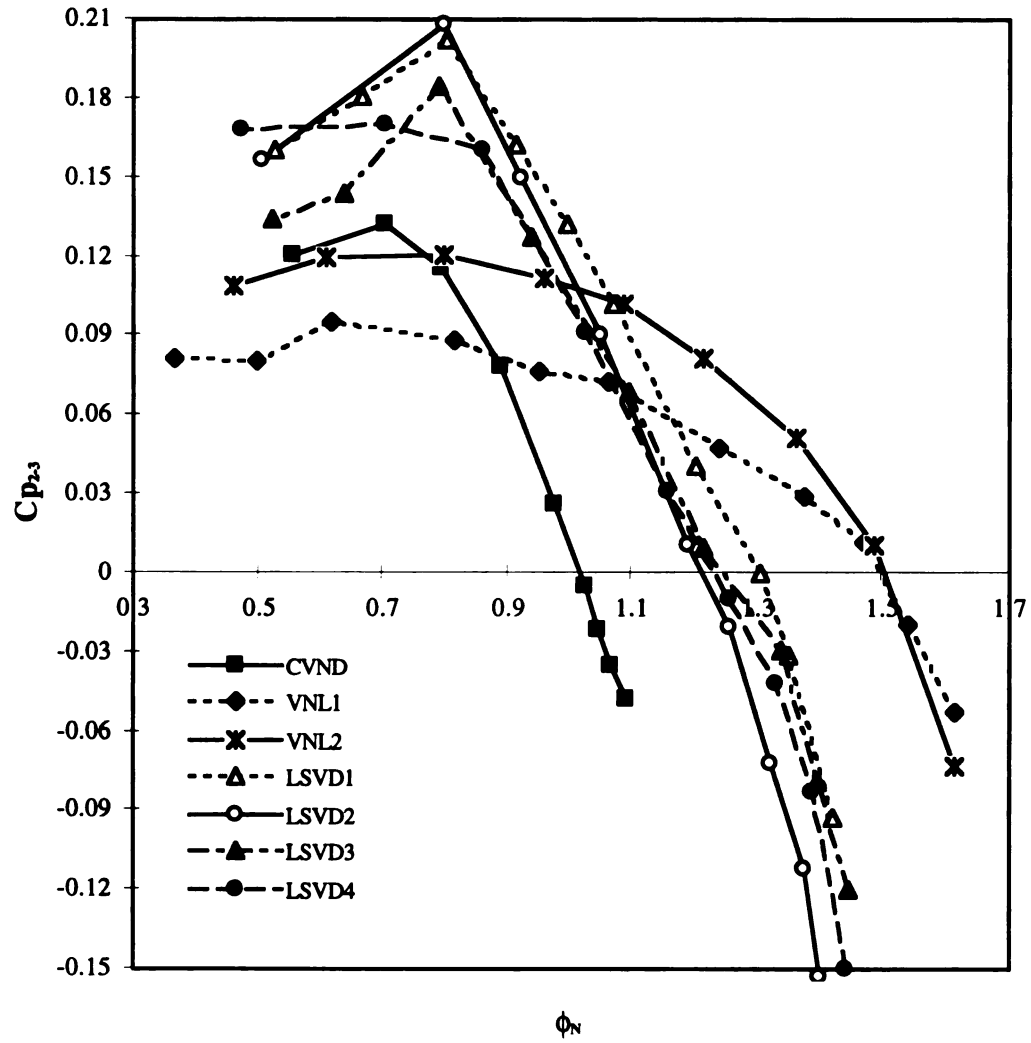**Figure 5.12. Diffuser pressure recovery at $M_t = 1.02$**
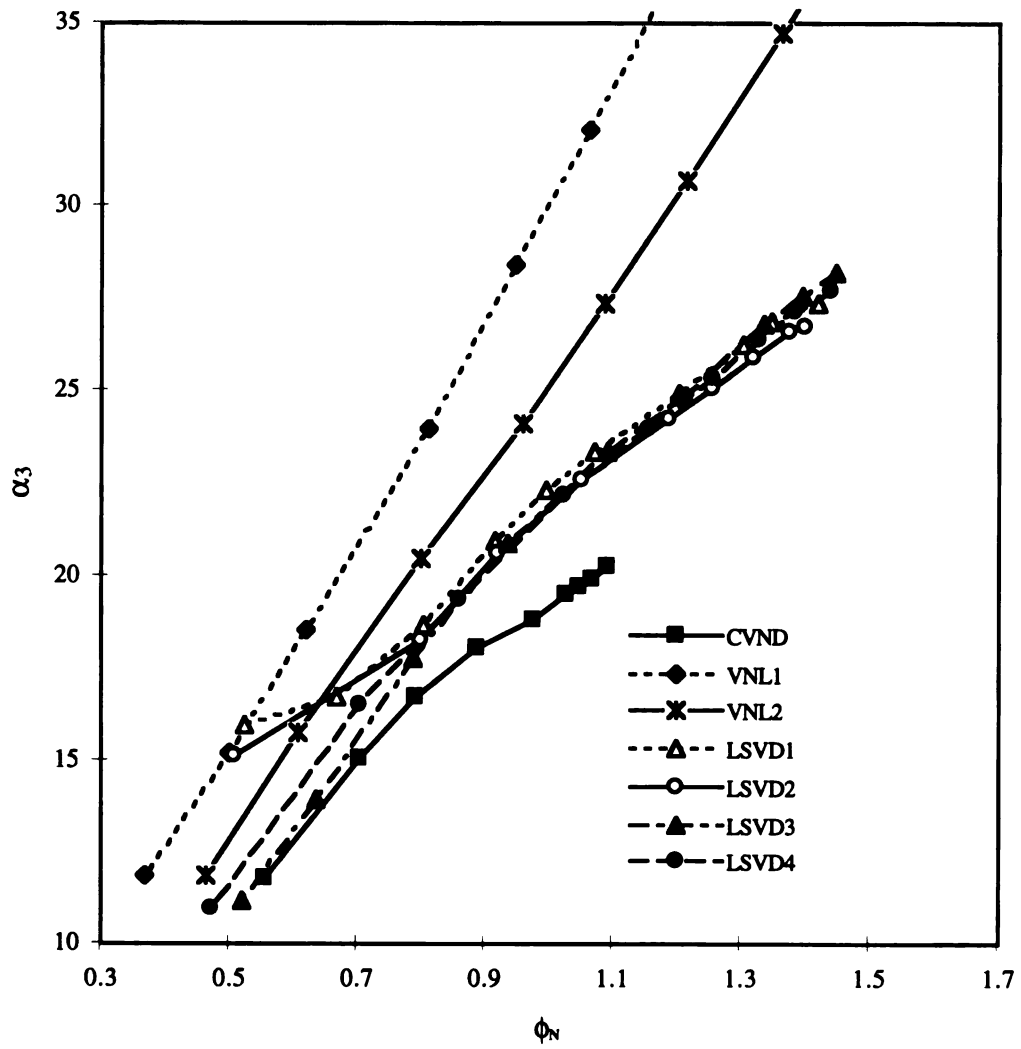
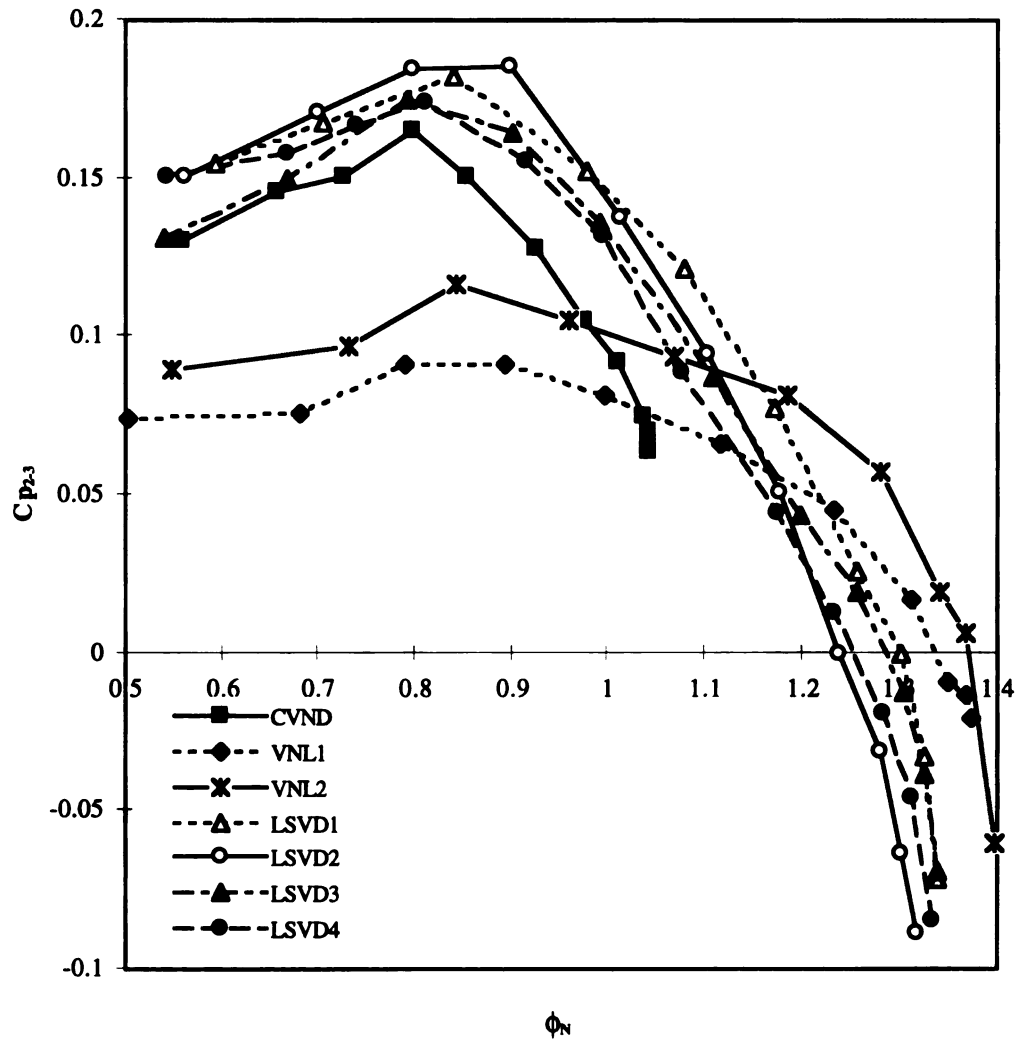**Figure 5.13.** Cp_{2-3} at $M_t = 0.69$

Figure 5.14. Impeller exit flow angle at M_t =0.69

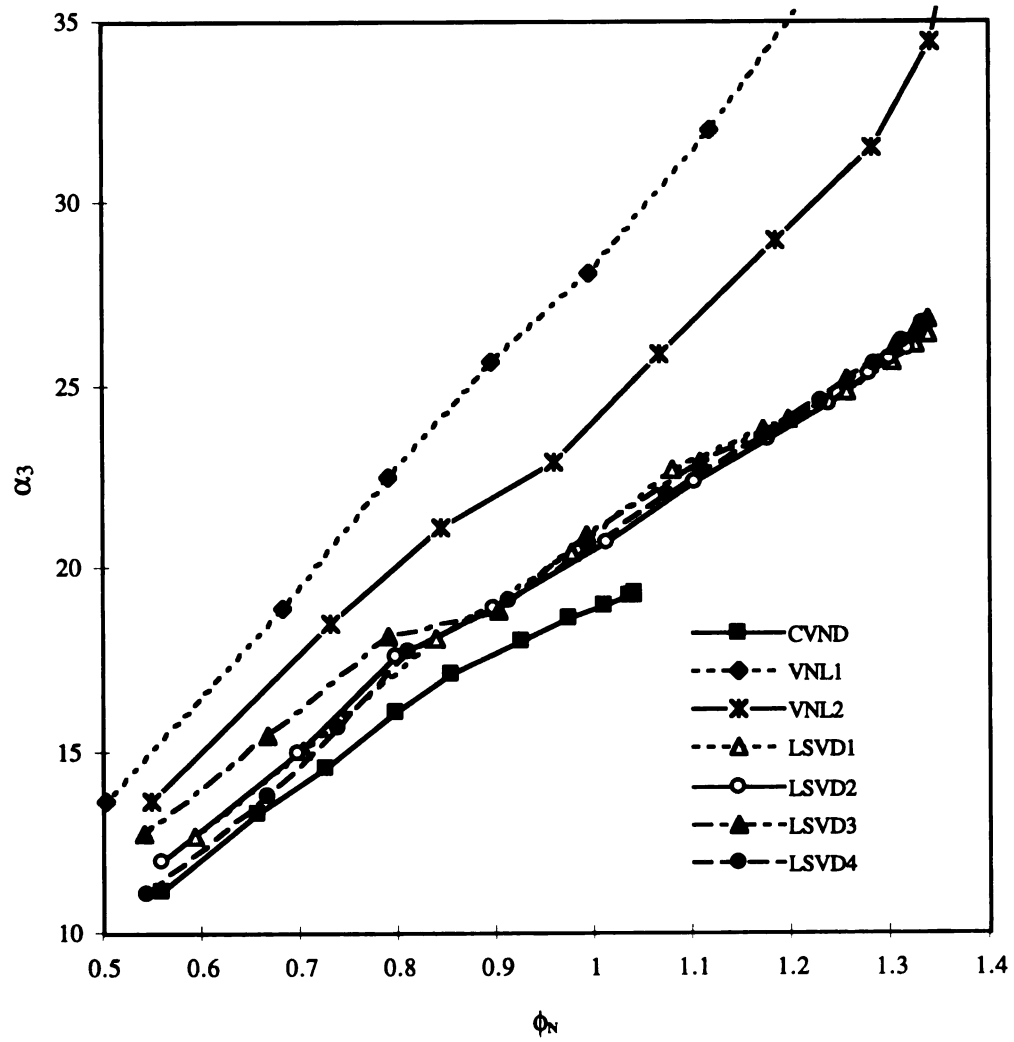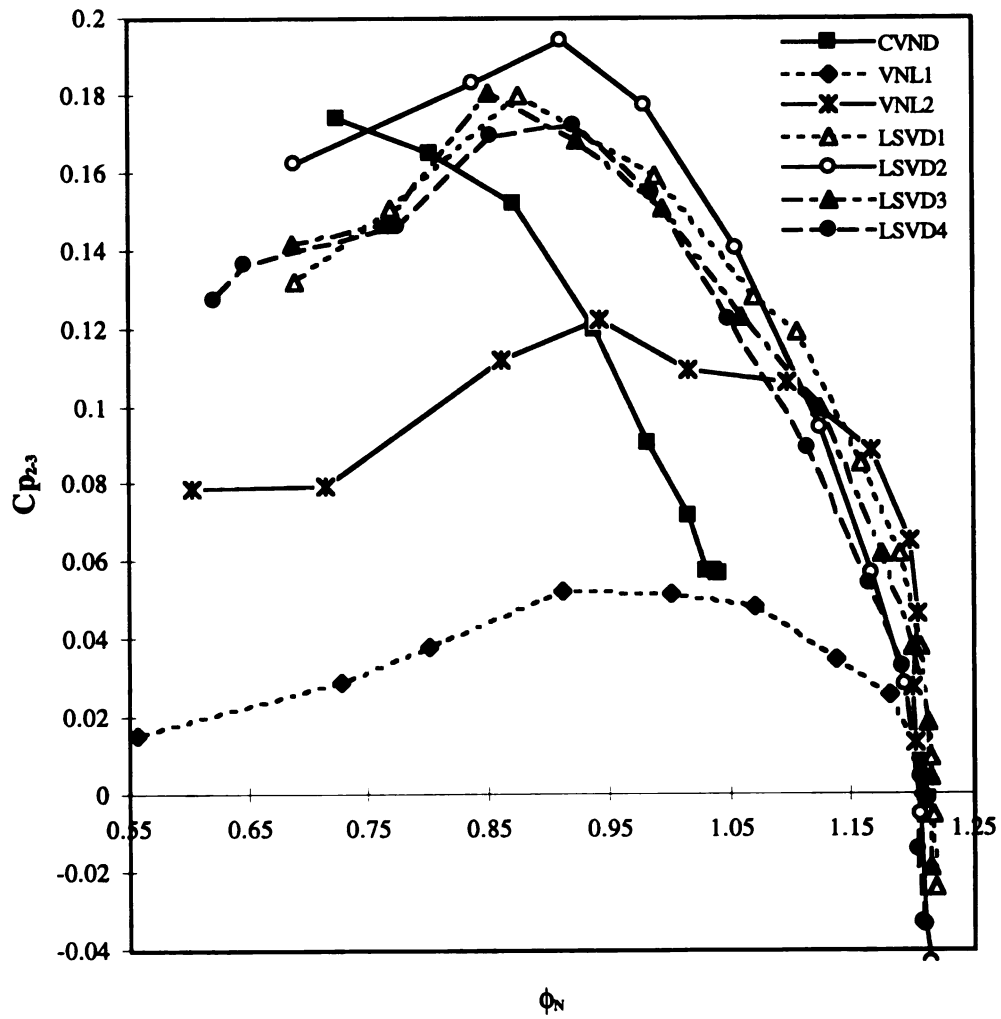**Figure 5.15. Cp_{2-3} at M_t =0.88**

Figure 5.16. Impeller exit flow angle at M_t = 0.88

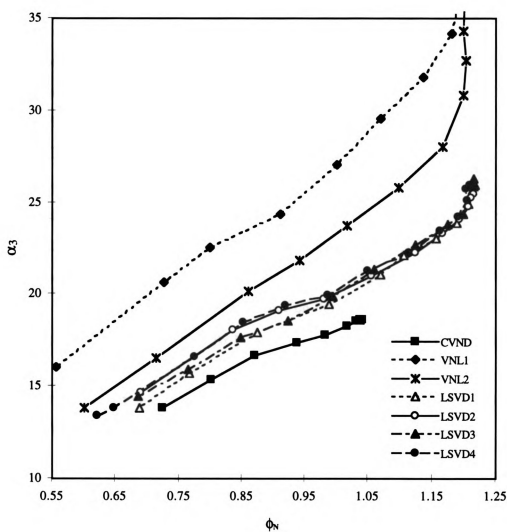**Figure 5.17. Cp_{2-3} at $M_t = 1.02$**

Figure 5.18. Impeller exit flow angle at $M_t = 1.02$

The presence of diffuser vanes is known to have great influence on the flow coming out of the impeller as discussed in section 2.4. It can be seen from the Cp_{2-3} curves of LSVDs and CVND that the diffuser vanes have caused considerable increase in Cp. The Cp_{2-3} of LSVDs at all speeds is almost more than twice that of the vaneless diffusers. Moreover the Cp_{2-3} of LSVDs is greater than the CVND at all speeds. Thus the vanes of the LSVDs have a greater influence on the flow than those of the CVND. The LSVDs with 0.7 solidity seem to attain greater Cp_{2-3} than the 0.6 solidity LSVDs. Moreover LSVD2 (16 Vanes, 0.7 Solidity) has the best Cp_{2-3} at all speeds, and LSVD4 (16 Vanes, 0.6 Solidity) has lowest Cp_{2-3} among all LSVDs. Thus there is an optimum vane number at each solidity which will attain highest Cp_{2-3}.

At all speeds Cp_{2-3} of the CVND and LSVDs tend to have a distinct peak after which the CP_{2-3} drops rapidly. This peak is reached when the incidence angle is equal to $0°$, which can be seen from the corresponding flow angles in the Figure 5.14, Figure 5.16 and Figure 5.18 respectively. As the positive incidence on the vanes increases the Cp_{2-3} of the LSVDs drops, indicating their sensitivity to incidence. The high sensitivity to incidence is due to the flat plate vanes, and this can be improved by using an airfoil shape vanes or increasing the vane leading edge nose radius. However at lower speeds (M_t = 0.88 and 0.69), LSVD4 seems to be more tolerant to positive incidence than the others, which explains the higher flow range attained by LSVD4.

5.4.2 Pressure Recovery in the Vaned Region (Cp_{3-4})

The pressure recovery between the vane leading edge radius and the vane trailing edge radius of the LSVDs along with the Cp of corresponding region of CVND and vaneless diffusers is given in Figure 5.19 through Figure 5.21 for different speeds. At all speeds the maximum Cp_{3-4} of CVND is almost thrice that of the vaneless or LSVDs. Cp_{3-4} of CVND corresponds to the pressure recovery between the vane leading edge and the

middle of the vaned channel. At high mass flow rates the throat chokes, and there are high losses due to the negative incidence on the vanes because of which there is no great pressure recovery. However as the mass flow rate decreases the flow after crossing the vane throat gets into a two dimensional diffuser passage and the Cp obtained is similar to any 2-D straight channel diffuser.

Even though the Cp_{3-4} of the LSVDs tend to behave like CVND at high mass flow rates due to negative incidence losses, at low mass flow rate it is as good as a vaneless diffuser. It can be seen at all speeds that the Cp_{3-4} of LSVD1 is highest and that of the LSVD4 is lowest, where as LSVD2 and LSVD3 seem to have nearly same Cp_{3-4}. This trend is as expected because LSVD1 ($\theta = 14.6°$) has highest blade turning angle and LSVD4 ($\theta = 11.1°$) has lowest, while LSVD2 ($\theta = 12.9°$) and LSVD3 ($\theta = 12.6°$) have nearly same amount of blade turning angle. However, it is hard to believe that a turning of 14.6° has not produced a Cp_{3-4} greater than the vaneless diffuser Cp_{3-4}. One of the possible reason for this is that the pressures were measured near the vane trailing edge pressure side and suction side only, due to which the measured pressures might have been lower than the pressure in the main flow. At the same time it was found that for all LSVDs and at all speeds the

$$Cp_{2-5} = Cp_{2-3} + Cp_{3-4} + Cp_{4-5}.$$

Each of these Cps were individually measured, thus indicating that the vanes of LSVDs were providing the turning to the flow with an accompanied loss in static pressure. In order to understand the actual dynamics of the pressure recovery in the vaned region of a LSVD, it might be important to measure pressures along the vanes and at several locations circumferentially between the two vanes.
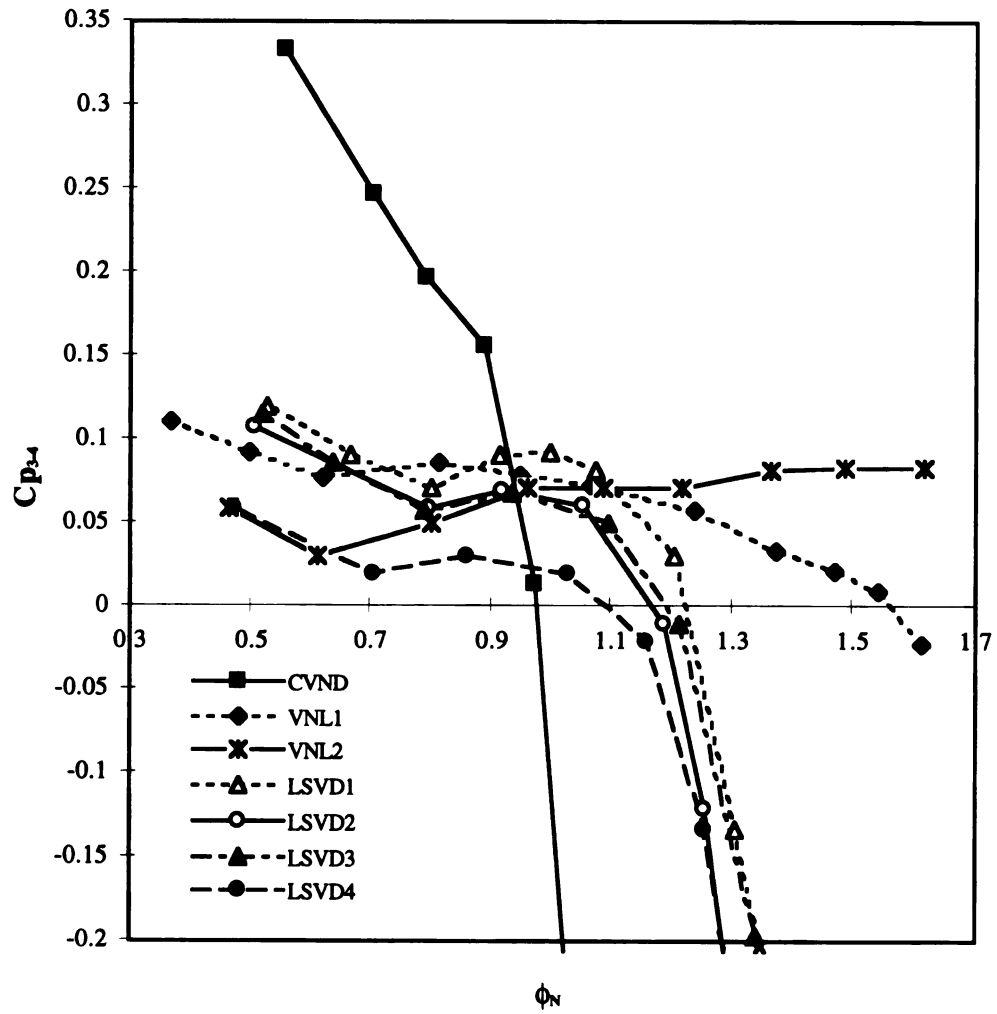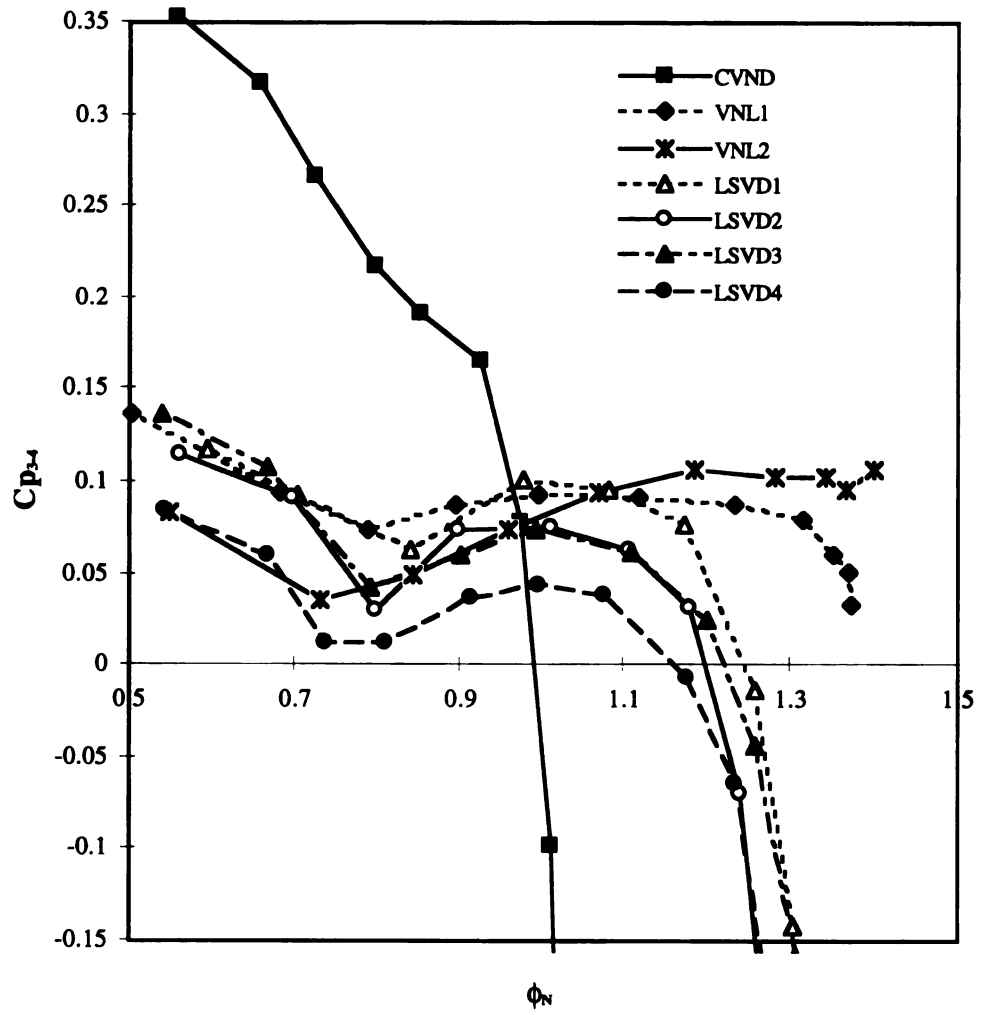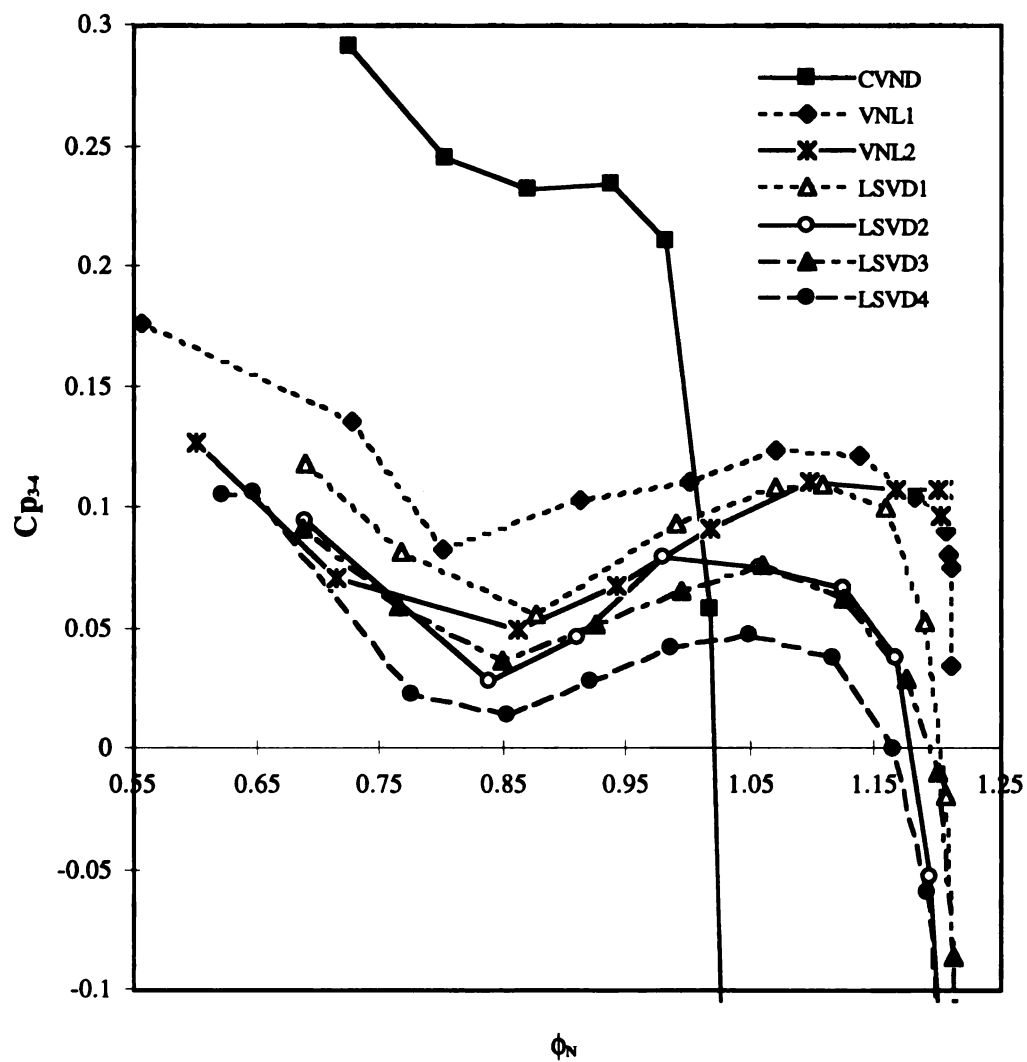
Figure 5.19. Cp$_{3-4}$ at M$_t$ = 0.69

Figure 5.20. Cp$_{3-4}$ at M$_t$ = 0.88

Figure 5.21. Cp$_{3-4}$ at M$_t$ = 1.02

5.4.3 Pressure Recovery Cp_{2-4}

By comparing the Cp_{2-5} (Figure 5.10 through Figure 5.12) and the Cp_{2-} (Figure 5.22 through Figure 5.24) curves one can see that more than 75% of the pressure recovery of the LSVDs occurs between the impeller exit (station 2) and the vane trailing edge radius (station 4). It can be seen that the Cp_{2-4} of LSVD1 is highest and that of LSVD4 is lowest in accordance with the blade turning angle, thus showing that the vanes with higher turning can attain higher Cp up to the vane exit radius. However from the Cp_{2-5} curves it can be seen that at low speeds ($M_t = 0.88$ and 0.69) and low mass flow rates the LSVDs with 0.6 solidity had better Cp_{2-5}. This shows that at low speeds there is an optimum vaneless space needed after the vanes of LSVDs. At high speed ($M_t = 1.02$) this phenomena is not seen as the diffuser stalls at higher mass flow rates. Thus the effectiveness of the downstream vaneless space is not clearly seen in Cp_{2-5} at high speed. Moreover the Cp_{2-4} attained by the LSVDs is similar to the pressure recovery of the conventional vaned diffusers between the diffuser inlet to the vane throat as reported by Baghdadi (1977), Kano et al. (1982) and Stein and Rautenberg (1988).

5.4.4 Downstream Vaneless Space Pressure Recovery (Cp_{4-5})

It can be seen that at all speeds the Cp_{4-5} of all diffusers is higher at high mass flow rates than at low mass flow rates (Figure 5.25 through Figure 5.27). This is because at high mass flow rates the flow angles are higher and thus the flow path is small and losses are lower. As the mass flow decreases the Cp_{4-5} of CVND decreases because the boundary layers along the channel walls become thick and separate. However the Cp_{4-5} of LSVDs at low mass flow rates is either equal to or a little less than the vaneless diffusers. Since the Cp_{2-4} of LSVDs is greater than that of the vaneless diffusers over a wide range of flow rate, the hub and shroud boundary layers at the vane exit of the LSVDs are thick due to which the Cp_{4-5} of LSVDs is not better than the vaneless diffusers.

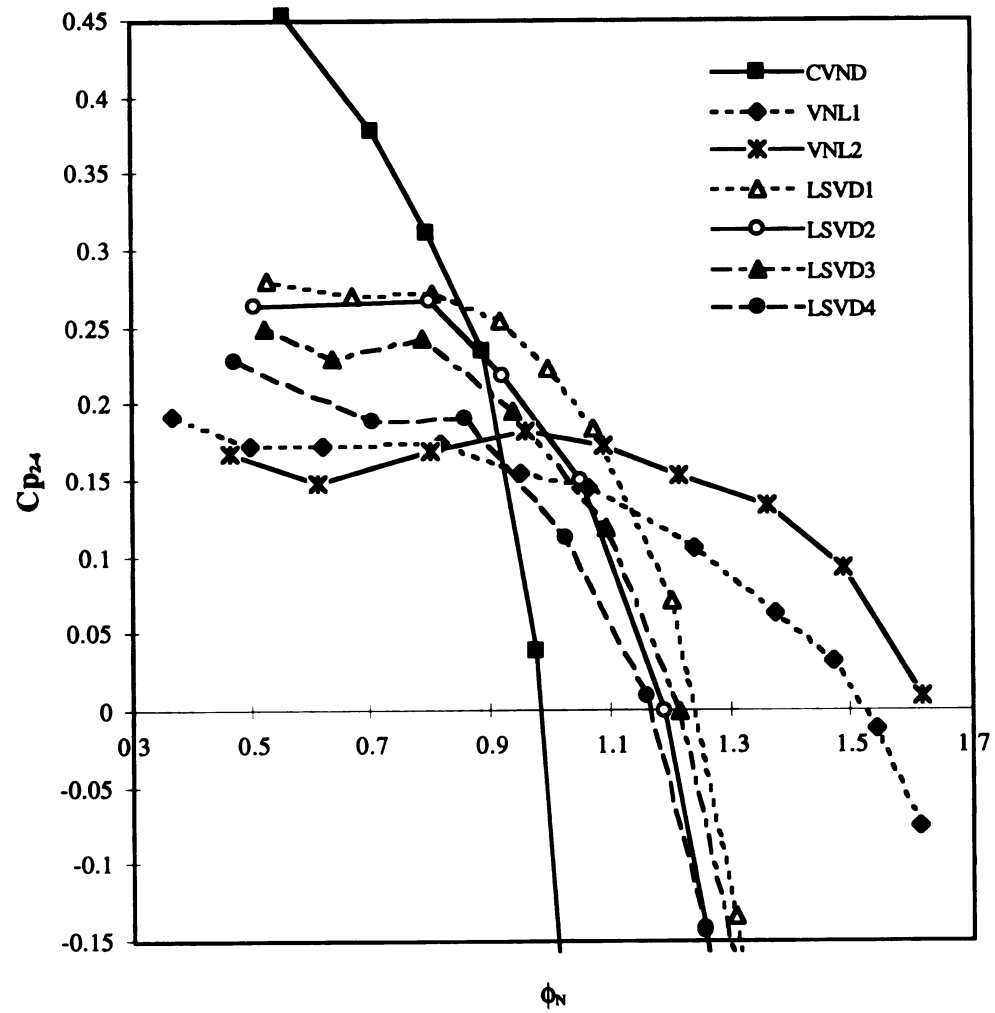**Figure 5.22. Cp_{2-4} at $M_t = 0.69$**

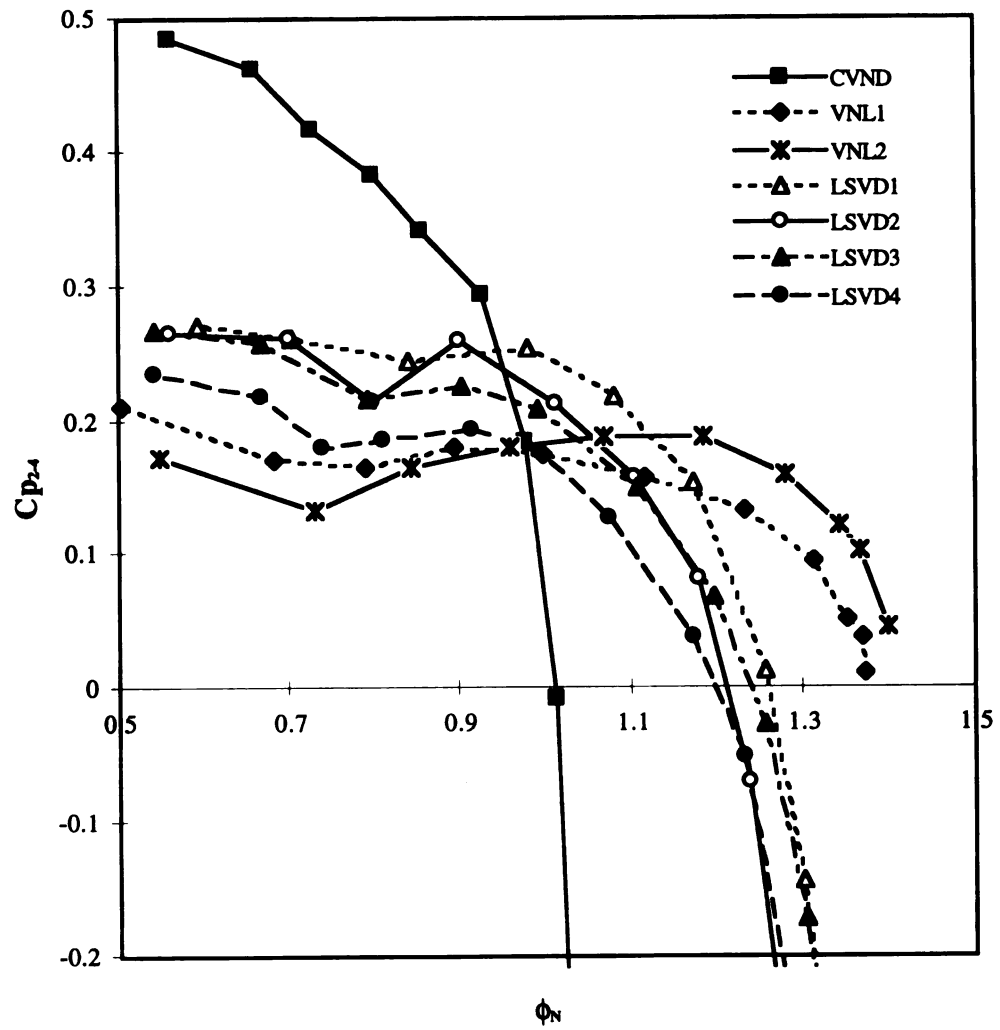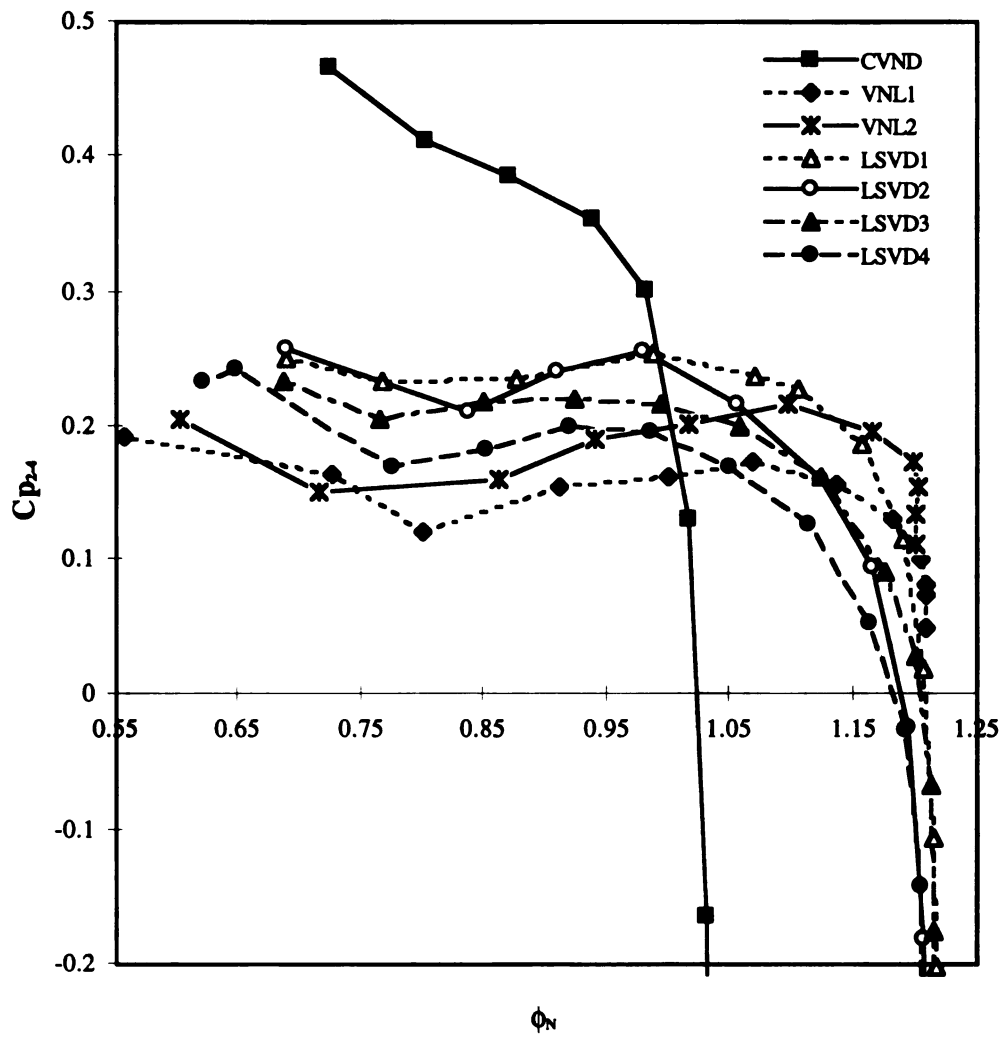**Figure 5.23. Cp_{2-4} at $M_t = 0.88$**

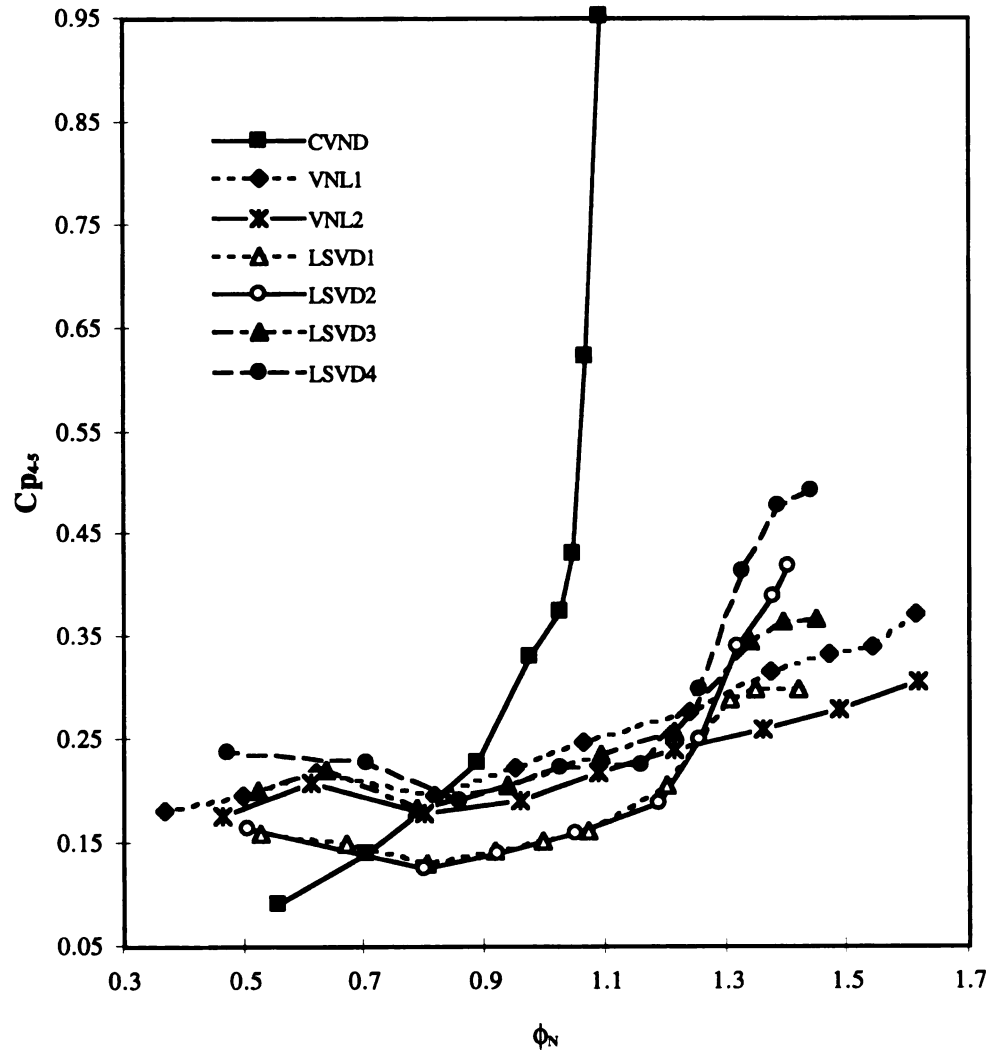**Figure 5.24. Cp_{2-4} at M_t = 1.02**

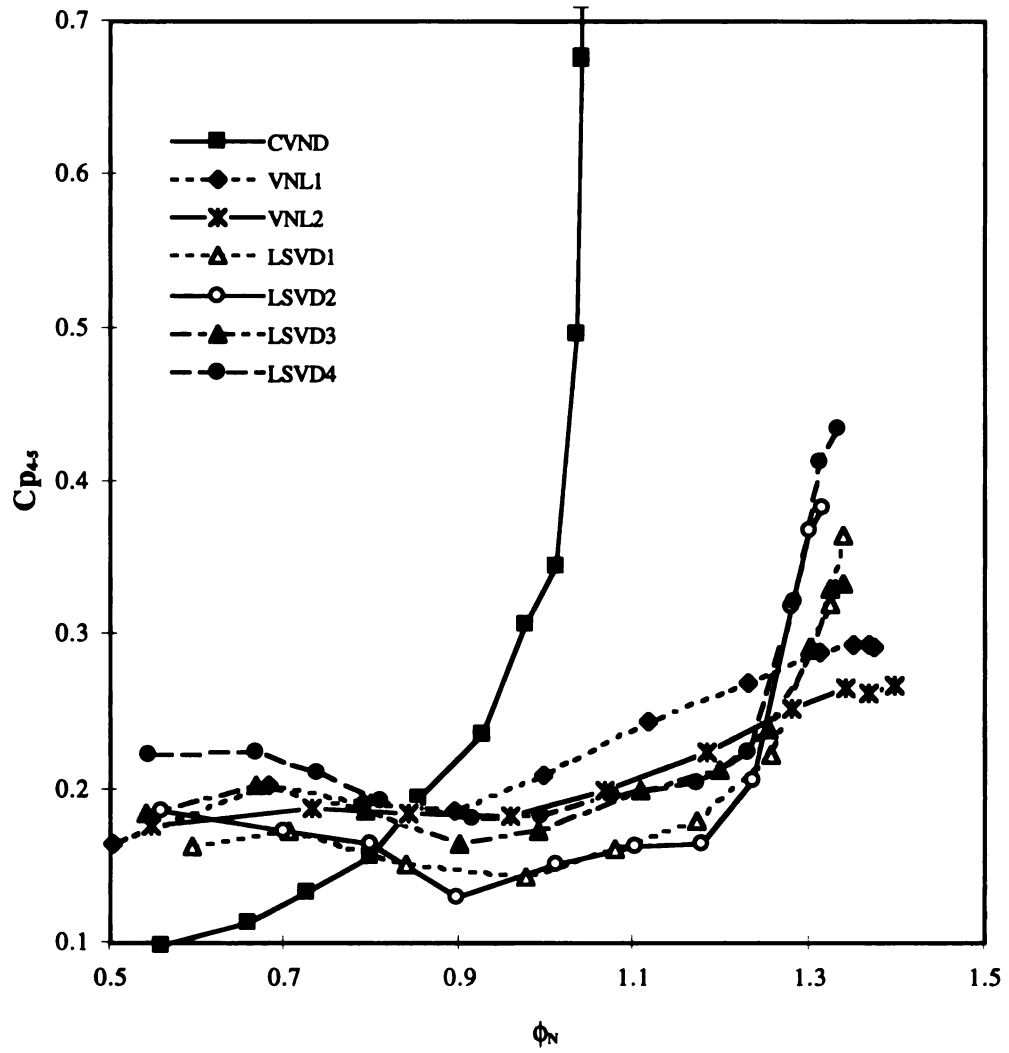**Figure 5.25. Cp$_{4.5}$ at M$_t$ = 0.69**
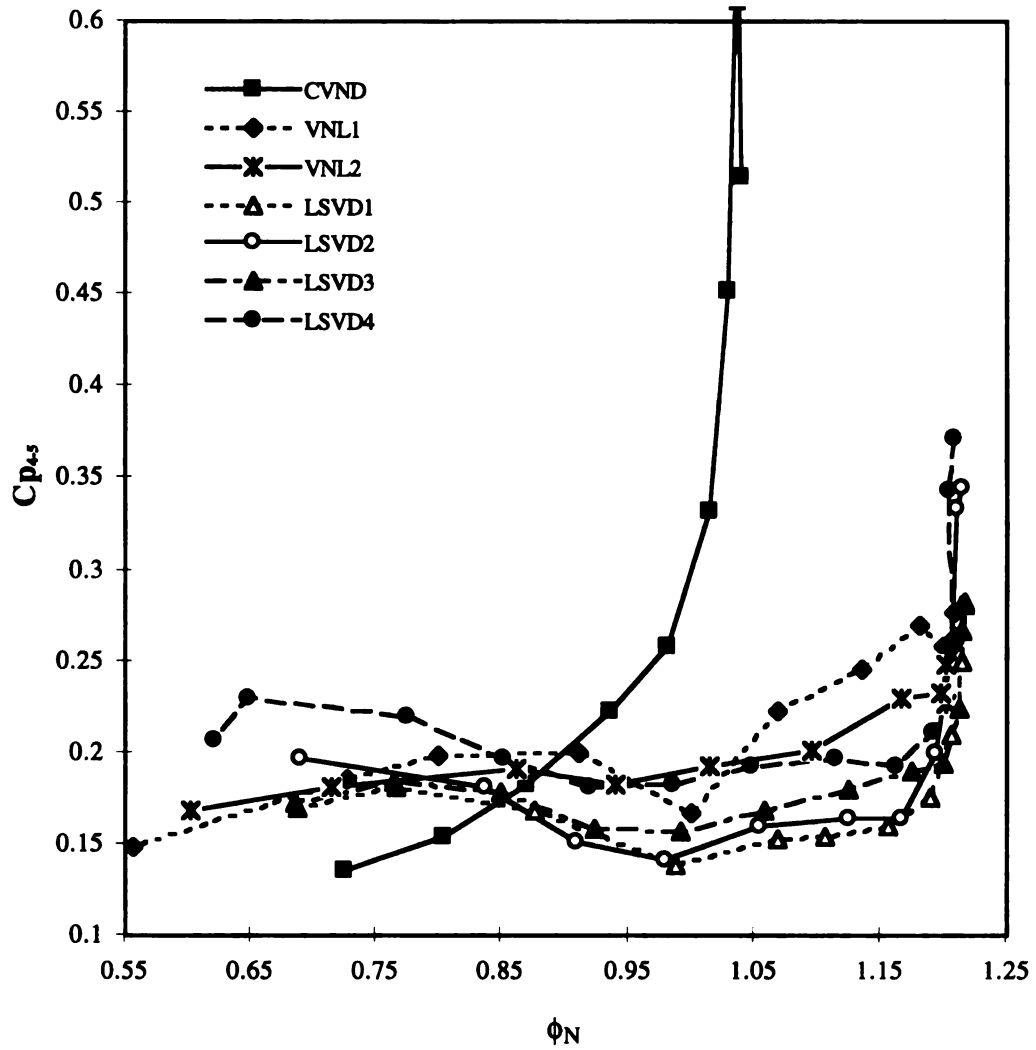
Figure 5.26. Cp_{4-5} at $M_t = 0.88$

Figure 5.27. Cp$_{4-5}$ at M$_t$ = 1.02

It can also be seen that the LSVDs with 0.7 solidity have lower Cp_{4-5} than the 0.6 solidity LSVDs. This could be explained from the lower Cp_{2-4} of 0.6 solidity LSVDs. As Cp_{2-4} is lower the boundary layers are more tolerant to the separation than those of 0.7 solidity LSVDs due to which 0.6 LSVDs tend to have better flow range too.

5.5 Loss Coefficient (ξ)

Figure 5.28 through Figure 5.30 show the loss coefficient of all the diffusers along with the downstream volute. At all speeds the loss coefficient of the CVND is highest at high mass flow rates and lowest at low mass flow rates. At the other extreme the vaneless diffusers have the lowest loss coefficient at high mass flow rates and highest loss at low mass flow rates. The LSVDs loss coefficients are in-between these two extremes at all mass flow rates. As a general trend the LSVDs with 14 vanes have lower loss coefficients than the 16 vane LSVDs at high mass flow rates at all speeds. However at low mass flow rates it will be unfair to draw any conclusions as the total pressures measured at station 3 are not reliable due to the highly unsteady flow at these flow rates.

5.6 Unsteady Behaviors in the Compressor Stage

The unsteady flow behaviors in the inducer, the impeller, and the diffuser were determined for all seven configurations at each operating point and at every speed. Because of similar patterns at all rotational speeds the data of $M_t = 1.02$ are presented here for VNL2, CVND and LSVD2 configurations. The data from transducer C are left out because they are almost the same as transducer B. Both transducer C and transducer B were located in the impeller at the same radius but different circumferential position.

Since most rotating stall signals reported in the literature were below the rotational speed of the impeller, the data between 0-500 Hz is plotted here. The following parameters were used for the calculation of spectral functions
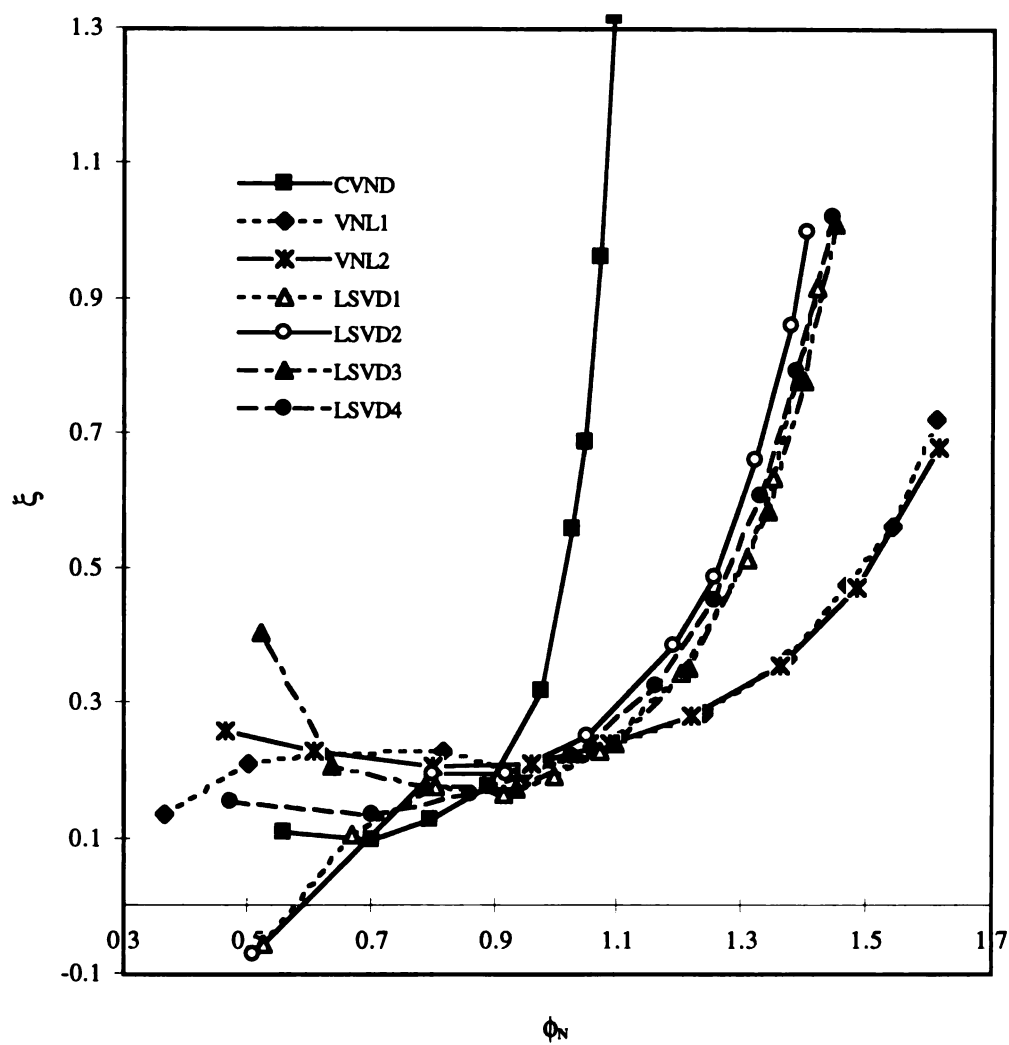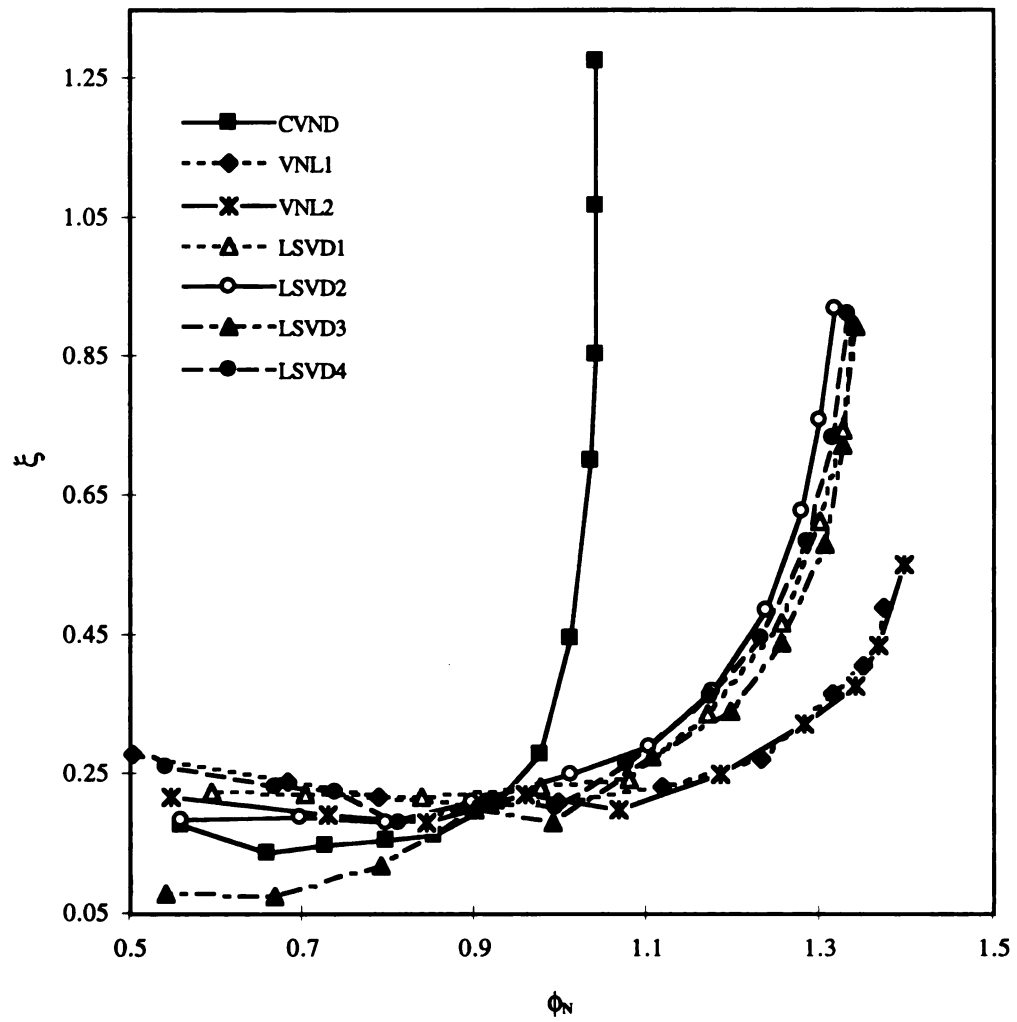
Figure 5.28. Loss coefficient at $M_t = 0.69$

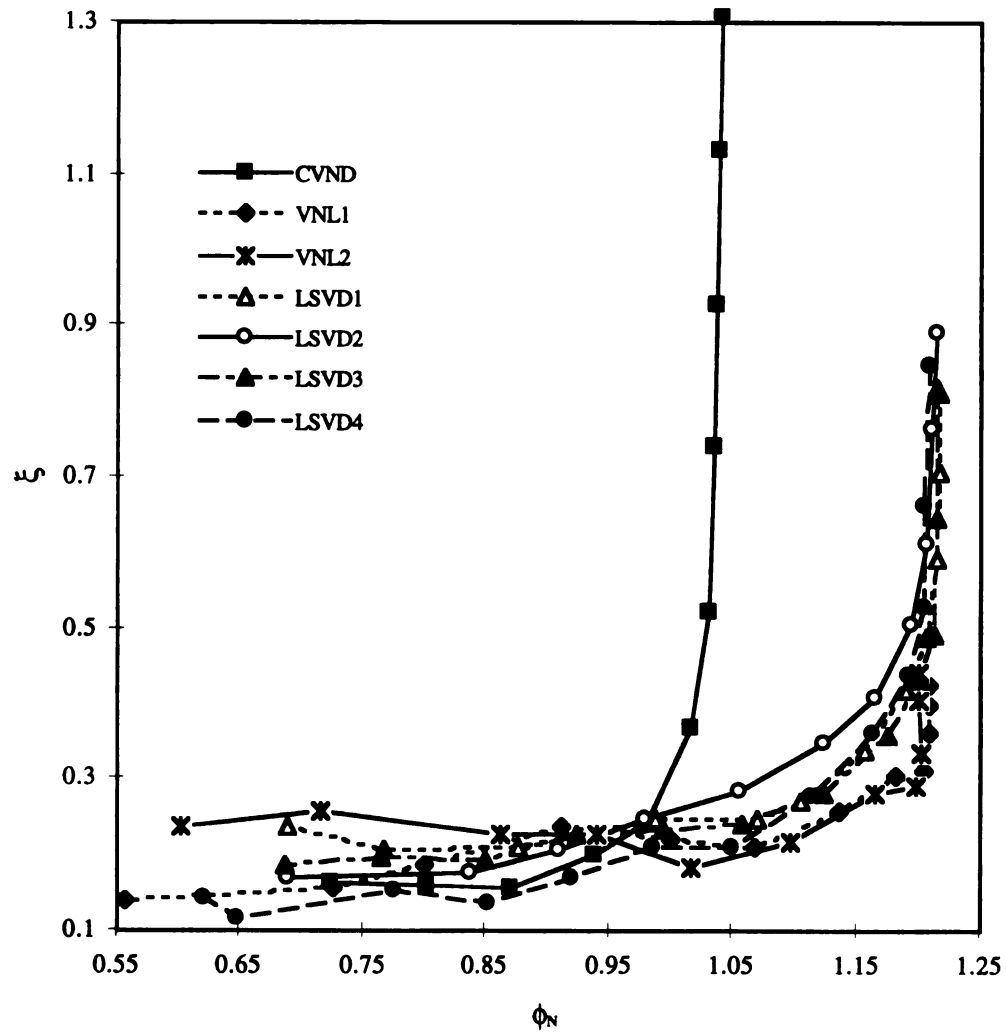**Figure 5.29. Loss coefficient at $M_t = 0.88$**

Figure 5.30. Loss coefficient at $M_t = 1.02$

• 8 records from each transducer were captured

• the sampling frequency was 2048 Hz

• each record had 1024 discrete points, which corresponds to 0.5 seconds

• all records were detrended

• a Hanning window was applied

• 50% overlapping was used

• the power spectrum, the cross spectrum, the coherence, and the phase shift were calculated

• the output is represented in terms of decibels, the reference being 1×10^{-3} bar.

5.6.1 Unsteady Flow in the Inducer

Figure 5.31, Figure 5.32, and Figure 5.33 are the power spectra of the signal from transducer A at high speed for VNL2, CVND and LSVD2 respectively. The rotational frequency of 460 Hz is clearly seen in all configurations along with a weak peak at 360 Hz. This weak peak was common to all transducers and occurred at $M_t = 1.02$ only. Thus, it is presumed that 360 Hz peak is either an electrical or rotodynamic component of the compressor system.

No significant pressure fluctuations are found in the inducer at high mass flow rates (Op#1), irrespective of the diffuser configuration. However at low mass flow rates the pressure fluctuations grow at Op#10 for VNL2 (Figure 5.31) and LSVD2 (Figure 5.33) configurations. These fluctuations indicate the onset of inducer stall in VNL2 and LSVD2 configurations. In the case of CVND (Figure 5.32) configuration no such fluctuations are seen at any operating flow point. Thus, clearly showing that the stage surge was caused due to the CVND diffuser stall at a higher flow rate than the flow rate causing critical incidence at the inducer.
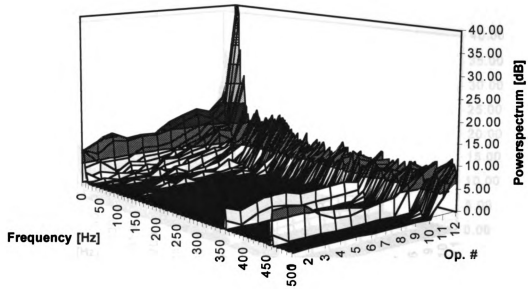
Figure 5.31. Power spectrum - Transducer A/VNL2
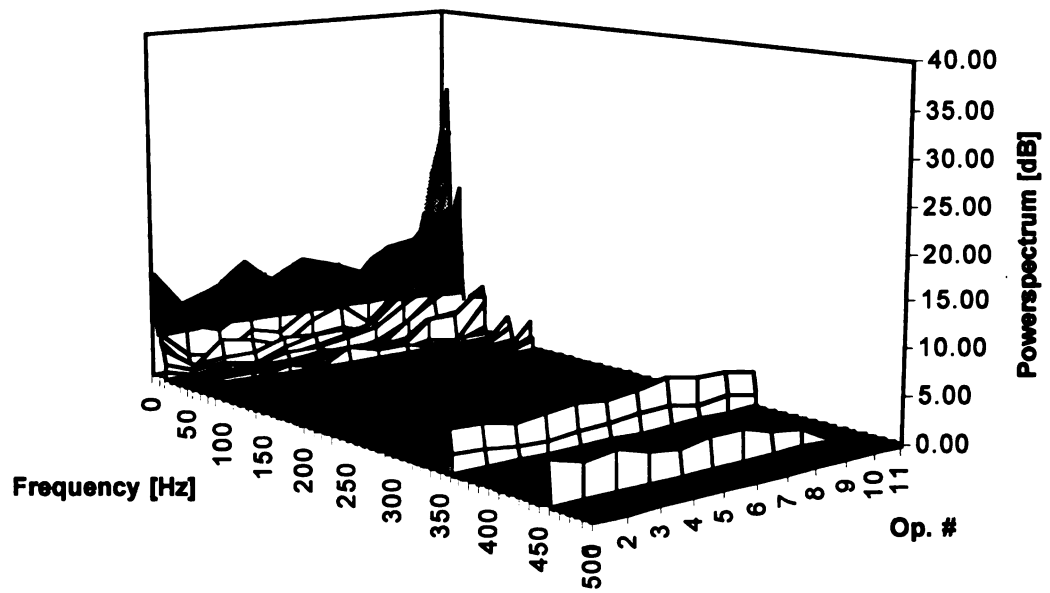
Figure 5.32. Power spectrum - Transducer A/CVND
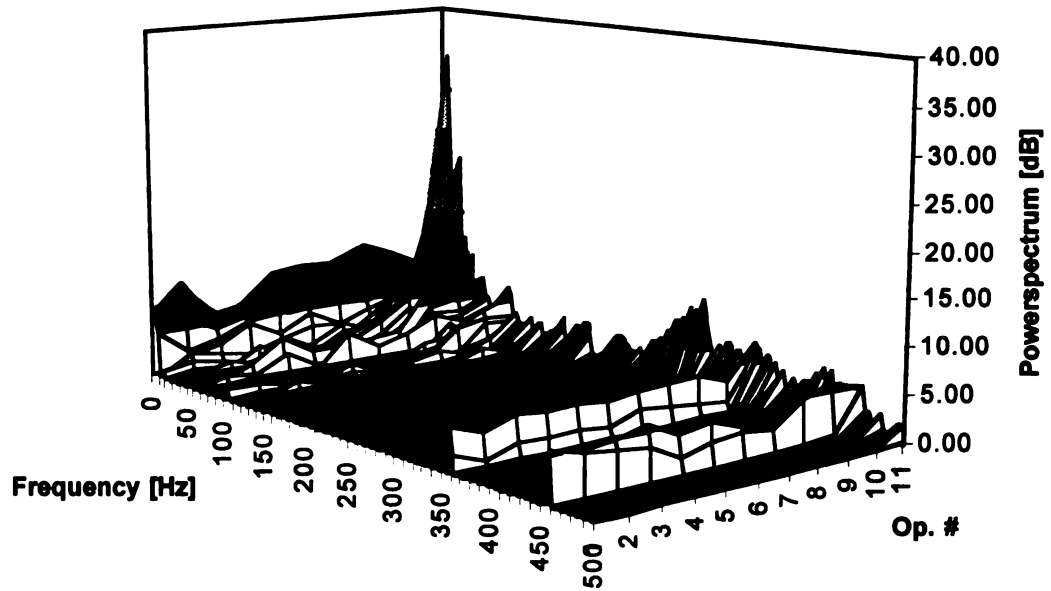
Figure 5.33. Power spectrum - Transducer A/LSVD2

A strong peak at 6 Hz is found in all transducers of VNL2 configuration, and a similar peak at 8 Hz was present in all transducers for CVND and LSVD2 configurations. The energy at this peak is between 30 and 46 dB which is much higher than at any other peak. Since the peak occurred at the same frequency in all transducer signals, it can be classified as surge peak. The peak in CVND configuration is weaker in energy than the peak at LSVD2 or VNL2 configuration indicating, the stage with CVND might have been operated just up to the onset of the surge.

5.6.2 Unsteady Flow in the Impeller

The power spectra of the signals obtained from transducer B for VNL2, CVND, and LSVD2 configurations are presented in Figure 5.34, Figure 5.35, and Figure 5.36 respectively. Since transducer B is located in the impeller, the energy of the signals is generally higher than in the inducer. The rotational frequency of 460 Hz is seen in all configurations with higher energy than in the inducer.

From Figure 5.34 it can be seen that the pressure fluctuations have medium level of energy over the whole frequency range at the first four operating points of the VNL2 configuration. The high energy in the fluctuations is due to the inducer choke and the associated losses. The level of energy decreases between the operating points 5 and 9 indicating that the flow in the impeller is stable. The operating range between Op#5 and Op#9 corresponds to the range where the stage had its best performance as seen in Figure 5.3. At Op#10 the fluctuations begin to increase and at Op#12, two peaks, one at 488 Hz and the other at 6 Hz are clearly seen. The peak at 6 Hz as mentioned earlier corresponds to the stage surge and the peak at 488 Hz was found to be due to a rotating stall in the diffuser.

Only small fluctuations are seen in the power spectra of transducer B for the CVND (Figure 5.35) configuration, except at the last operating point. Thus, the impeller is not the
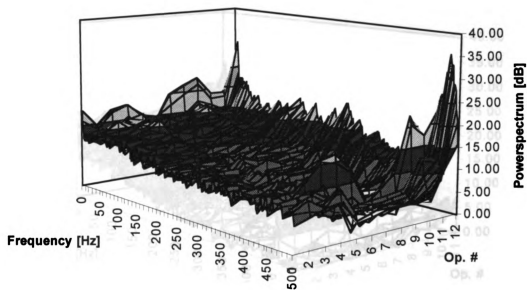
Figure 5.34. Power spectrum - Transducer B/VNL2
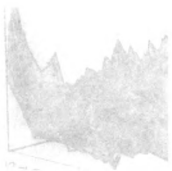
Figure 5.35. Power spectrum - Transducer B/CVND

Figure 5.36. Power spectrum - Transducer B/LSVD2

critical component for this configuration and the 8 Hz peak seen at the last operating point is the surge.

The unsteady patterns in LSVD2 configuration (Figure 5.36) are similar to the patterns found in VNL2 configuration. The energy level over the whole frequency range is slightly higher at first three operating points and then decreases betwe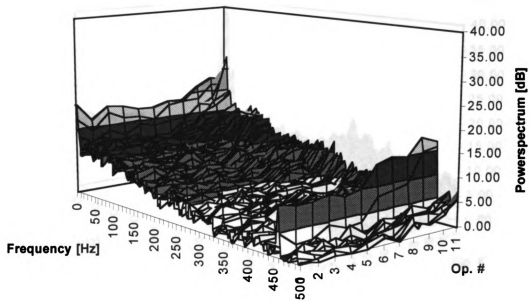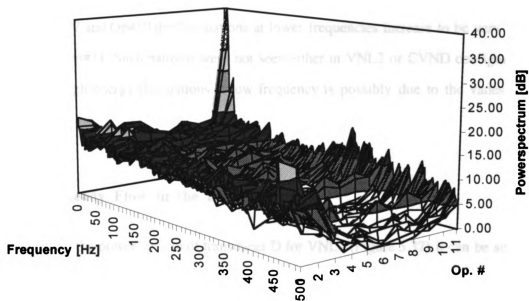en Op#4 and Op#6. The higher energy at the first three operating points is due to the inducer choke. However between Op#7 and Op#10 the fluctuations at lower frequencies increase to be very high at Op#10 and Op#11. Such patterns were not seen either in VNL2 or CVND configurations. Thus, this high energy fluctuations at low frequency is possibly due to the vanes of the LSVD2.

5.6.3 Unsteady Flow in the Diffuser

From the power spectra of transducer D for VNL2 (Figure 5.37) it can be seen that the pressure fluctuations have very low energy for the first nine operating points. Thus, the diffuser operates very stable in the operating range and has no negative effects on the stage stability. Between the Op#10 and Op#12 the fluctuations increase over the whole frequency range. The peak at 6 Hz has the highest energy level at transducer D than at any other transducer. This is expected as transducer D is located in the diffuser and the static pressure is highest in the diffuser.

In the case of CVND configuration no instabilities are seen between Op#1 to Op#4, as the diffuser is choked (Figure 5.38). The pressure fluctuations increase between the operating point 5 and 7. These increased fluctuations are caused by the pressure side stall of the vanes at negative incidence. However, operating points 8 and 9 seem to have much less fluctuations than at Op#7. From Figure 5.3 it can be seen that the stage attained highest head (ψ_N) at these operating points, thus the flow is stable. The fluctuations again increase

Figure 5.37. Power spectrum - Transducer D/VNL2
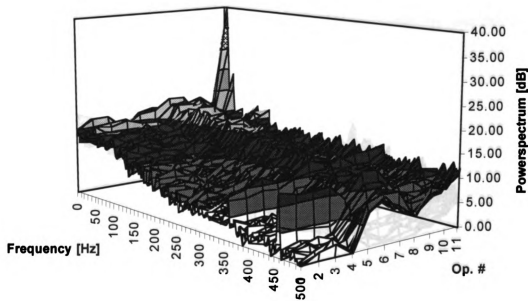
Figure 5.38. Power spectrum - Transducer D/CVND

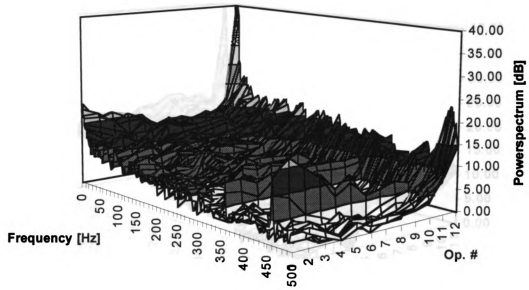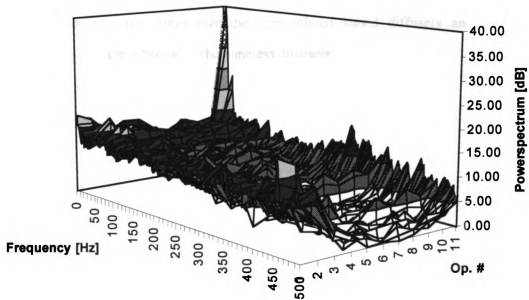**Figure 5.39. Power spectrum - Transducer D/LSVD2**

from Op#10 and the surge peak at Op#11 can be seen with 8 Hz frequency.

Figure 5.39 shows the power spectra of transducer D in LSVD2. Very high fluctuations are seen in the first two operating points due to the pressure side stall of the vanes. The fluctuations between Op#4 and Op#10 are small indicating that the diffuser does not cause any instability in this operating range. However at operating point 11 the energy in the fluctuations increases and the surge peak is seen at 8 Hz. Thus, LSVDs seem to have a wider stable operating range than the conventional vaned diffusers and this stable operating range is almost equal to the vaneless diffusers.

6. CONCLUSIONS AND RECOMMENDATIONS

The low solidity vaned diffusers, which have emerged as possible alternative to the vaneless and conventional vaned diffusers for the centrifugal compressors were studied both numerically and experimentally. The numerical analysis of the flow through the low solidity vaned diffusers provided vital information regarding the aerodynamic and geometric parameters affecting the performance. The results of 3-D viscous calculations qualitatively compared well with the experimental observations, and it was found that the low solidity vaned diffusers stalled when the vane suction surface separation was accompanied by the end wall separation. The numerical experimentation with the geometric parameters revealed that the vane stall of low solidity vaned diffusers could be delayed by reducing the blade loading or blade turning angle at the cost of pressure recovery of the diffuser. It was also observed that the stable operating range of the compressor with low solidity vaned diffusers could be increased by decreasing the solidity. However, by reducing the solidity the blade turning angle was increased, which would have provided higher pressure recovery, and needed experimental verification.

Based on the observations of numerical analysis and a detailed study of the conventional vaned diffuser design and flow phenomena, four new low solidity vaned diffusers were designed for experimental analysis. The new designs were conceived with a view to study the effect of blade loading or the blade turning angle and the solidity of the vanes.

The four new low solidity vaned diffusers were tested downstream of the same impeller along with two vaneless diffusers and one conventional vaned diffuser. The

experiments were performed at three different impeller tip Mach numbers to study the effect of rotational speed on the performance of the diffusers. The comparison of the overall performance of the low solidity vaned diffusers with the vaneless and vaned diffusers showed the clear advantage of the low solidity vaned diffusers over vaneless and vaned diffusers in terms of both the flow range and the efficiency. The peak efficiency of the compressor increased with an increase in the blade turning angle of the low solidity vaned diffuser while the flow range suffered. It was observed that below an optimum blade turning angle the low solidity vaned diffusers tend to behave like a vaneless diffuser in terms of operating flow range. Moreover, for a given M_t there seemed to be an optimum blade turning angle which would provide highest peak efficiency without significant loss in flow range. The effect of the solidity on the peak efficiency of the compressor stage was very small while lower solidity diffusers were able to provide better flow range. These observations from the experiments confirm the numerical results: by lowering the solidity flow range can be improved without any significant loss in performance.

In addition to studying the overall performance of the stage with different diffusers, the pressure recovery phenomena in each diffuser was studied in detail. The low solidity vaned diffusers were divided into three regions 1) the upstream vaneless space, 2) the vaned region, and 3) the downstream vaneless space, to analyze the pressure recovery in the diffuser. From this analysis it was found that nearly 75% of the total pressure recovery in the low solidity vaned diffusers occurred between the impeller exit and the vane trailing edge radius. It was also found that the pressure recovery between impeller exit and vane leading edge was much higher in the case of low solidity vaned diffusers than the conventional vaned or vaneless diffusers. While the pressure recovery of the vaned region of the low solidity vaned diffusers was no better than the corresponding region of a vaneless diffuser, in spite of the high loading of the vanes. From the experimental results, it was clear that having large vaneless space downstream of the low solidity vanes would

only provide a marginal improvement in the pressure recovery with added danger of diffuser stall.

From the results of present experiments and the data available in the public domain, correlation of blade turning angle and the solidity to the pressure recovery of the low solidity vaned diffusers can be drawn and assimilated into a 1-D prediction procedure for centrifugal compressor. The result would be a preliminary prediction procedure of future designs of low solidity vaned diffusers.

It is recommended that the pressure recovery in the vaned region be analyzed by measuring the static pressure distribution both around the vane and across the two adjacent vanes. This can be accomplished by having static taps at regular intervals around the vane to cover both the suction and the pressure surfaces. In addition to these, static taps at several radii between the vane leading edge and trailing edge are needed across two vanes, in order to obtain a complete pressure distribution which will reveal the details of pressure recovery phenomena.

The reduction of solidity has proved to be advantageous both in terms of flow range and peak efficiency. However, in the present study the reduction in solidity caused a reduction in blade turning angle too. Thus, it will be interesting to test some low solidity vaned diffusers of lower solidity and high blade turning angles, to observe if there is any optimum relation between the solidity and blade turning angle with respect to the performance.

However, much testing remains to be done with regards to some of the parameters such as the leading edge radius ratio, the vane shape and the vane downstream vaneless space, which were not addressed in the present study. Moreover, the effect of the low solidity vaned diffuser vanes on the impeller internal and discharge flow is vital and needs investigation.

Even though many more investigations are needed to completely understand the flow and pressure recovery phenomena in the low solidity vaned diffusers, they have

certainly shown promise both in terms of higher operating flow range and high efficiency. Thus, it will not be too ambitious to say that the low solidity vaned diffusers are going to be the diffusers of future for centrifugal compressors, and it is only a matter of time before they find wide use in all kinds of centrifugal compressor applications.

BIBLIOGRAPHY

BIBLIOGRAPHY

Aungier, R. H., 1988, "A Systematic Procedure for the Aerodynamic Design of Vaned Diffusers," *Flow in Non Rotating Turbomachinery Components*, ASME FED - Vol. 69, pp. 27-34.

Aungier, R. H., 1990, "Aerodynamic Performance Analysis of Vaned Diffusers," *Fluid Machinery Components*, ASME FED - Vol. 101, pp. 37-44.

Baghdadi, S., 1977, "The Effect of Rotor Blade Wakes on Centrifugal Compressor Diffuser Performance -- A Comparative Experiment," ASME *Journal of Fluids Engineering*, Vol. 99, pp. 45-52.

Baldwin, B., and Lomax, H., 1978, "Thin Layer Approximation and Algebraic Model for Separated Turbulent Flows," AIAA Paper No. 78-257.

Bammert, K., Jansen, M., and Rautenberg, M., 1983, "On the Influence of the Diffuser Inlet Shape on the Performance of a Centrifugal Compressor Stage," ASME Paper No. 83-GT-9.

Carlson, J. J., Johnston, J. P., and Sagi, C. J., 1967, "Effect of Wall Shape on Flow Regimes and Performance in Straignt, Two Dimensional Diffusers," ASME *Journal of Basic Engineering*, Vol. XX, pp. 151-160.

Camatti, M., Betti, D., and Giachi, M., 1995, "Vaned Diffusers Development Using Numerical and Experimental Techniques," ASME Paper No. 95-WA/PID-4.

Casey, M. V., and Dalbert, P., and Roth, P., 1992, " The Use of 3D Viscous Flow Calculations in the Design and Analysis of Industrial Centrifugal Compressors," ASME *Journal of Turbomachinery*, Vol. 114, pp. 27-37.

Clements, W. W., and Artt, D. W., 1987, "The Influence of Diffuser Channel Geometry on the Flow Range and Efficiency of a Centrifugal Compressor," *Proceedings Institute of Mechanical Engineers*, Vol. 201, pp. 145-152.

Clements, W. W., and Artt, D. W., 1988, "The Influence of Diffuser Channel Length - Width Ratio on the Efficiency of a Centrifugal Compresor," *Proceedings Institute of Mechanical Engineers*, Vol. 202, pp. 163-169.

Conrad, O., Raif, K., and Wessels, M., 1980 "The Calculation of Performance Maps for Centrifugal Compressors with Vane - Island Diffusers," *Performance Prediction of Centrifugal Pumps and Compressors*, ASME, pp. 135-147.

Dalbert, P., Gyarmathy, G., and Sebestyen, A., 1993, "Flow Phenomena in a Vaned Diffuser of a Centrifugal Stage," ASME Paper No. 93-GT-53.

Drtina,P., Dalbert, P., Rutti, K., and Schachenmann, A., 1993, "Optimization of a Diffuser with Splitter by Numerical Simulation," ASME Paper No. 93-GT-110.

Dawes, W. N., 1991, "A Computer Program for the Analysis of Three Dimensional Viscous Compressible Flow in Turbomachinery Blade Rows," *BTOB3D Manual*.

Dawes, W. N., 1988, "Development of a 3-D Navier Stokes Solver for Application to all Types of Turbomachinery," ASME Paper No. 88-GT-70.

Dean, R. C. Jr., 1974,"The Fluid Dynamic Design of Advanced Centrifugal Compressors," Creare TN-185.

Eckardt, D., 1975, "Instantaneous Measurements in the Jet - Wake Discharge Flow of a Centrifugal Compressor Impeller," ASME *Journal of Engineering for Power*, Vol. 97, pp. 337-346.

Fisher, E.H., and Inoue, M., 1981, "A Study of Diffuser/Rotor Interaction in a Centrifugal Compressor," *Journal of Mechanical Engineering Science*, Vol. 23, pp. 149-156.

Ghose, S., and Kline, S. J., 1978, "The Computation of Optimum Pressure Recovery in Two Dimensional Diffusers," ASME *Journal of Fluid Engineering*, Vol. 100, pp. 419-426.

Hathaway, M. D., Chriss, R. M., Wood, J. R., and Strazisar, A. J., 1993, "Experimental and Computational Investigation of the NASA Low Speed Centrifugal Compressor Flow Field," ASME *Journal of Turbomachinery*, Vol. 115, pp. 527-542.

Hayami, H., Senoo, Y., and Utsunomiya, K., 1990, "Application of a Low Solidity Cascade Diffuser to Transonic centrifugal Compressor," ASME *Journal of Turbomachinery*, Vol. 112, pp. 25-29.

Hohlweg, W. C., Direnzi, G. L., and Aungier, R. H., 1993, "Comparison of Conventional and Low Solidity Vaned Diffusers," ASME Paper No. 93-GT-XX.

Inoue, M., and Cumpsty, N. A., 1984, "Experimental Study of Centrifugal Impeller Discharge Flow in Vaneless and Vaned Diffusers," ASME *Journal of Engineering for Gas Turbine and Power*, Vol. 106, pp. 455-467.

Jiang, T., and Yang, T., 1982, "Improved Vane Island Diffusers at High Swirl," ASME Paper No. 82-GT-68.

Johnson, M. W., and Moore, J., 1980, "The Developemnt of Wake Flow in a Centrifugal Impeller," ASME *Journal of Engineering for Power*, Vol. 102, pp. 382-390.

Johnson, M. W., and Moore, J., 1982, "The Influence of Flow Rate on the Wake in a Centrifugal Impeller," ASME Paper No. 82-GT-45.

Johnson, M. W., and Moore, J., 1983, "Secondary Flow Mixing Losses in a Centrifugal Impeller," ASME *Journal of Engineering for Power*, Vol. 105, pp. 24-32.

Kaneki, T., and Ohashi, S., 1982, "High Efficiency Multistage Centrifugal Compressor," *Hitachi Review*, Vol. 31, pp. 287-291.

Kano, F., Tazawa, N. and Fukao, Y., 1982, "Aerodynamic Performance of Large Centrifugal Compressor," ASME Paper No. 82-GT-17.

Kenny, D. P., 1972, "A Comparison of the Predicted and Measured Performance of High Pressure Ratio Centrifugal Compressor Diffusers," *Advanced Radial Compressors*, VKI Lecture Series 50.

Kenny, D. P., 1979, "A Novel Correlation of Centrifugal Compressor Performance for Off - Design Prediction," AIAA Paper No. 79-1159.

Kline, S. J., Abbott, D. E., and Fox, R.W., 1959, "Optimum Design of Straight Walled Diffusers," ASME Journal of Basic Engineering, Vol. XXX, pp. 321-331.

Krain, H., 1981, "A Study on centrifugal Impeller and Diffuser Flow," ASME *Journal of Engineering for Power*, Vol. 103, pp. 688-697.

Krain, H., 1988, "Swirling Impeller Flow," ASME *Journal of Turbomachinery*, Vol. 110, pp. 122-128.

Miller, R. W., 1992,"Flow Measurement Engineering Handbook," *Second Edition*, Mc Graw Hill.

Mounts, J. S., and Brasz, J., J., 1992, "Analysis of Jet/Wake Mixing in a Vaneless Diffuser," ASME Paper No. 92-GT-418.

Osborne, C., and Sorokes, J., 1988, "The Application of Low Solidity Diffusers in Centrifugal Compressor," *Flow in Non Rotating Turbomachinery Component*, ASME FED-Vol. 69, pp. 89-101.

Pampreen, R. C., 1972, "The Use of Cascade Technology in Centrifugal Compressor Vaned Diffuser Design," ASME *Journal of Engineering for Power*, Vol. 94, pp.187-192.

Pinarbasi, A., and Johnston, M. W., 1994, "Detailed Flow Measurements in a Centrifugal Compressor Vaneless Diffuser," ASME Journal of Turbomachinery, Vol. 116, pp. 453-461.

Reeves, G. B., 1977, "Estimation of Centrifugal Compressor Stability With Diffuser Loss Range System," ASME *Journal of Fluid Engineering*, Vol. 99, pp. 76-83.

Reneau, L.R., Johnston, J. P., and Kline, S. J., 1967, "Performance and Design of Straight, Two - Dimensional Diffusers", ASME *Journal of Basic Enginnering*, Vol. 89, pp. 141-150.

Rodgers, C., 1982, "The Performance of Centrifugal Compressor Channel Diffusers," ASME Paper No. 82-GT-10.

Runstadler, P. W. Jr., and Dolan, F. X., 1973, "Further Data on the Pressure Recovery Performance of Straight Channel, Plane Divergence Diffusers at High Subsonic Mach Numbers," ASME *Journal of Fluid Engineering*, Vol. XX, pp. 373-384.

Runstadler, P. W. Jr., and Dean, R. C. Jr., 1969, "Straigth Channel Diffuser Performance at High Inlet Mach Numbers," ASME *Journal of Basic Engineering*, Vol. 91, pp. 397-422.

Senoo, Y., 1984, "Low Solidity Cascade Diffusers for Wide Flow Range Centrifugal Blowers," *Flow in Centrifugal Compressors*, VKI Lecture Series, 1984-07.

Senoo, Y., Hayami, H., and Ueki, H., 1983, " Low Solidity Tandem Cascade Diffusers for Wide Flow Range Centrifugal Blowers," ASME Paper No. 83-Gt-3.

Senoo, Y., 1978, "Japanese Patent Application Disclosure," 119411/78 (*In Japanese*).

Sorokes, J. M., 1993, "The Practical Application of CFD in the Design of Industrial Centrifugal Impellers," *Proceedings of the Twenty Second Turbomachinery Symposium*, Taxas A&M University, pp. 113-124.

Sorokes, J. M., and Welch, J. P., 1992, "Experimental Results on a Rotatable Low Solidity Vaned Diffuser," ASME Paper No. 92-GT-19.

Sorokes, J. M., and Welch, J. P., 1991, "Centrifugal Compressor Performance Enhancement Through the Use of a Single Stage Development Rig," *Proceedings of the Twentieth Turbomachinery Symposium*, Taxas A&M University, pp. 101-112.

Stein, W., and Rautenberg, M., 1988, "Analysis of Measurements in Vaned Diffusers of Centrifugal Compressors," *Journal of Turbomachinery*, Vol. 110, pp. 115-121.

Stein, W., and Rautenberg, M., 1985, "Flow Measurements in Two Cambered Vane Diffusers With Different Passage Widths," ASME Paper No. 85-GT-46.

Wilmsen, B., 1996, "Design and Development of an Unsteady Data Acquisition System (UDACS) for Centrifugal Compressor," *A Thesis*, Michigan State University.

Yoshinaga, Y., Gyobu, I., Mishina, H., Koseki, F., and Nishida, H., 1980, "Aerodynamic Performance of a Centrifugal Compressor With Vaned Diffuser," ASME *Journal of Fluid Engineering*, Vol. 102, pp. 486-493.